

# **Numerical Modeling of Polyvinyl Alcohol (PVA) Swelling and Dissolution in Water**

by  
Sebastian Emilio Yazigi-Richoux

A Thesis Submitted to the Faculty of the Department of Mechanical Engineering,  
University of Houston

In Partial Fulfillment of the Requirements for the Degree of  
Master of Science  
in Mechanical Engineering

Chair of Committee: Dr. Li Sun

Committee Member: Dr. Haleh Ardebili

Committee Member: Dr. Jiming Bao

Committee Member: Dr. Dong Liu

University of Houston  
August 2020

## **Acknowledgments**

I would foremost want to express my deepest gratitude to my advisor, Dr. Li Sun for his guidance, encouragement, support, teachings, expertise, and patience towards me during these last few years.

I wish to also give thanks to Dr. Ardebili, Dr. Bao, and Dr. Liu for taking valuable time to review and evaluate this presented work. I am also grateful for the rest of the faculty of the University of Houston for their teachings during my undergraduate and graduate career.

I would also like to give thanks for the other members of Dr. Sun's group for their friendship, support, encouragement, and assistance over the last two years. I would also like to thank former team member Dr. Min Liu for his guidance and teaching me the ropes with respect to research and lab matters.

I would also like to thank members of Dr. Ardebili's lab; especially Mr. Qiang Fu for teaching me how to use lab instruments.

## **Abstract**

This study investigates the numerical models for polymer dissolution, with a long-term goal of developing high performance dissolvable elastomer from Polyvinyl Alcohol (PVA) replacing current not dissolvable rubber based materials. With fast development of hydraulic-fracturing in past 15 years, the oil and gas industry is in great need of dissolvable materials to fabricate certain temporary downhole tools in replacing traditional metals/rubbers/composite parts. Such dissolvable tools can eliminate the current downhole milling and back-flush operations to meet the high pressure ( $>70\text{MPa}$ ) and high temperature ( $>100^\circ\text{C}$ ) working environment, most of current “dissolvable” elastomers are mixtures of rubber and dissolvable polymers (such as Polylactic acid and poly(glycolic acid)) to achieve high ductility. These mixtures are only degradable and will break into small pieces after reactions. Starting from 2016, our group has been developing PVA based elastomer that will have comparable properties as acrylonitrile butadiene rubber (NBR). PVA is a known biocompatible and water dissolvable plastic material. What make it interesting is that water can act as a very effective plasticizer and alter its mechanical properties. PVA shows glassy mechanical behavior at nominal conditions, but becomes rubbery-like from water addition. With enough water, PVA molecules will disperse in water and form a solution. This study looks at the numerical solution of the PVA swelling and dissolving process in water.

Our polymer dissolution model uses thermodynamics and kinematics. Thermodynamics explains why dissolution happens in the PVA/water looking at free energy differences for the initial and end states of polymer solvent system. Kinematics gives an insight to the process of polymer dissolution. At first the polymer only swells as small amount of solvent penetrates it and no dissolution occurs. Local solvent concentration is low and water molecules within the polymer act as a plasticizer. Accompany the increasing water concentration, there is a corresponding minimum time called de Gennes’s reptation time, after which individual polymer chains is considered to disentangle from the bulk polymer. This moment defines the time after which the polymer dissolution begins. Here proposed our own numerical polymer dissolution model building on the kinematic models from literature. In solving the double moving boundary problems of swelling and dissolution, Landau transform is introduced to deal with the changing domains. An iterative scheme to track the location of the moving boundary demarking the polymer-solvent intersection at every time step has been developed to solve the problem. Therefore, our own methods and algorithms are introduced.

The model's results showed good qualitative agreement with published experimental results from others. A quantitative analysis showed that total polymer amount is not conserved through time initially. Conservation was obtained by modifying the governing equation of the moving boundary. Our model is a good foundation, but potential enhancements such non-linearization and expansion two dimensions are good opportunities for further work.

## **Table of Contents:**

Acknowledgments.....	1
Abstract.....	2
Table of Contents:.....	4
List of Tables:.....	5
List of Figures.....	6
Chapter I: Introduction & Background.....	1
Hydraulic Fracking and Frac Plug Problem.....	1
Thesis Overview.....	9
Chapter II: Polymers.....	13
Overview of Polymers.....	13
Polymer Glass Transition Temperature.....	17
Classification of Polymers.....	27
Elastomers and Plastics.....	29
Elastomers in the Oil and Gas Industry.....	31
Polyvinyl Alcohol.....	33
Chapter III: Polymer Dissolution Models.....	37
Thermodynamics of Polymer Solubility.....	37
Review of Kinematic Polymer Dissolution Models.....	47
Chapter IV: Own Polymer Dissolution Model.....	73
Set-up of the Model.....	73
The Stefan Problem and the Landau Transforms.....	80
Finite Difference Method and Solver Algorithms.....	83
Model Results and Modifications.....	97
Chapter V: Conclusion & Future Work.....	102
Conclusion.....	102
Future Work Suggestions.....	103
References.....	106
Appendices.....	115
A. MATLAB Script.....	115

## List of Tables:

TABLE 1 VOID SIZE DISTRIBUTION WITH RESPECT TO DRAW RATIO( STRAIN).TABLE TELLS HOW MANY VOIDS ARE PRESENT IN THE MATERIAL DENSITY WISE WITH RESPECT TO THE STRAIN. VALUES ARE VOID QUANTITY PER CUBIC NANOMETER. FROM [39].	24
TABLE 2 NUMBER OF CLUSTERS FOR PEN AND PET THAT ACCOMMODATE TWO TYPES OF RADII: POSITRONIUM AT THE MIDDLE COLUMN AND OXYGEN MOLESCULES AT THE RIGHT COLUMN. FROM [40].	26
TABLE 3 GLASS TRANSITION TEMPERATURE VS RH FOR PVA FILMS. FROM: [69].	35
TABLE 4 CHANGE IN MECHANICAL PROPERTIES DUE TO RH. FROM [72].	36

## List of Figures

FIGURE 1 US FOSSIL FUEL PRODUCTION TRENDS BY YEAR. MOST OF THE PRODUCTION INCREASES ARE FROM SHALE. FROM: [2].	2
FIGURE 2 SIMPLE SCHEMATIC OF A SHALE PRODUCTION WELL, WHICH SUCCESS RELIES ON THE EFFECTIVENESS OF HORIZONTAL DRILLING AND HYDRAULIC FRACKING. FROM: [3].	2
FIGURE 3 PERFORATING GUN ( IN GREEN) WITH FRAC PLUG ( RED) IN THE HORIZONTAL WELL SECTION. FROM: [4].	3
FIGURE 4 BOSS HOG FRAC PLUG WITH COMMON FEATURES NUMBERED ACCORDINGLY. FROM: [5].	3
FIGURE 5 FRAC PLUG AND A MILL BIT. THE CIRCLED TEETH KEEP THE PLUG IN PLACE DURING DRILLING. ONCE TOO DAMAGED, THE PLUG WILL BECOME LOOSE. FROM: [10].	4
FIGURE 6 ALL METAL INNOVEX FRAC PLUG. FROM: [11].	7
FIGURE 7 THE CONTACT REGION OF A METAL-ON-METAL SEAL. THE GROOVES AND VALLEYS ARE EXAGGERATED IN SIZE TO SHOW THE TOPOGRAPHY. FROM: [14].	7
FIGURE 8 THE THREE DIFFERENT SURFACE ALIGNMENT CONFIGURATIONS SIMULATED IN. FROM: [14].	8
FIGURE 9 PERMEABILITY FOR EACH CONFIGURATION USED WITH RESPECT TO COMPRESSION LOAD APPLIED. FROM: [14].	9
FIGURE 10 THE EVOLUTION OF BULK POLYMER UNDERGOING DISSOLUTION. FROM: [16].	11
FIGURE 11 POLYSTYRENE CHAIN MADE UP OF INDIVIDUAL ETHYLENE UNITS. FROM: [22].	13
FIGURE 12 AMORPHOUS AND SEMI-CRYSTALLINE POLYMER. FROM: [21].	14
FIGURE 13 STRESS RELAXATION IN PROGRESS AND HOW A SPRING-DASH SYSTEM CAN REPRESENT IT. FROM: [30].	16
FIGURE 14 DOMINANT ELASTIC VS DOMINANT VISCOUS RESPONSE OF SILLY PUTTY UNDER VARIOUS CONDITIONS. FROM: [32].	17
FIGURE 15: DIFFERENT REGIONS THAT MAKE UP THE TOTAL VOLUME OF THE SYSTEM. FROM: [34].	18
FIGURE 16 TWO TEMPERATURE SHOWING HOW INCREASING THE TEMPERATURE GIVES THE MOLECULE MORE 'RANGE'. FROM: [37].	20
FIGURE 17 THE VORONOI TESSELLATION METHOD FOR TWO DIMENSIONAL POLYMER CHAIN SYSTEMS. THE BLACK DOTS REPRESENT THE ATOMS OF THE POLYMER CHAINS AND ALSO THE CENTER OF EACH POLYGON. FROM [39].	23
FIGURE 18 TETRAHEDRON MADE BY THE DELAUNEY TESSELLATION METHOD. EACH VERTEX IN THE SYSTEM IS THE LOCATION OF AN ATOM. FROM [40].	25
FIGURE 19 SHOWING POLYMER CHAINS WITH AND WITHOUT PLASTICIZER. FROM: [41].	27
FIGURE 20 SOME OF THE POLYMER CHAIN TOPOLOGY CLASSIFICATIONS. FROM: [21].	28
FIGURE 21 GENERAL STRESS-STRAIN CURVE OF AN ELASTOMER. FROM: [44].	30
FIGURE 22 FRAC PLUG SEAL BEFORE AND AFTER BEING ACTIVATED BY SQUEEZING. FROM: [10].	32
FIGURE 27 PLOTTING OF VARIOUS SOLVENT AND STATING ON WHETHER OR NOT THESES SOLVENTS WILL DISSOLVE CELLULOSE NITRATE. THE VOLUME IS SPHERICAL AND PLOTTED OUT BY THE RADIUS. FROM: [67].	46
FIGURE 28 THE HANSEN SPHERE. ANY MATERIAL THAT LIES WITHIN THE GRAY SPHERE SURFACE WILL UNDERGO DISSOLUTION. FROM: [74].	47
FIGURE 29 THE MAIN STEPS OF POLYMER DISSOLUTION: (A) SHOWS THE ORIGINAL BULK POLYMER BEFORE ANY DISSOLUTION OCCURS; (B) SHOWS THE POLYMER SWELLING AS SOLVENT HAD PENETRATED IN; (C) IS AFTER ENOUGH ELAPSED TIME SUCH THAT SINGLE POLYMER CHAINS LEAVE THE BULK. FROM [15].	48
FIGURE 30 THE THREE MAIN REGIONS FOR TU & OLANO'S SET-UP AT INITIAL TIME.	49
FIGURE 31 TU & OLANO'S BULK POLYMER DISSOLUTION SOLUTION DEVELOPMENT WITH RESPECT TO TIME. THE BLUE DOTS MARK THE POLYMER-SOLVENT BOUNDARIES AT EACH TIME INCREMENT. EACH CURVE	

IS ALSO LABELED WITH INCREASING TIME INCREMENTS. THE INITIAL POLYMER VOLUME FRACTION CURVE IS THE CURVE #1. FROM: [75].	54
FIGURE 32 THE SPHERICAL COORDINATE SYSTEM. THE POLYMER PELLETT WILL BE DEFINED BY THESE COORDINATES, BUT THE SYMMETRY ALLOWS ONE TO IGNORE THE ANGLES OF THETA AND PHI. FROM: [77].	55
FIGURE 33 SHOWING DEVOTTA ET AL PROBLEM SET UP. HERE SPHERICAL PELLETT IS IMMERSSED WITHIN A SOLVENT. THE RED BOX EMPHASIZES THE 1-D SIMPLIFICATION DUE TO SYMMETRY.	55
FIGURE 34 BOUNDARY CONDITIONS SET UP BASED ON FIGURE ABOVE. LEFT END IS NEUMANN BC AND FIXED WHILE RIGHT END IS DIRICHLET BC AND ALLOWED TO MOVE WITH REGARDS TO SPACE.	56
FIGURE 35 RESULTS FROM DEVOTTA ET AL SHOWING SIMULATION VS EXPERIMENTAL RESULTS FOR POLYSTYRENE PELLETT SUBMERGED IN CYCLOHEXANE. BOTH MODEL AND DATA SHOW HOW DECREASING SIZES DECREASES DISSOLUTION TIME UP TO A POINT UNTIL IT FLATTENS OUT. FROM: [76].	60
FIGURE 36 POLYMER-SOLVENT SYSTEM OF PEPPAS & WU.	60
FIGURE 37 MAXWELL MODEL ANALOG. THE VISCOELASTIC BEHAVIOR OF A POLYMER CAN BE REPRESENTED WITH THIS SPRING-DASHPOT ARRANGEMENT.	62
FIGURE 38 PIERRE-GILLES DE GENNES' REPTATION SET-UP. FROM: [19].	68
FIGURE 39 SCHEMATIC OF THE MOLECULAR CLOCK IN ACTION.	71
FIGURE 40 EXPERIMENTAL AND NUMERICAL RESULTS OF THE SOLVER FOR POLYSTYRENE IMMERSSED IN MEK. FROM: [17].	72
FIGURE 41 REGIONAL SET-UP OF THE PROBLEM. REGION I IS BULK POLYMER AND REGION II IS SOLVENT	73
FIGURE 42 CHANGE IN REGIONAL SIZES AND DOMAINS AS THE POLYMER DISSOLUTION MODEL PROGRESSES WITH RESPECT TO TIME.	74
FIGURE 43 CLASSICAL STEFAN PROBLEM SET-UP. FROM: [82].	80
FIGURE 44 CONTINUOUS VS DISCRETE SPACE TIME FOR REGION ONE OF THE PROBLEM. THE DISCRETE REGIONS ARE ONLY SET FOR THE INTERSECTIONS OF BLACK LINES. THE ANALYTICAL HAS AN INFINITE NUMBER OF LOCATIONS, REPRESENTED AS THE RED FIELD. THE BLUE COLORED LINES ARE KNOWN INITIAL AND BOUNDARY CONDITIONS THAT ARE USED TO COMPUTE THE RESULTS.	87
FIGURE 45 SHOWING THE IMAGINARY NODE HALFWAY TIME-WISE AS A RED CIRCLE. THIS NODE WILL BE DEFINED BY THE SIX ADJACENT C-LABELED NODES.	87
FIGURE 46 TO SOLVE THIS COARSE GRID, ONE WILL NEED THREE IMAGINARY HALF-WAY NODES MARKED AS THE THREE RED CIRCLES.	91
FIGURE 47 SHOWING HOW THE 'C' NODES WITH SUBSCRIPT OF -1 DO NOT EXIST IN PHYSICAL SPACE. THESE NODES ARE CALLED 'GHOST NODES'.	93
FIGURE 48 MATRIX RE-ARRANGEMENT OF THE ABOVE EQUATIONS. THIS RESULTS IN A SYSTEM WITH 3 UNKNOWN AND 3 INDEPENDENT EQUATIONS.	94
FIGURE 49 POLYMER CONCENTRATION PROFILE AT START. THE BLUE ASTERISK MARKS THE BOUNDARY BETWEEN THE BULK POLYMER AND THE SOLVENT.	98

# **Chapter I: Introduction & Background**

## **Hydraulic Fracking and Frac Plug Problem**

In the last decade, there has been a significant technological revolution in the fossil fuel energy industry. New and improved drilling and processing techniques, mainly the hydraulic fracking and horizontal drilling processes, have enabled drilling operations to reach both oil and natural gas resources in the shale formation that once were too cost-intensive for extraction. Thanks to these technologies, oil and gas production in the United States has dramatically increased since 2010, as shown in figure 1. The United States is on track to become energy independent and less affected by the geopolitics involving oil-rich nations and cartels such as the Organization of Petroleum Exporting Countries (OPEC) [1]. This increases are mostly due to shale production growth, in which most of the product is natural gas. Compared to coal, burning natural gas emits CO<sub>2</sub> but in far less quantities and does not release additional dangerous particulates such as lead and sulfur dioxide. Natural gas can also serve as a ‘bridge’ as the overall energy infrastructure undergoes the slow but steady transition to renewable energy. Natural gas power plants can potentially complement and aid renewable power sources to cover for their two biggest obstacles that prevent their universal usage: intermittent qualities of renewable energy and a lack of methods to store energy at a large scale [1, 2].

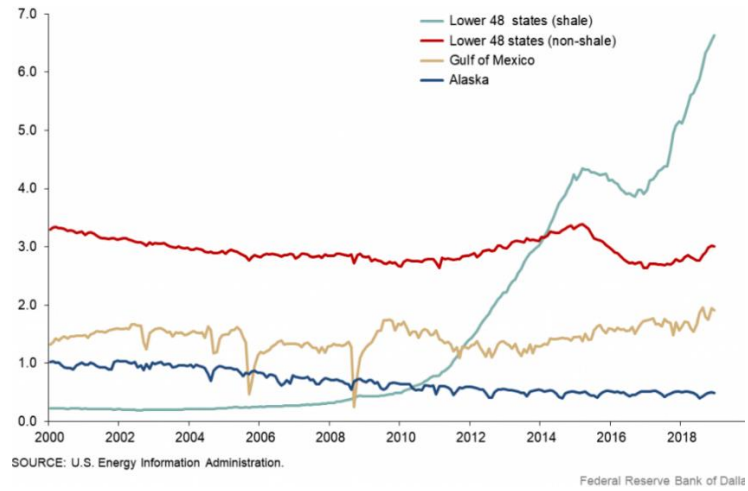


Figure 1 US fossil fuel production trends by year. Most of the production increases are from shale. From: [2].

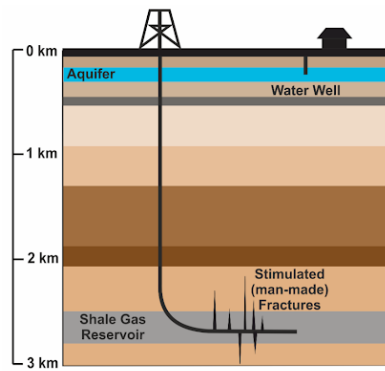


Figure 2 Simple schematic of a shale production well, which success relies on the effectiveness of horizontal drilling and hydraulic fracturing. From: [3].

One of the critical technologies in unconventional formation production is hydraulic fracturing or better shortened as ‘fracking’, which only became realistic at the turn of century. Sections of a horizontally drilled well are isolated sequentially and pressurized fracking fluid

composed of mainly water and proprietary additives is applied to fracture the nearby rock formations to reach the natural gas [1, 3]. Figure 2 shows a schematics of shale well.

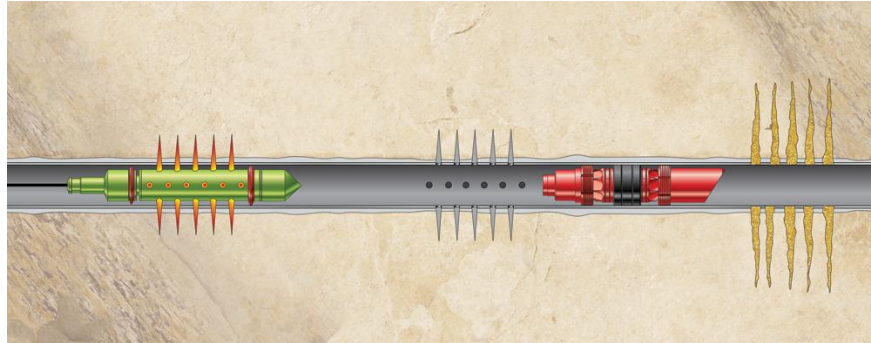


Figure 3 Perforating gun ( in green) with frac plug ( red) in the horizontal well section. From: [4].

A device called a frac-plug is used to isolate parts of the well such that the fracking is done section by section. Figure 3 shows the frac plug isolating a well section. The perforating gun on figure 3 induces local cracks into the well deposit. The well section is then pressurized such that the cracks grow to access and extract the fossil-fuels within the rock. There is a wide variety of designs of frac-plugs made by oil service and tooling companies ranging from independent manufacturers (Magnum) to conglomerates such as Schlumberger and Baker Hughes [6, 8]. Figure 4 shows the representative components of a frac plug, it normally consists of are three main category of parts made from different materials as follows [5-7]:

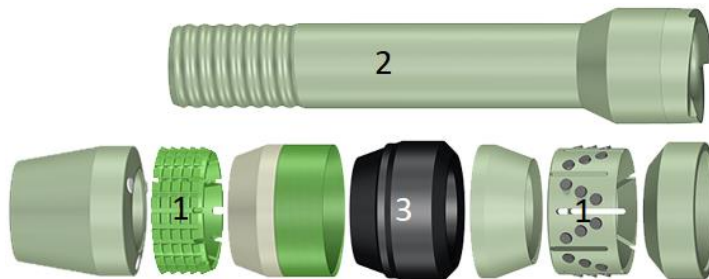
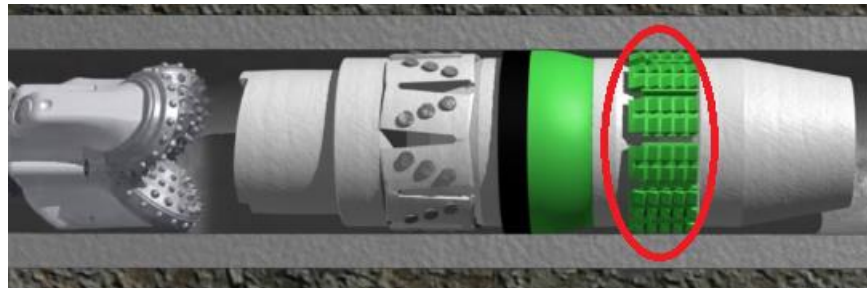


Figure 4 Boss Hog frac plug with common features numbered accordingly. From: [5].

1. Front and rear metal slips with ‘teeth’. The ‘teeth’ anchor the frac plug to the drill pipe casing. Slips can be made from “hardened metal or composite with ceramic buttons.

2. Hollow mandrel and connecting/support components. All frack components are assembled on the mandrel to function. The mandrel helps isolate a well section when a frac-ball is dropped from upstream and seal the hollow end-the right side. The mandrel and other structural parts are usually made of an epoxy composite material.
3. A middle packer that expands to isolate an inner well section. The packer will expand radially during frac plug setting to seal up the section of the drill casing for fracking, it is made of a polymeric elastomer.

After the fracking operation is done for all the isolated sections, these conventional frac plugs must be removed such that the natural gas can be brought to the surface. This removal is usually done by using a drill mill to destroy every frac plug [9]. One must carefully choose the correct type of mill for the frac plug drill-out depending on the materials used. Different mill bits cut the frac plug in a specific way. An example is the mill tooth bit. The mill tooth's action consists of penetrating, stretching, and finally pulling loose bits of material from the plug. The mill tooth bit is best for using against plugs made of composite materials, and that is the reason why current drillable frac plugs use as much of composite material as possible. This bit also performs decently against conventional cast iron slips. But hardened iron components can be a challenge and will quickly wear down and damage the mill bit. Another type of mill bit is the Tungsten Carbide Insert tricone bit. This bit crushes rather than cuts the frac plug. This mill bit is not as efficient as the mill tooth bit. But the tricone bit is better at drilling through hardened iron components. Plug manufacturers often give their own set of guidelines and recommendations with respect to what mill bit to use for a specific plug model [9].



*Figure 5 Frac plug and a mill bit. The circled teeth keep the plug in place during drilling. Once too damaged, the plug will become loose. From: [10].*

One challenge encountered during drilling is that the whole plug can rotate during the milling process when contacting with the spinning mill bit. The friction between the plug components in contact with the inner casing and the mandrel help reduce the plug's spin. But the mill must be able to overcome the plug's spin to destroy the frac plug. Figure 5 shows a frac plug about being drilled. The cast iron slip with teeth (in the circled region) again plays a crucial role during the milling operation. These 'teeth' are solely responsible in keeping the frac plug from moving along and around casing during the milling operation. The 'teeth' keep the plug in place until they themselves are milled. Once the teeth are gone, the rest of the intact plug is free to move along the casing. The procedure is then for the drill to push the what remains of the plug further downstream until it comes into contact with the front portion of another plug downstream. The end part of the remaining frac plug must lock with the front of a frac plug downstream for further successful milling. This locking is necessary to prevent the remaining frac plug from spinning with the drill such that further milling out will occur. Pushing the drill against the plug can help squeeze the two plugs together to assist in the locking [6, 9].

The whole milling process must be done with extreme care. Any mistake can damage the milling equipment or lead to the failure of fully destroying a frac plug. The milling process itself also requires a skilled and knowledgeable operator to mill each plug efficiently and without errors. It takes on average about thirty minutes to drill through a frac plug in the case where no problems are encountered. Any errors or accidents made during a milling operation will add time and cost resources. Thirty minutes may not appear to be much, but a single horizontal well can have tens of frac plugs [6, 9]. One proposed passive solution is to make the frac plugs themselves dissolvable such that they do not need to be milled [11].

Fracking itself is nothing new but dissolvable frac plugs are a recent innovation to the field. The necessity to reduce labor and material costs in order for fracking firms to be competitive not only with each other but also against conventional fossil fuel resources has allowed various frac

plugs to exist. The first generation dissolvable frac plugs were not fully dissolvable; only some parts of the plug underwent complete dissolution. The objective of these plugs was not to replace the milling operation, but to rather make it easier. The obvious drawback here is that plug components such as ‘teeth’ and buttons still remained. One had to deal with these undissolved pieces by coiled tubing intervention before proceeding any further [11]. Magnum Oil Well Tools introduced the first fully dissolvable frac plug onto the market in late 2014. This plug’s main material components are a dissolvable metal along with a dissolvable polymer packer. Dissolvable alloys replace the conventional frac plug materials of cast iron and composites. The high temperature inside a well can also assist the dissolution to occur within an acceptable time. Each material component dissolves at different times, and the whole plug is fully dissolved in about 72 hours at 250 Fahrenheit [8]. The applications of the Magnum plugs led to an average saving of about 300,000 dollars for the whole life cycle of a single fracking well [12].

Clean-up of the well by coil tubing must be carried out before the well can be put into hydrocarbon production. This is because various materials accumulate inside the well during the continuous fracking job and the dissolution of multiple frac plugs. In addition, materials such as drill cuttings, fracking proppants such as sand, are in the well. All of these materials must be removed to ensure no restrictions to production [13]. Chauffe [11] saw that dissolvable plugs left no milling debris or drill cuttings. This resulted in less remaining material and thus easier well cleaning.

Other firms followed Magnum Oil Well Tools with their own designs and materials for dissolvable plugs. Chauffe [11] published a report on the application of the dissolvable, all metal frac plugs made by Innovex. These fracking plugs used in various sites showed good performance. In one case, 20 out of 23 plugs underwent full dissolution in one site and 64 out of 72 plugs underwent dissolution at another. The not fully dissolved plugs had to be milled, but it took far

less time for completion. An average of 1.5 to 2 minutes was needed per plug. This is a vast improvement to the thirty minutes of conventional plugs.



*Figure 6 All metal Innovex frac Plug. From: [11].*

The Innovex plug uses a “unconventional design” metal seal to both anchor the plug to the drill casing and to seal the well rather than use a conventional elastomer packer. Metal seals play a critical role in environments where other seal materials fail such as in nuclear power applications. Despite their potential, there has been very little investigation and quantitative understanding into their working and failure mechanisms [11]. They are known to be very complicated because of surface properties. Perez-Rafol et al. [14] carried out a numerical simulation study on the leakage mechanism between two metallic annular contact seals. Because of the turning process, both seals had a rough surface with alternating grooves in the radial direction and finer grooves in the circumferential direction. Figure 7 shows the contact topography of the two seals.

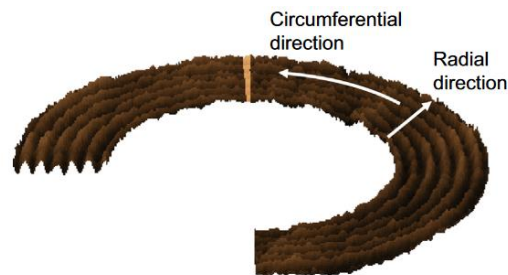


*Figure 7 The contact region of a metal-on-metal seal. The grooves and valleys are exaggerated in size to show the topography. From: [14].*

The authors modeled a small area of the both metal seals- the area modeled is the orange colored wedge on figure 7. This is because the varying surface roughness made the problem computationally costly. The orange slice has the whole radial length being used and has the inner pressure as the inner radial boundary condition and zero pressure as the outer radial boundary condition. The incomplete circumferential ends had periodic boundary conditions meaning that each end was mirrored to the other one. The authors ran three cases with respect to the alignment of the contact surface roughness as shown in figure 8.

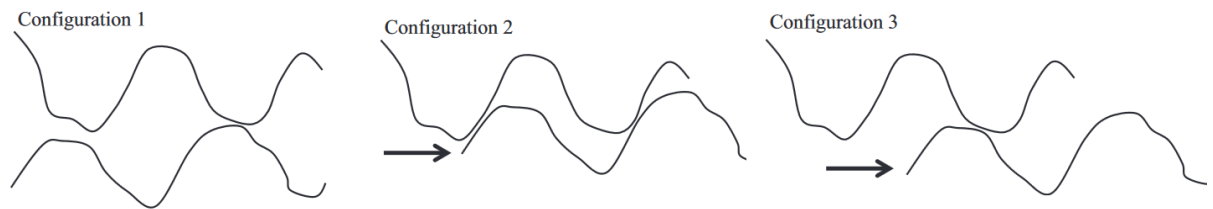


Figure 8 The three different surface alignment configurations simulated in. From: [14].

Three types of contact surface morphologies and corresponding contact mechanics were analyzed upon compression. The load pushes the rough surfaces against each other and leads to changes in surface topography. Compression also led to changes to the gaps between the compressed surface. These gaps along with the changed topography form possible pathways for leaks. The Reynolds equation was used to obtain the pressure distribution through the possible pathways to see if leaks appeared. The pressure dropped along the radial direction was the preferred direction for flow. However, the flow could also take a circumferential direction but without a drop in pressure. This resulted in the flow having a meandering path from the inner to outer radius of the seal and leak.

Figure 9 shows the results of permeability with respect to compressive load for the three cases. This shows a universal drop in permeability with greater compression and that the initial contact arrangement can have a dramatic effect on the permeability.

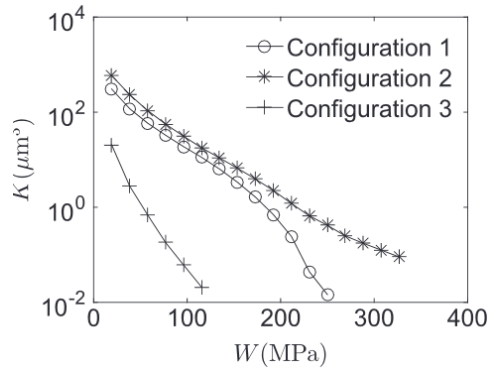


Figure 9 Permeability for each configuration used with respect to compression load applied. From: [14].

A satisfactory seal should get consistent and efficient preventions against leaks under different conditions- not just works only for a specific configuration, such as three as shown in figure 8. Configuration three shows the best performances but it can be argued that the metallic surface is sensitive to any sort or type of surface damage such as scratches. How this damage on the grooved surfaces would affect the performance is presently unknown and t seals will contain various defects before or during their application [14]. The fracking plug is an excellent example as the plug is pushed down a pipeline at fairly fast speeds to isolate well sections. Thus while metal seals do have potential, their limitations both known and unknown are present. In comparison, elastomers have a long history of use and development as seal components. The first filed patent for an elastomer seal, the O-ring, can be dated back to 1896 in Sweden [15].

## Thesis Overview

The focus of this study is to investigate and reveal the properties and characteristics of dissolvable polymer: Polyvinyl alcohol (PVA) and to develop its application as the critical middle seal part of a dissolvable plug. PVA can completely dissolve in water. For dissolvable frac plug applications, the packer component has to sustain a fracking pressure (normally at 10,000psi) for the fracking operation (6-18 hours). Then the material needs to dissolve within a desired period of time (days to weeks). Thus, an understanding of how PVA functions under the high pressure and

temperature during fracking is critical. Other researchers may find this investigation useful in situations where polymers undergo a similar dissolution process.

The main goal is to develop a numerical model to understand the entire process from the initial contact of PVA with water to complete dissolution. The work discussed here builds on existing models of polymer dissolution. During such a polymer dissolution process, first polymer swells once it is in contact with solvent enters the polymer. While the solvent penetrates the polymer, dissolution is not immediate. The penetrating solvent changes the local properties of the polymer such as the elastic modulus and ductility. It takes certain amount of time for physically entangled polymer chains to disentangle from each other due to solvent penetration [16]. This time is defined a reptation time [17, 18], a concept proposed by de Gennes to describe the time polymer chains need to disentangle [19, 20]. After the reptation time, single loose polymer chains leave the bulk polymer into the surrounding solvent. The entire dissolution process is illustrated in figure 10. There are four main stages. Here we assume a symmetric one dimensional dissolution problem where the polymer sample is in contact with solvent on both the left and right sides. The dashed middle lines symbolize the mirror plane and the problem can be solved from one end. The first schematic shows the status when polymer just gets in touch with the solvent. The second stage is where the local polymer swells as the solvent begins to penetrate the bulk polymer for time shorter than the reptation time. Region 'R' represents the un-swelled glassy state of the polymer while region 'S' represents the swelled rubbery portion of the polymer. The third stage describes the extension of the glassy/rubbery interface into the glassy state together with the dissolution of the surface rubbery state. The final stage shows the take-over of the swelled rubbery state with continued polymer surface dissolution [16].

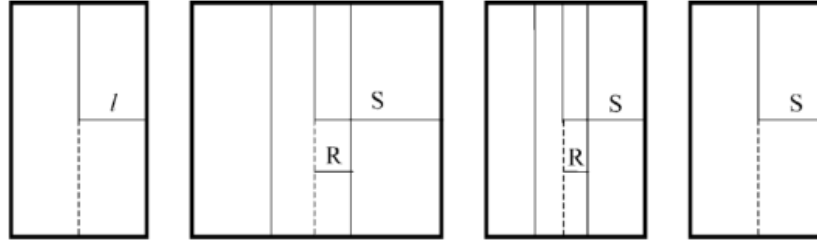


Figure 10 The evolution of bulk polymer undergoing dissolution. From: [16].

There are various mathematical models to describe the phenomena just discussed. The work covers three of these models in-depth to give an understanding on how one can use numerical methods to simulate polymer dissolution. The models reviewed break up the polymer-solvent system into two regions. One region where the bulk polymer is at and another region demarks the bulk solvent. Each region has its own set of governing equations along with boundary and initial conditions. Because the polymer swells and dissolves during the process, the size of each one of these regions changes with respect to time. Two of the models add an additional region located at the boundary where the polymer and solvent regions meet. The governing equations at the third region help characterize the polymer's initial swelling and eventual dissolution. The other model introduces the concept of a molecular clock to deal with the polymer's eventual dissolution.

The work also introduces own polymer dissolution model building on the previous models. In this model, the problem is broken up into three main regions: the bulk polymer, the bulk solvent, and finally the region connecting the bulk polymer to the bulk solvent. Each region has its own governing equation along with additional conditions. Moreover, the location of the last region changes with respect to time to characterize the swelling and dissolution of the polymer-solvent system. The work introduces and applies the concept of the Landau Transform to deal with swelling and dissolution phenomena. Additionally, finite differences methods along with iterative scheme solvers are introduced and applied to solve the polymer dissolution problem numerically. The work also presents the results of the final model along with modifications done to it.

To summarize, this thesis is divided into five parts in chapter arrangement. The first chapter gave a background on fracking and the necessity of dissolvable plugs. The second chapter gives a background on the classification and properties of polymers, specially the application of elastomers in the oil and gas field. This chapter also gives in-depth information on PVA. The third chapter deals with polymer dissolution. First the thermodynamics of dissolution are presented and discussed. Then three kinematic models of polymer dissolutions are reviewed to give an insight into the mechanisms and phenomena that occur during polymer dissolution. In the next chapter, the authors own polymer dissolution model is presented. The model builds on the presented models and gives an in-depth look into the analytical, numerical, and computational methods that this model uses to solve the polymer dissolution problem. The chapter closes by presenting the results of the solver along with changes resulting from applied modifications. The final chapter is the conclusion and gives a final review of the complete work. In this chapter, the authors give some additional suggestions for further work that regretfully could not be carried out and published.



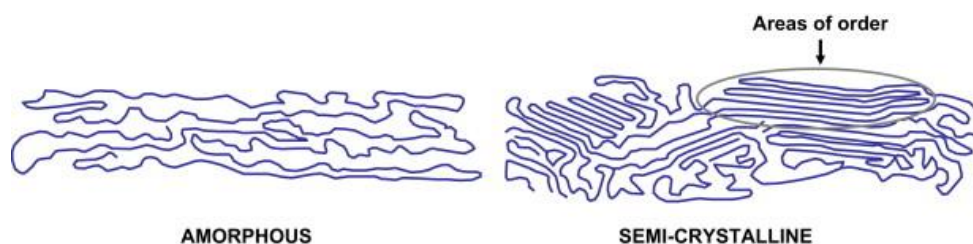


Figure 12 Amorphous and semi-crystalline polymer. From: [21]

Individual polymer chains can also be linked together. This is done by chemically altering the side groups of a polymer. From these reactions, side groups within a chain can chemically bond to other base units belonging to other polymer chains. This whole process is called chemical cross-linking and results in a polymer network [23]. The properties of the chemical groups within the chains along with the architecture of the chains can give the polymers a wide range of physical properties.

While scientific inquiry into polymers is fairly recent, humanity has used naturally-derived polymers since before recorded history. People first used naturally-derived polymers to make clothing. For example, in ancient China natural silk was also spun to make beautiful and delicate garments. Straw was also used to mechanically strengthen mud used for buildings. Mankind saw the value of polymers from the very beginning [24]. The manufacture of man-made polymer started in the 19<sup>th</sup> century; around the same time that the word ‘polymer’ came to be. Two polymers artificially made in this era were Parkesine and Celluloid. Both of these polymers were used as a substitute for ivory [25]. It was not until the 1920s that the modern concept of polymers was developed. Staudinger postulated that macromolecules in the size of millions of repeated atomic units were possible. He at first received heavy resistance from the scientific community of his time. One of his first experiments showed that rubber that underwent hydrogenation still retained a high molecular weight. This experiment contradicted the temporary scientific understanding that rubber was composed of aggregated isoprene units held together by non-covalent bonds. The

hydrogenation of rubber should have destroyed the aggregation and lowered the molecular weight [25]. Additional experiments eventually proved Staudinger's conjecture to be correct and won him the Nobel prize for Chemistry in 1953 [24, 25]. Ever since, there has been an explosion in the research and application of polymers such that financial consultants expect the polymer industry to have a market size of 158 billion dollars by 2026 [27].

Polymers have wide applications due to their unique properties. Two main very attractive properties are the light weight along superior manufacturability. The variety in structure, chemical groups, and architecture allows polymers to have a wide range of mechanical, thermal, and even electrical properties and makes them appealing to material scientists [26]. Polymers mechanically behave in very noticeably different ways when compared to traditional materials such as metals and ceramics. Metals normally show linear elastic behavior followed by a limited amount of ductility. Polymers show time-dependent viscous and elastic behavior when loaded or strained. Such dynamical character is called viscoelasticity. There are many physical and mathematical models simulating this behavior. The simplest models combine springs and dashpots in certain arrangements to characterize both the viscous and elastic behavior [28, 30].

The spring and dashpot assembly shown in figure 13 captures one of the important viscoelastic properties of polymer: the relaxation time,  $t_{relax}$ . When a polymer is strained to a fixed amount, the stress decreases even though the strain is kept constant. The relaxation time is approximately how long it takes for the stress to decay and can be approximated as

$$t_{relax} \approx \frac{\eta}{E}, \quad (1)$$

where  $\eta$  is the viscosity of the dashpot element and  $E$  is the Elastic Modulus of the spring element [29].

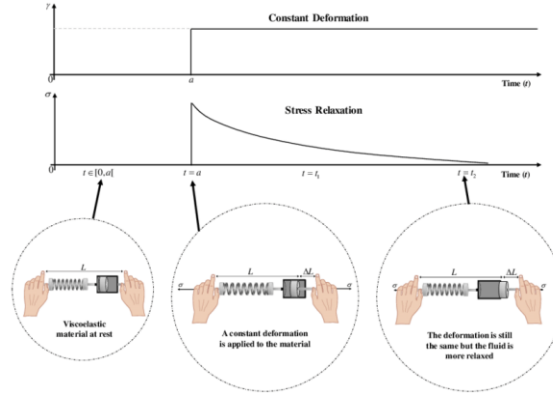


Figure 13 Stress relaxation in progress and how a spring-dash system can represent it. From: [30].

Relative to the polymer's own relaxation time, loads applied swiftly lead to a more elastic response. While loads applied more slowly lead to a more viscous response. Reiner [31] developed a dimensionless number called the Deborah number named after the prophetess in the Book of Judges. The relationship is

$$Deborah\ Number = \frac{t_{relax}}{t_{observation\_time}}, \quad (2)$$

where  $t_{observation\_time}$  refers to the time of loading. The plastic toy silly-putty gives an excellent example of how loading time can influence polymer behavior. When thrown against a surface, the  $t_{observation\_time}$  is short and thus the Deborah number is large. The putty shows an elastic response by bouncing. Letting the putty sit on a surface leads to a large  $t_{observation\_time}$  and a low Deborah number during which gravitational and contact forces act on the putty. This results in the putty showing a viscous response and 'melting' on the surface. Figure 14 shows these two scenarios [32].

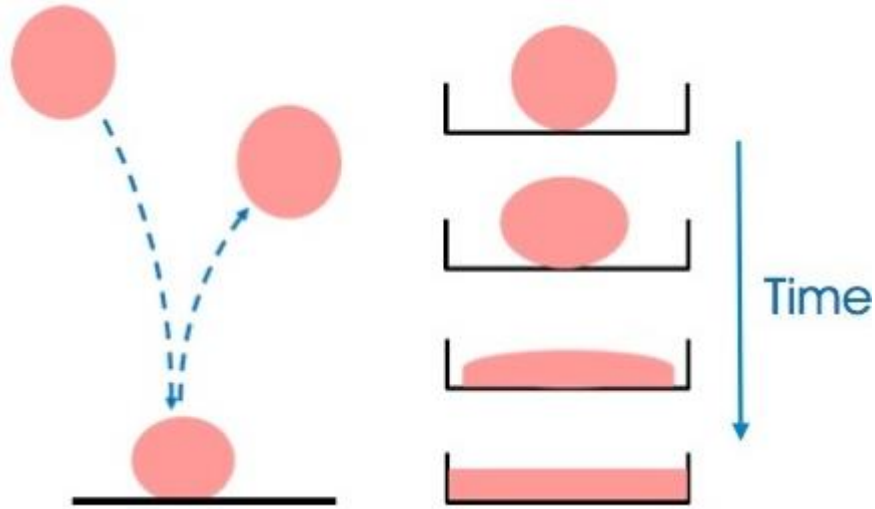


Figure 14 Dominant elastic vs dominant viscous response of silly putty under various conditions. From: [32].

## Polymer Glass Transition Temperature

In addition to time scale, the temperature also plays a significant role in polymer behavior. All polymers have an unique temperature point known as the glass transition temperature,  $T_g$ . The physical properties of the polymer such as coefficient of thermal expansion, viscosity, and specific heat undergo a large change in quantity when  $T_g$  is reached [25, 33]. This normally occurs without visible appearance change in the polymer. But during such transition mechanical parameters, such as the Elastic Modulus, can drop by three orders of magnitude when the polymer is heated to the  $T_g$ . The  $T_g$  should be taken more as a region rather than a specific point for the polymer. The reason for doing this is because the  $T_g$  for a polymer in question also depends on the cooling rate [33].

Various models exist to explain the glass transition temperature and the most successful models are based on free volume. One problem with such models is that each of them defines free volume in a distinct way. Here we illustrate different types of free volumes based on figure 15 [34]. Here  $V_{hc}$  is the volume of the atoms or molecules themselves; the space that a molecule takes up and consists of the black regions in the figure.  $V_{free:vib}$  is the volume taken up by the by the

atoms/molecules' vibrations. Sum of  $V_{hc}$  and  $V_{free:vib}$  become  $V_{vib}$ , the volume occupied by individual atoms/molecules.  $V_{free:exs}$  is the remaining volume of the system.

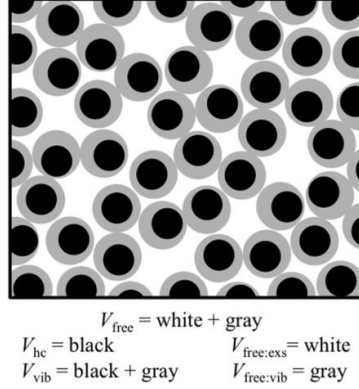


Figure 15: Different regions that make up the total volume of the system. From: [34].

Turnbull and Cohen [35] came up with a qualitative model to explain how free volume relates to the glass transition with respect to temperature. The model starts by first defining an average free volume

$$\bar{v}_f = \frac{V_{free}}{N}, \quad (3)$$

where  $N$  is the number of molecules in the system. Every molecule is in a 'cage' bounded by the its nearest neighbor molecules. While the  $\bar{v}_f$  is the average 'cage' size for each molecule. The free volume of each molecule can vary and thus a probability distribution will exist. The free volume corresponding to a molecule is denoted as

$$v = v_f + v_c, \quad (4)$$

where  $v_f$  is volume that can be obtained from redistributing  $V_{free}$  among the molecules without free energy increase, while  $v_c$  does. Turnbull and Cohen's argument is that the free volume of a molecule can reach a critical size denoted by  $v^*$ . When the free volume of a caged molecule reaches this critical size, it is possible for another molecule to move into this void. Therefore, the process results in a diffusion process that does not depend on activation but rather in the re-distribution of free volume of the system. The contribution of a single molecule to diffusion is

$$D(v) = ga(v)\vec{u}, \quad (5)$$

where  $D$  is the diffusion coefficient,  $g$  is a geometric factor,  $a$  is the diameter of the cage, and  $\vec{u}$  is the molecular velocity. Diffusion will not occur until the critical free volume size is achieved

$$D(v) = 0 \text{ if } v < v^*. \quad (6)$$

Moreover, an average diffusion coefficient can be obtained by integrating the contribution of all molecules

$$D = \int_{v^*}^{\infty} D(v)p(v)dv, \quad (7)$$

where  $p(v)$  is the probability of finding a cage with a free volume of  $v$ .  $p(v)$  can be obtained by considering the total number of possible ways to redistribute the total free volume,  $V_{free}$ , between all molecules without adding free energy. Turnbull and Cohen integrated eq. (7) to end up with

$$D = ga^*\vec{u}e^{-\left(\frac{\gamma v^*}{v_f}\right)}, \quad (8)$$

where  $a^*$  is the molecular diameter and  $\gamma$  is a numerical factor to correct any free volume overlap. This formula explains how the movement of molecules occurs and how this helps explain the glass transition of materials.

Turnbull and Cohen [36] published work to help explain how temperature plays a role in the redistribution of free volume and  $v^*$ . Assuming intermolecular interactions can be described by Lennard-Jones type of potential well and the potential energy is function of the molecule's position:  $V(r)$ . Figure 16 shows The Energy with respect to atomic distance between two molecules. The distance with the lowest energy is at  $r_0$  and is 'the bottom of the well'. There is a high repulsive interaction at small molecular separation when the hard spherical molecules come into contact with separation below equilibrium distance  $r_0$ . Each molecule is vibrating with vibrational energy is related to temperature. Increase in temperature will result in larger

molecular vibration amplitude and have a greater average  $r$  than  $r_0$ . Due to the anharmonicity of the potential well, thermal expansion is observed as the molecules spend more time at greater  $r$  values [37]. Figure 16 shows how the increase of temperature gives the molecule a greater range within the well.

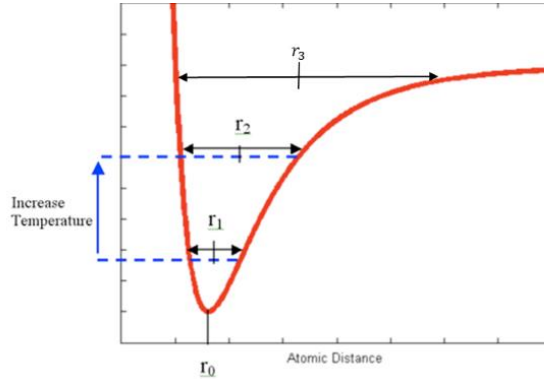


Figure 16 Two temperature showing how increasing the temperature gives the molecule more 'range'. From: [37].

The Lennard-Jones potential along with the influence temperature laid the foundation in Turnbull and Cohen's explanation. There is a proportional relationship between the average radius of the all the cages to free volumes. This proportionality can be expressed as

$$\frac{V_{free}}{V_{hc}} \propto A(\bar{r} - r_0), \quad (9)$$

where  $\bar{r}$  is the average radius of all molecular cages,  $A$  is a fitting parameter, and  $r_0$  is the equilibrium molecular separation at 0K. One can get a clearer understanding when looking at what happens at different temperatures as shown in figure 16. For a low temperature case where  $\bar{r} \approx r_0$ , potential energy would be minimized when the excess free volume and thus  $\bar{r}$  is distributed as narrowly as possible. In fact, additional energy would be needed to broaden the radius distribution. Increasing the radius of one cage while keeping  $\bar{r}$  constant requires other radii to decrease. Increasing the one  $r$  costs energy due the large slope of potential energy with respect to  $r$ . Decreasing the other radii increases the potential energy due to high repulsive forces from hard sphere contact. For higher temperatures, less additional energy is needed and a broader  $r$

distribution will result. This is because both the potential energy slope is less steep and the average radii is large enough that the hard sphere contact forces do not come into play. At  $\bar{r} = r_3$  for example, no additional energy is needed to have a very broad radius distribution. The radius distribution can be related to the free volume probability distribution. The portion of the excess free volume that can be unevenly redistributed between molecules with no energy is the free volume. This free volume is what allows the probability distribution in volume,  $p(v)$ , to exist.  $p(v)$  will broaden at higher temperatures and thus more critical volumes at or above  $v^*$  exist. And thus enable molecular movement to occur. The derivation given by Turnbull and Cohen above is qualitative, but has far-reaching implications. The most notable one is that all materials “would go through the glass transition if sufficiently undercooled and crystallization did not occur [34].”

The derivation above is simple, elegant, and gives an idea of how temperature induces glass transition in a material by considering free volume. However, polymers are composed of long repeated chains that are entangled with each other. Cohen and Turnbull’s model falls short here, as they modeled the material as hard spheres, each one with its own assigned free volume. Their method gave a good qualitative analysis and closed form solutions.

However, the free volume in polymers is much more complicated than this and closed-form solutions are out of the question. Barring this, experimental methods serve as a way to investigate the free volume of polymers. The most robust of these methods is Positron Annihilation Life-time Spectroscopy (PALS). Here one bombards the material with ortho-positronium particles consisting of a positron-electron pair. When this particle interacts with an electron within the material, annihilation occurs. To conserve energy, there is also a release of high frequency photon particles from the mutual electron-positron destruction. The life-time of these positronium pair particles helps correlate the electron density within the polymer and thus free volume within the material. If the free volume inside the material is ASSUMED to be

spherical, the life-time of the positronium particles within the material can be correlated to the free volume size [40]. While PALS is a robust experimental technique and has wide-spread use, there are some drawbacks. Foremost, is the labor-intensiveness and cost of carrying out the experiments along with problems dealing with interpreting the results. Results are hard to interpret because data is limited. One can bombard the material with a limited quantity of positroniums prior to permanently damaging and altering the material. The fact that the free volume of the material is taken to be spherical as a priori is also problematic [Dong and Jacob].

Another method to investigate the free volume of polymers involves computational modeling. This involves using Density Functional Theory (DFT) or Molecular Dynamics (MD) to numerically model polymer chain systems. With these methods, one builds polymer chains and uses numerical methods based on physical laws to solve for properties of the polymer in question.

Dong and Jacob [39] used both MD and the method of Voronoi Tessellations to compute the free volume of polymer chains. The purpose of their work was to see how free volume changes with respect to changes in polymer chain architecture from stretching. The chains within a relaxed polymer have random configuration, but when strained the polymer chains undergo some alignment along the strain direction. On their model, the quantity, distribution, and shape of free volume ‘holes’ with respect to the architecture of polymer chains is tracked as the bulk polymer is strained.

The model involves the construction of linear polyethylene polymer chains. The whole volume is broken up into grids. These grids help characterize the free volume of the polymer. Grid volume locations with no polymer hard atoms present are taken to be ‘free’. Adjacent ‘free’ grid cells are connected to each other to form free volume voids throughout the whole system. The solver not only tracks the size of these voids, but also their shape.

The Voronoi Tessellation method was also used to see how the free volume changes with respect to strain and polymer atom location. This method allowed to track how the free volume changes with respect to *locations* within the polymer chain. Figure 17 shows Voronoi Tessellations in two dimensions. Each atom within the polymer chain serves as ‘nucleation’ point for the polygons to grow and expand. They do so until they come into contact with other polygons. Thus, each polygon minus the hard sphere area of the atoms is the free area. The two dimensional method is similar to the three-dimensional one, except that polyhedral are used instead to obtain free volume.

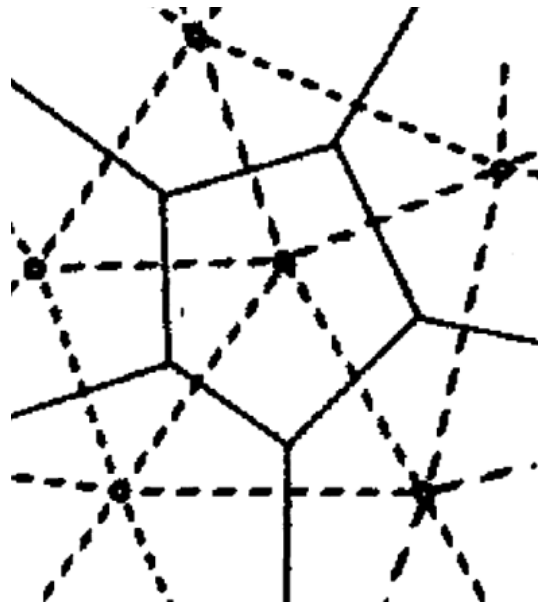


Figure 17 The Voronoi Tessellation method for two dimensional polymer chain systems. The black dots represent the atoms of the polymer chains and also the center of each polygon. From [39].

By using the grid and Voronoi Tessellation methods above, Dong and Jacob computed how free volume changes with respect to the straining polymer system. With increasing strain, the number of free volume voids with greater volume increase, at the cost of smaller volume voids. Additionally, the *total* void free volume decreases with greater strain. The table below shows the results of this. At 1 draw ratio, there are no large voids, but at higher draw ratios larger voids appear. Moreover, the shape of these voids changes with respect to strain. At higher strains, the

larger voids that appear overall more elliptical like in shape. The smaller volume voids in average remain unchanged and more spherical-like in shape.

*Table 1 Void size distribution with respect to draw ratio( strain).Table tells how many voids are present in the material density wise with respect to the strain. Values are void quantity per cubic nanometer. From [39].*

**Table 1. Distribution of Void Size at Different Draw Ratios (Unit Is number/nm<sup>3</sup>)**

void size (Å <sup>3</sup> )	draw ratio			
	1	2.4	5.0	7.4
<5	75.816	65.608	56.869	53.294
5–10	2.404	2.438	2.150	1.755
10–20	1.435	1.833	1.440	1.318
20–40	0.491	0.834	0.710	0.685
40–60	0.032	0.197	0.200	0.150
60–100	0.000	0.064	0.072	0.072
≥100	0.000	0.000	0.006	0.013
total	80.178	70.974	61.446	57.287

The Voronoi Tessellation methods allows one to see how free volume changes at different locations within the chain. This method allows one to assign a free volume to each atom in the chain and comparing how the free volume at respective atom locations changes with respect to strain, one can see how the free volume distribution also changes along a chain. The polyhedral from the Voronoi methods are redrawn at each new draw ration (strain) of the polymer chain system to track local changes in free volume. From these computations, Dong and Jacob saw the average free volume at the ends of the polymer chains increased with respect to straining. On the other hand, the average free volume for atoms far away from the polymer chain ends decreased.

Thus, the work of Dong and Jacob not only shows that for polymers free volume is more complicated, but also that it is heavily dependent on the architecture of the polymer chains themselves. The computational models also showed that free volumes do not have to be spherical and in fact become more elliptical like at higher strains, giving some doubt to the spherical priori for PALS experimental analysis. When strained, the polymer chains undergo limited alignment and thus better packing. This packing allows the polymer chains to fit better with respect to each

other and reduce the total free volume [39]. Polymer architecture is not the only variable that influences free volume in polymer. Others such as stereochemistry, back-bone rigidity, side-groups, and others also play a part [40].

In his Doctorate Thesis, Callander [40] carried out MD simulations of Polyethylene terephthalate (PET) and Polyethylene naphthalate (PEN) compute the free volume of these two different polymers. These two polymer have different molecular structures and one of the thesis' goals was to see how these differences influenced free volume properties. Specially how free volume helped explain the superior  $O_2$ solubility of PEN.

Callander also used MD and DFT to help build the respective polymer chain ensembles for each material. Because PEN and PET have different chemical formulas, different chain assemblies were allowed for each. To calculate the free volume for each material, Callander used Delauney Tessellation. This method is similar to the previous Voronoi approach, but now atoms serve as vertices for the free volume tetrahedral. Figure 18 below show a tetrahedral made by using atoms as vertices. To finalize the volume, the hard sphere volume of each atom section within the tetrahedral is subtracted.

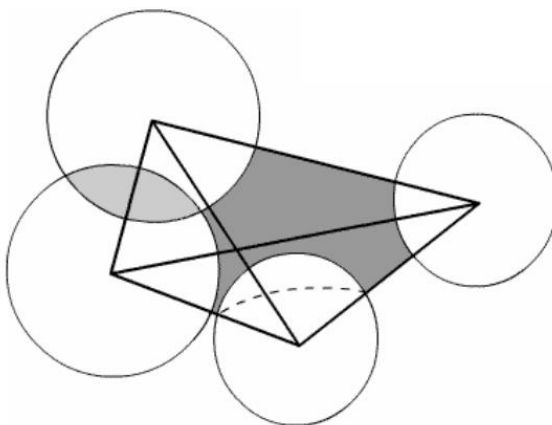


*Figure 18 Tetrahedron made by the Delauney Tessellation method. Each vertex in the system is the location of an atom. From [40]*

Similar like in Dong and Jacob, adjacent polyhedral were grouped together to form clusters. Additionally, various properties with regards to free volume such as size, shape and overall distribution within each material system were also obtained. Initial analysis showed that PET and PEN had very close average penetrant radius, where the penetrant radius is the radius of a penetrant that can access a tetrahedral free volume in question. Analysis regarding connecting adjacent and alike tetrahedral gave divergence in the results. By linking nearby clusters that could accommodate the penetration radius of an  $O_2$  molecule, PEN had a larger average number of these clusters than PET. This was not case in accommodating the penetration radius of positronium, where there was a much closer average quantity. Table 2 shows this.

*Table 2 Number of clusters for PEN and PET that accommodate two types of radii: positronium at the middle column and Oxygen molecules at the right column. From [40].*

**Table 3-7:** Average number of clusters for PET and PEN at o-Ps and  $O_2$  penetrant radii at 95 % confidence limits

<b>Polymer</b>	<b>Average Number of o-Ps clusters per model</b>	<b>Average Number of <math>O_2</math> clusters per model</b>
PET	92.833 ± 4.006	27.700 ± 2.361
PEN	88.408 ± 2.922	35.076 ± 3.191

Callander carried out a student's t statistical analysis to show this difference was statistically significant. Moreover, the difference in cluster quantity that made this difference involved clusters made out of less than 10 tetrahedrals and with an average volume between 20 to 30 cubic Angstrom. It is these additional clusters that give PEN greater oxygen solubility than PET.

Callander's work showed how two polymers, because of different chemical properties such as back-bone rigidity and side-groups, had different free volume properties. Dong and Jacob's work showed how the polymer chain architecture of a polymer of the same type affects the free volume properties. Thus, for a polymer free volume is much more complex and yet

richer. A further discussion with respect to polymer free volume is beyond the scope of this work, but it is hoped that the reviewed works give an appreciation into how much more different a realistic assessment of free volume with regards to polymers is when compared the Cohen and Turnbull's simple but elegant model.

The Turnbull derivation above explains how temperature induces the glass transition. But glass transition can also be altered by methods other than temperature. One of these approaches is to use plasticizers. Plasticizers are additives with a low molecular weight, thus much smaller sizes when compared to an average polymer macromolecule. Adding plasticizers to a polymer will reduce efficient packing of the polymer chains. The plasticizer will get in between the polymer chains of the polymer as shown in figure 19. This will increase the excess free volume in the system ( $V_{free:exs}$ ). The increase of  $V_{free:exs}$  will allow polymer chain segments to have more freedom in reconfiguration and movement. Sufficient amount of plasticizer with appropriate properties can lower the glass transition to the operational temperature, changing the polymer mechanical behavior to rubbery-like [41]. In the current study, water is found to be not only a solvent but also a very effective plasticizer for PVA.

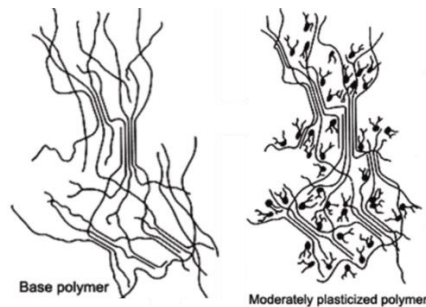
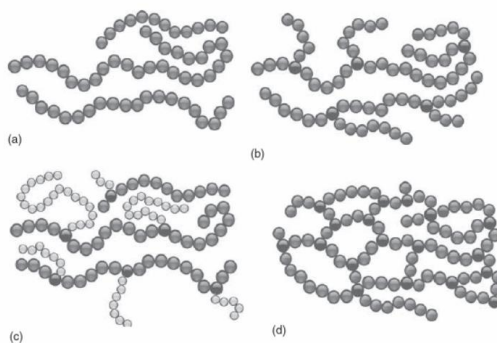


Figure 19 Showing polymer chains with and without plasticizer. From: [41].

## Classification of Polymers

Polymers include a large variety of organic species and more are added every year through organic synthesis. The polymer industry has come up with various classifications scenarios to assign to categorize them to make the ever-growing quantity of polymers more manageable and easier to deal with. Saldivar-Guerra et al. [21] summarize some of the following classifications.

One important classification approach is based on polymer chain topology. Polymers having the same chemical formulas can have different properties due to a different chain structure. Four main types are shown in figure 20. Polymer chains can be linear meaning all repeating units only have two chemically bonded nearest neighbors. Branching is one topological variation. In branching, some of the repeated units have three chemically bonded nearest neighbors, leading to a ‘branch off’ from the main chain. If the repeated units on the branches are different from the main chain, the topology is that of a graft-polymer. Cross-linked polymers are polymers with chains chemically bonded to others polymers and form a network. One property of such cross-linked structures are they are normally insoluble [21].



*Figure 20 Some of the polymer chain topology classifications. From: [21].*

Polymer classification can also be based on what atom types make the backbone chain of the polymer. Polymers with a carbon backbone are classified as organic polymers and polymers with the backbone made of Si, P, O<sub>2</sub>, or other non-carbon atom are called inorganic polymers. In addition, a polymer chain does not have to be made up of the same base unit. When a polymer

chain consists of more than one type of base units, they are called copolymers. A polymer can also be classified as a homo-polymer or a copolymer [21].

## **Elastomers and Plastics**

Another widely adopted polymer classification method is based on their physicochemical properties, and among with the mechanical behaviors is the most often used [42]. Polymers belonging to the elastomer family often show elastic mechanical behavior when deformed. This means when that when the polymer is stretched it will return to its original size quickly when unloaded [43]. The Modulus of elastomers will not remain constant with respect to the applied strain [23] and are often much lower than the typical metals, ceramics, and the other polymer family: plastics. Plastics are often referred to the polymers exhibits much brittle mechanical performances. A plastic will undergo minimal elastic deformation with the rest being permanent when loaded [43]. Plastic polymers can also fracture when strained. How much straining is possible before failure depends on the specific plastic in question. Figure 21 summarizes the typical stress-strain curves for the polymers classified as elastomers and plastics. For example, polyethylene can sustain irreversible stretching up to 400% without fracturing while polystyrene fractures when stretched at about 10%. [23].

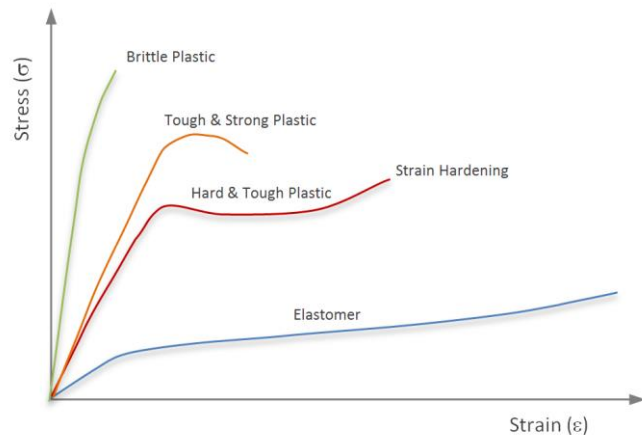


Figure 21 General stress-strain curve of an elastomer. From: [44].

$T_g$  indicates the temperature range where transitions between glassy and rubbery states takes place. At lower temperature polymers will be more mechanically stronger and brittle to behave as plastics. With increasing temperature and existence of a glassy transition, some plastics behave as an elastomer at temperatures above  $T_g$ . One criterion for such as plastic-elastomer transition can be summarized in the following sentence: “Any low crystallinity amorphous polymer with a flexible chain can be in principle be made into an elastomer by cross-linking [43].” Cross-linking is necessary, but it does not have to be a chemical cross-link involving covalent bonds; physical cross-link also works. In the meanwhile, a flexible backbone chain is also needed because such chains can move with greater ease. Thus is best to use polymers whose backbone consists of simple units for example C-C or C-O units [43] to introduce such a transition. Backbones with cyclic or benzene rings will make the chain stiffer and unfavorable for elastomers [45]. The polymer must also have a high molecular weight along with low intermolecular interaction energy between chains [46]. Another factor in play is the cis- and trans- nature of polymer chains. Trans-polymer chains will be more favorable towards crystallization and will lead to both a higher  $T_g$  and more importantly increase the overall crystallinity of the polymer. High crystallinity makes a polymer unfavorable to become an elastomer [45].

The opposite is also true. An elastomer can behave mechanically like a plastic below the  $T_g$ . The mechanical behavior will change from elastic rubbery to the more brittle, glassy behavior of plastics. Thus operational environment must be taken to account when using an elastomer for any application. Failure to account for this can be catastrophic. The best known and one of the most catastrophic examples deals with the Challenger Space Shuttle Disaster. The ill-fated shuttle launch occurred during an exceptionally cold morning. In this low temperature the FKM elastomer seal on a booster rocket underwent glass transition from rubbery to glassy. The elastomer's much brittle properties caused the seal to not function properly and caused hot gases escape. This led to one of the Shuttle's solid booster rocket to explode in midflight, killing all on board [47, 48].

## **Elastomers in the Oil and Gas Industry**

Elastomers have widespread engineering applications with the most visible use in everyday life as the vulcanized rubber used in tires. Tires all the way from bicycles to 18-wheelers are made from vulcanized rubber. A less visible use of elastomers for laypeople but still important to make everyday life possible is the use of elastomers within the oil and gas industry. Elastomers used in oil and gas applications need to meet high operational requirements. These requirements arise from the deep underground and subsea environments where elastomers are used. These environments have high pressure, either very high or very low temperatures, corrosive substances, and the presence of hydrogen sulfide,  $H_2S$  [49].

The oil and gas industry uses a wide variety of elastomers at these challenging environments. Some of these elastomers are the NBR (Nitrile Butadiene Rubber), EPDM (Ethylene Propylene Diene Monomer), HNBR (Hydrogenated Nitrile Butadiene Rubber), FKM (Fluoroelastomers), FEPM (Perfluoroelastomers), and FFKM (Perfluorocarbon Elastomer) [50]. Very generally, FKM, FEPM, and FFKM show better chemical resistance and tolerate high operational temperatures but have low mechanical strength and are more expensive [51]. NBR is

cheaper and has good mechanical properties, but unsuitable in wells where H<sub>2</sub>S is present. Here the interaction with H<sub>2</sub>S causes NBR to become brittle and glassy-like [52]. NBR, EPDM, and HNBR perform well at low operation temperatures [53]. From the examples above, no elastomer is truly best. Each one has its own strengths and limitations.

The oil and gas industry uses elastomers to manufacture parts such as seals, gaskets, and O-rings. These are crucial components in blow out preventers (BOP), packers, completion equipment, line hangers, and many others [49]. In frac plugs, the function of packers is to isolate and to prevent fluids or gases from reaching a certain area. Most elastomer packers become activated by energization. This means that work is done on the seal to activate it and make the packer capable of blockage [50]. The elastomer packer of the plug is squeezed along the axial direction (through an operation procedure called “setting”). This squeezing causes the elastomer to expand outwardly in the radial direction and make contact with the inner casing of the well and thus isolate the well section. This isolation is needed for the fracking job to be done successfully.

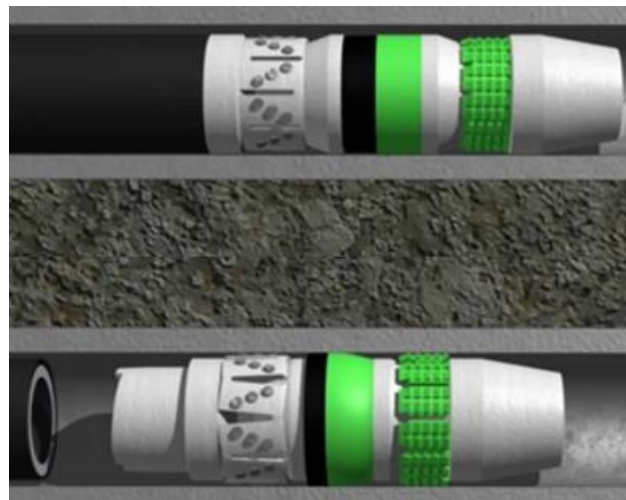


*Figure 22 Frac Plug seal before and after being activated by squeezing. From: [10].*

## Polyvinyl Alcohol

Polyvinyl Alcohol (PVA) is a fairly old and established polymer age-wise. Two German chemists, Herman and Hoehnel, first synthesized PVA from polyvinyl ester in 1924. PVA is a fully synthetic polymer, as it is not found or extracted in any natural resource. Mass production of PVA for various uses in the United States began in 1939 [54]. The world's total industrial output of PVA for various applications and uses was one million tons in 2010 [55]. The future looks bright for PVA. Investment and traders estimate that by 2024, in the centennial of its discovery, PVA will be an enterprise with a market size of 1.4 billion dollars in the United States alone [58].

PVA has many industrial uses. One of the main uses of PVA is as a sizing agent in the textile and paper industries. Here PVA is added to the textile and paper fibers. Doing so gives the fibers higher strengths while at the same time provides protection against oils and greases. This protection is because PVA is a polar polymer while most oils and greases are highly non-polar. Another common application is making food packaging films out of PVA. Chemically cross-linked PVA provides an excellent barrier against moisture and other contaminants [54]. The films serve in both preventing matter from reaching food and in isolating the food itself to preserve properties such as taste for a longer time. Crosslinking results in PVA chains being connected to one another by strong chemical bonds. These bonds increase the size of PVA chains. PVA that has chemical crosslinks *resists* instead of undergoing dissolution in water.

Cross-linked PVA is a very specific case. Conventional PVA is an ensemble of long chains with repeated base units. The structural formula of the PVA base unit is on figure 21 [54, 56]. The base unit has a chemical formula of  $[CH_2CH(OH)]_n$  consisting of a carbon backbone with a

hydroxyl side group. This hydroxyl side group has a high polarity. Water is the most common solvent used to dissolve PVA and is easily available in most situations, and also has a high polarity.

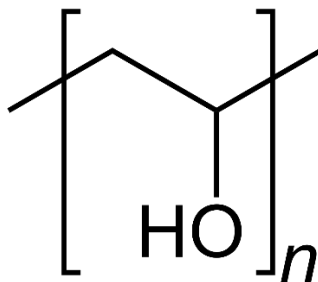


Figure 23 PVA unit monomer. Notice the important OH side group sticking out. From: [56].

The most common synthesis approach of PVA begins with making another polymer: Polyvinyl Acetate (PVAc). PVAc is made by conventional methods and by using vinyl acetate as the monomer units, resulting in linear chains. The PVAc chains then undergo saponification. Saponification is the process where the acetate side group in each repeated unit undergoes hydrolysis such that only Hydroxyl remains. PVAc must be immersed in an aqueous solution of lye (NaOH) and methanol to carry out saponification. The chemical process is illustrated in figure 24. It is also possible to use other vinyl-ester-polymer systems such as those with side groups of formate and chloroacetate to synthesize PVA, but such processes are rarely used when compared to using PVAc to get PVA [51, 54].

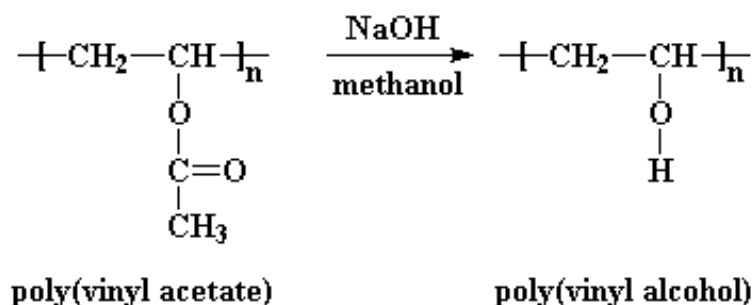


Figure 24 PVAc undergoing saponification to make PVA. From: [57].

PVA also has many varieties based on their distinct chemical structures. Some of PVAs behave like plastics in ambient environment. But parameters such as temperature can change their

properties. As we discussed in previous session, polymers will have rubbery characteristics at temperatures above  $T_g$ , It is well known that  $T_g$  of PVA depends on intrinsic properties such as molecular weight and chemical composition [59].

In addition,  $T_g$  can be tuned by adding plasticizers to the base polymer. Konidari et al. [60] plasticized films made of un-crosslinked PVA by using water. The group first made thin films of PVA and desiccated them to make sure there was no water remaining. Then the film samples were placed in airtight chambers with controlled humidity (RH) [61]. By weighing the sample before and after treatment, water concentration in PVA can be determined. Using differential scanning calorimetry (DSC),  $T_g$  of these samples are determined as function of water intake. Table 3 below shows the tabulated results.

*Table 3 Glass transition temperature vs RH for PVA films. From: [69].*

<b>Mean Values of <math>T_g</math> and <math>w_1</math> Equilibrated at Different RHs</b>		
RH (%)	$T_g$ (° C)	$w_1$
0	$73.8 \pm 2.0$	$0.00 \pm 0.00$
42	$33.0 \pm 3.5$	$0.034 \pm 0.010$
65	$10.6 \pm 3.6$	$0.082 \pm 0.003$
86	$-14.0 \pm 1.5$	$0.141 \pm 0.005$

The results clearly demonstrates the downward drifting in  $T_g$  of PVA as a function of increasing water concentration. In the meanwhile, tensile tests performed on these samples (Table 4) shows a transition from plastic to elastomer behavior under the same room temperature, driven by the increasing amount of water in samples. The mechanical properties for each film

under nominal temperature and pressure are in table 4. Like with  $T_g$ , PVA films that were put in the same chamber are grouped together to end up with averages.

Table 4 Change in Mechanical Properties due to RH. From [72].

RH (%)	Film	$E$ (GPa)	$\Delta L/L_o$	Tensile strength (MPa)
0	PVA-1 (seven samples)	$2.26 \pm 0.15$	$0.10 \pm 0.03$	$137 \pm 22$
0	PVA-2 (six samples)	$2.32 \pm 0.23$	$0.088 \pm 0.026$	$121 \pm 9.8$
42	PVA-1 (five samples)	$2.13 \pm 0.20$	$0.16 \pm 0.07$	$98 \pm 12$
65	PVA-3 (seven samples)	$0.42 \pm 0.05$	$1.70 \pm 0.30$	$49 \pm 8.3$
65	PVA-4 (four samples)	$0.42 \pm 0.02$	$1.48 \pm 0.39$	$43 \pm 2.4$
86	PVA-1 (five samples)	$0.10 \pm 0.01$	$1.64 \pm 0.49$	$38 \pm 7.3$

Konidari's data shows that increasing the water content in PVA effectively lowers  $T_g$  and this in turn influences the mechanical properties of PVA. This trend is similar to figure 19. Here water is the plasticizer for PVA. Its penetration can cause PVA swelling and with increasing concentration to form a PVA gel. In other words, if a PVA sample is immersed in water, we can observe a gelling process accompanied by gradual dissolution. This process will be discussed in the next chapter [16].

This PVA can also be made into so called hydrogels, which has subtle differences from the gel state discussed here PVA hydrogels are normally made by first dissolving PVA in water and letting the PVA solution undergo cycles of freezing and thawing. Crystallites can be produced from these cycles that act as physical cross-links. These cross-links allow the PVA molecule to form a "high molecular weight" structure and thus be a gel. A PVA hydrogel formed likes this will contain large amount water but will NOT undergo any dissolution in water due to the formation of these crystallites throughout the system. The only way to recover solubility is by first destroying the crystallites [62].

## Chapter III: Polymer Dissolution Models

### Thermodynamics of Polymer Solubility

A polymer may or not undergo dissolution when immersed in a liquid. Dissolution means that the polymer-solvent system went from one equilibrium separate state to another equilibrium solution state. The use of thermodynamics and equilibrium states gives the most compelling argument of why the polymer either did or did not undergo dissolution [63]. For any process to happen thermodynamically the system's Gibbs free energy change must be negative when comparing the equilibrium end state to the beginning state. Gibb's free change energy equation is

$$\Delta G_m = \Delta H_m - T\Delta S_m, \quad (10)$$

where  $\Delta G_m$  is change in Gibbs free energy for the two states,  $\Delta H_m$  is the change in enthalpy,  $\Delta S_m$  is the change in entropy and  $T$  is the temperature of the system. An event will occur only if

$$\Delta G_m < 0. \quad (11)$$

Flory [63,64] gave a derivation of entropy change of a polymer-solvent system. The derivation included the modification of the classical entropy of mixing entropy for a binary liquid system under ideal conditions

$$\Delta S_{mixing} = -R(n_1 \ln(X_1) + n_2 \ln(X_2)), \quad (12)$$

where  $n$  is the number of moles of the respective liquid 1 or 2 while  $X$  denotes the respective mole fractions. Flory's model includes following assumptions. First, the model assumes the polymer-solvent to have a quasi-solid lattice structure. Figure 25 shows that the total space for this model breaks up into lattice cells. The second assumption is that solvent molecules and repeated polymer units are equal in size and only one of either type is able to occupy a lattice cell at a time. The third assumption is that all lattice cells are occupied; there is no free volume. The fourth assumption is

that all polymer chains have the same length or in other words every polymer chain contains the same number of repeated base units. The last assumption deals with the assembly of the polymer chains within the lattice. Here every polymer repeated unit must have at least two nearest neighbors to make a proper linear polymer chain [63]. These assumptions result in an entropy change due to mixing per number of possible sites in the lattice. This relationship is

$$\frac{-\Delta S_m}{\# \text{ of sites}} = k_b \left( \frac{\Phi_p}{m_p} \ln(\Phi_p) + \frac{\Phi_s}{m_s} \ln(\Phi_s) \right), \quad (13)$$

where the  $\Phi_s$  is the volume fraction of the solvent and  $\Phi_p$  is of the polymer. The  $m_p$  is related to the total number of repeated base units that make up a polymer chain. While  $m_s$  is for the solvent and always set equal to one. These are shown in figure 23: solvent molecules as white units and a polymer base units as black units. One can see that the both volume fractions will be less or equal to one and that the summation of two volume fractions must be one. A consequence of this is that both  $\ln(\Phi_p)$  and  $\ln(\Phi_s)$  will be negative in eq. (13). The large  $m_p$  for the polymer term makes first term on the right-hand side small. This is because polymer chains have thousands or even millions of monomers on average, and thus  $m_p$  will be large. The second term on the right hand side is larger than the first one since  $m_s = 1$  for the solvent. The entropy change term is always negative as mixing increases the entropy of the system.

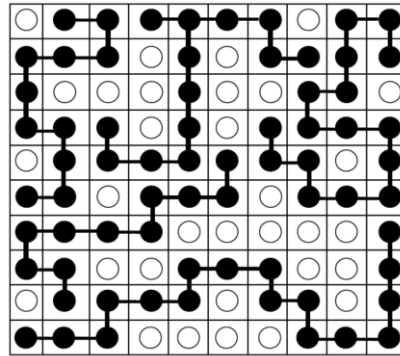


Figure 25 Lattice set up of the Flourey-Huggins. Here the dark units are the monomer segments that make up the polymer while the light units make up the solvent molecules. From: [65].

The entropy change will always be negative, but the enthalpy change from dissolution also plays a role. Flory [63] assumed that there are three types of nearest neighbor energy pair interactions that make up the enthalpy term. These three types are: polymer unit to polymer unit, polymer unit to solvent unit, and solvent unit to solvent unit. Each of these pair types has its own potential energy function. Only the first and the last type of pair interactions are present at the initial equilibrium state where the polymer and the solvent are fully separated from each other. All three types of interactions are possible in the end equilibrium state where the polymer and solvent are fully mixed.

By considering only nearest neighbor interactions, the interaction potential energy for equal pairs for the solvent (solvent to solvent) will be

$$z\epsilon_{SS}, \quad (14)$$

where  $\epsilon_{SS}$  is the potential energy for one pair of solvent molecules and  $z$  is the coordination number, or the total number of nearest neighbor solvent molecules to a single solvent molecule. During mixing, some of the solvent molecules will become nearest neighbors to polymer unit molecules. This will lead to a change in potential energy of the system. The change due to one pair of polymer solvent nearest neighbor interaction is given by

$$\Delta\epsilon_{PS} = \epsilon_{PS} - \frac{\epsilon_{SS} - \epsilon_{PP}}{2}. \quad (15)$$

This change is due the energy difference between a new solvent polymer unit nearest neighbor pair,  $\epsilon_{PS}$ , that replaces both a solvent to solvent neighbor pair,  $\epsilon_{SS}$ , and a polymer to polymer neighbor pair,  $\epsilon_{PP}$ . The division by two is needed since the change from one initial pair of both polymer to polymer and one solvent to solvent nearest neighbor interactions results into a final state of two pairs of polymer to solvent interactions. The change in total enthalpy of the system can be obtained by determining how many new nearest neighbor pairs of polymer to solvent interactions arise at the end equilibrium state. Thus, the change is

$$\Delta H_m = n_s \Phi_p z (\Delta \epsilon_{SP}). \quad (16)$$

Enthalpy change depends on the volume fraction of the polymer,  $\Phi_p$ , and on the total number of solvent molecules,  $n_s$ , but because not *all* polymer and solvent molecules will become polymer- to- solvent nearest neighbor pairs, Flory defined a parameter in the following way

$$\chi = \frac{z \Delta \epsilon_{PS}}{k_B T}, \quad (17)$$

where the denominator consists of Boltzmann's constant along with the temperature such that to make the parameter dimensionless. The parameter depends only on the material properties of the solvent and polymer. Hildebrand and Scatchard [66] came up with an additional relationship for the change of enthalpy due to mixing term  $\Delta H_m$  of eq. (16). The interaction energy for one solvent molecule will involve all nearest neighbor interactions to other solvent molecules. Models like the Lennard-Jones potential mathematically show both the attractive dispersion force and the repulsive Pauli force for a pair interaction involving the solvent molecule and one of its neighbors. A solvent molecule escapes all Lennard Jones potential wells when it moves very far away from all its neighbors. By using this argument, Hildebrand made this potential energy equal to the energy of vaporization for the solvent. The vaporization energy will account for the forces holding the solvent together at the liquid state. This energy of vaporization can be expressed as

$$-\Delta E_V = H_V - RT, \quad (18)$$

where  $H_V$  is the enthalpy (heat added),  $T$  is the temperature, and  $R$  is the ideal gas constant. One can express the energy of vaporization as a cohesive energy density term in the following way

$$C_{SS} = \frac{\Delta E_V}{V}, \quad (19)$$

where  $C_{SS}$  denotes the cohesive energy density for a solvent molecule interacting with another solvent molecule. The  $V$  terms is the volume of the solvent or polymer to turn eq. (19) into an energy density term. Accordingly,  $C_{ps}$  defines cohesive energy density for a polymer-solvent interaction and  $C_{pp}$  for a polymer-polymer interaction. Only some polymer molecules will end up

interacting with the solvent at the final state and the probability of this is proportional to the volume fractions of both the polymer and the solvent. This gives the change in enthalpy due to mixing as [25,66]

$$\Delta H_m = (n_s + n_p)V_m\Phi_s\Phi_p(2C_{ps} - C_{ss} - C_{pp}), \quad (20)$$

where, the  $n_s$  and  $n_p$  are the number of solvent and polymer units respectively, while  $V_m$  is the molar volume. Thus, the change in enthalpy is related to the total energy change due to changes in interaction types due to mixing. Prior to mixing, there are only two types of interactions: polymer to polymer and solvent to solvent ( $C_{ss}$  &  $C_{pp}$ ). After mixing there exists an additional type of interaction: polymer to solvent ( $C_{ps}$ ). To see how the enthalpy changed because of mixing, one only needs to account for how many new solvent polymer molecules nearest neighbor pairs arose from mixing. Since the total quantity of polymer and solvent molecules is constant, the new interaction type comes at the cost of the two old types. One polymer to polymer and one solvent to solvent nearest neighbor interaction can turn into two polymer to solvent interactions. The terms in parenthesis at eq. (20) does this.

Figure 26 represents this graphically. The left sub-image is the polymer chains and the solvent before any mixing. Here, the only present nearest neighbor interactions are polymer to polymer ( $C_{pp}$ ) marked as a blue box and solvent to solvent ( $C_{ss}$ ) marked as a red box. After mixing the new nearest neighbor interaction type regarding polymer and solvent ( $C_{ps}$ ) is also present and denoted as a green box. The red and blue boxes still exist after mixing but in lesser quantity than in prior to mixing state.

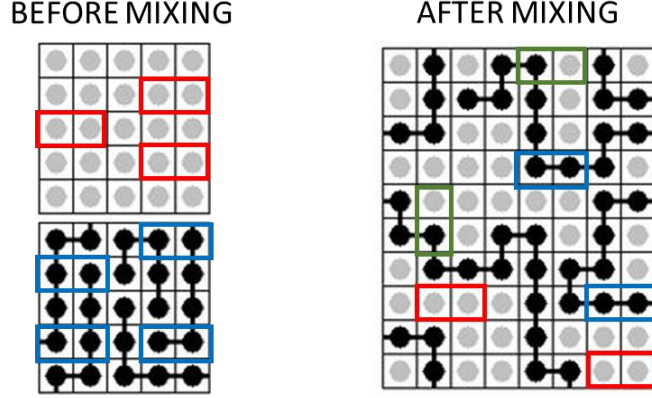


Figure 26: The polymer-solvent system before and after mixing. From: [65].

A fundamental problem exists in expressing  $C_{ps}$  in terms of  $C_{pp}$  and  $C_{ss}$ . Combination rules exist for doing so. Scatchard used the geometric mean between the pure polymer and pure solvent cohesive energy densities to obtain

$$C_{ps} = \sqrt{C_{pp}C_{ss}}. \quad (21)$$

The use of a geometric mean for this approach is strictly empirical based on the work of Galitzine [66]. Eq. (20) can be altered using eq. (21). The enthalpy change is now given as

$$\Delta H_m = (n_s + n_p)V_m\Phi_s\Phi_p(\delta_{ss} - \delta_{pp})^2, \quad (22)$$

where  $\delta_{ss} = \sqrt{C_{ss}}$  and  $\delta_{pp} = \sqrt{C_{pp}}$ . These two terms are called the Hildebrand solubility parameters for both the pure solvent and the pure polymer, respectively. All the derivations above allow one to finally get to relate the Flory parameter to a quantity that can be obtained experimentally: the heat of vaporization. The Flory parameter is now equal to

$$\chi = \frac{V_r}{RT}(\delta_{ss} - \delta_{pp})^2, \quad (23)$$

where  $V_r$  is the volume of a solvent molecule. A problem from this derivation is that it is almost impossible to get cohesive energy from the polymer vaporization energy. This is because a polymer often breaks down into simpler components as energy is added such that the polymer as a whole will not undergo vaporization intact. A method to solve this is to break down the polymer unit and

to look at the group contributions of all the components that make up a polymer unit, to determine the contributions of each functional group of the polymer unit individually and adds them up to get the total  $C_{pp}$ . These individual functional group contributions are available in the literature. [25].

Other methods also exist to obtain the Hildebrand solubility parameter. For example, one can use experimentally indirect methods such as viscosity measurement and ultraviolet-visible spectroscopy. Carvalho et al. [68] obtained the parameters of both unsulfonated and sulfonated polystyrene by using these two experimental methods. The parameters obtained by each method for each polymer were close and in agreement with other published results [68].

Executing one of the methods above allows one to fully solve for the enthalpy term. Now the Gibbs free energy change is

$$\Delta G_m = \Delta H_m - T\Delta S_m \Rightarrow \frac{\Delta G_m}{RT} = n_p \ln(\Phi_p) + n_s \ln(\Phi_s) + n_s \Phi_p \chi. \quad (24)$$

Eq. (23) shows that the Flory parameter term will always be positive because of  $(\delta_{ss} - \delta_{pp})^2$ . The change in entropy term is always negative but at the same time small. The Gibbs free energy change in eq. (24) must be negative for dissolution to occur. The Hildebrand solubility parameters of the pure polymer and solvent must be as close as possible to each other to make the Flory parameter small and thus dissolution thermodynamically possible. The Flory-Hildebrand model for polymer dissolution works well, but the model does have its limitations. The limitations are as follows [25]:

1. The model ignores free volume (all spaces in the lattice are filled)
2. The model assumes that the polymer chains undergo random mixing for computing entropy and uses segment approach for computing enthalpy
3. The model uses a lattice model which itself is an approximation for computing the free energy
4. The model works only for nonpolar polymers and solvents

The last limitation is the most unsettling one. The derivation given by Hildebrand for relating cohesive energy to the energy of vaporization is scientifically correct. The drawback of Hildebrand's method is that the underlying assumption is that all the interaction types are grouped

together with the energy of vaporization to end up with a single parameter:  $C$  or  $\delta$  [67]. A single parameter is easier to deal with, but does not account for the individual contributions from each type of cohesion force. The preceding Flory-Hildebrand dissolution model described above correctly predicts dissolution between nonpolar materials such as those used in the lacquer industry. But further experimental testing showed failure to predict solubility in compounds that were known to have either polar or Hydrogen bonds [69]. PVA is a polymer with high polarity and the Flory-Hildebrand model cannot account for its dissolution [67, 69]. Hansen et al. [69] solved this problem by introducing the Hansen Solubility Parameter (HSP). Hansen realized that during vaporization three different types of bonds could break. This meant that one must account for the cohesion energy contribution of each bond type individually to come up with more accurate results. The Hansen model expands Hildebrandt's single cohesive energy term into three main parts.

The first part is the dispersion energy which arises from the atomic dispersion forces between atoms. This force comes from randomly, temporarily induced dipoles between molecules and is the London dispersion interaction. The second one considers the polar effect and includes the energy between the interactions of permanent dipoles known as the Keesom interaction. This term also accounts for when a molecule's permanent dipole induces a temporary dipole in another molecule- the Debye interaction. The last term is the hydrogen force which occurs when a hydrogen atom in a molecule strongly attracts electrons located in other molecules and thus forms a protonic bridge between molecules. The hydrogen bond is the strongest among these three terms [67]. The energy of vaporization of eq. (18) is expanded. This gives the equivalence as

$$-(H_V - RT) = E_V = E_D + E_P + E_H, \quad (25)$$

where  $E_D$  is the dispersion energy term,  $E_P$  is the polar energy term, and  $E_H$  is the energy from hydrogen bonds. Eq. (25) is similar to eq. (18), but now the three types of bond interaction

energies are considered. Similarly, Hansen expanded Hildebrand's single solubility parameter [70]. This expansion is expressed as

$$\frac{E_V}{V} = \frac{E_D}{V} + \frac{E_P}{V} + \frac{E_H}{V} = \delta^2 = \delta_D^2 + \delta_P^2 + \delta_H^2, \quad (26)$$

where  $\delta_D$  is the dispersion parameter,  $\delta_P$  the polar parameter, and  $\delta_H$  the hydrogen parameter. Hansen's derivation resulted in three independent parameters for each pure solvent or polymer. These three parameters make up the so-called Hansen solubility parameters (HSPs). A solvent can be plotted out in three dimensional space where each HSP serves as an axis. In his thesis, Hansen plotted out various solvents this way. He also experimentally determined whether each solvent did or did not dissolve a specific polymer. Plotting the solvents out in the HSP space and determining whether or not each one dissolved a specific polymer resulted in spherical volume in the 3-d space demarked by the location of various solvents. In figure 27, Hansen plotted out various solvents and tested whether each solvent was capable of dissolving cellulose nitrate. Using the solvent as data-points, Hansen came up with the spherical volume for cellulose nitrate. The results allowed one to determine whether or not a new solvent will or will not dissolve cellulose nitrate. Here one just obtains the HSP for the solvent in question and plots it. If the coordinates fall inside the spherical volume, the solvent can dissolve cellulose nitrate [70].

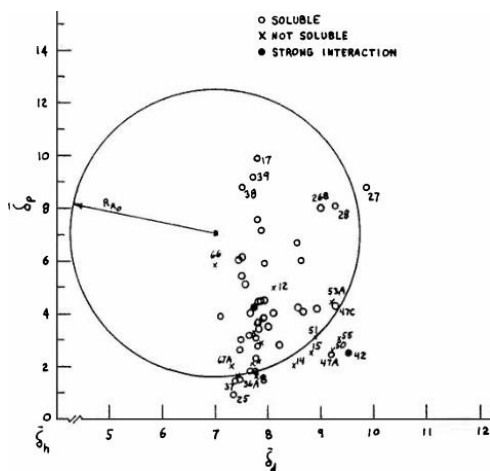


Figure 23 Plotting of various solvent and stating on whether or not these solvents will dissolve cellulose nitrate. The volume is spherical and plotted out by the radius. From: [67].

Building on this work, Hansen derived a graphical relationship between the HSPs of a solvent and those of a polymer [71]. This relationship is given by the equation

$$(R_a)^2 = 4(\delta_{DP} - \delta_{DS})^2 + (\delta_{PP} - \delta_{PS})^2 + (\delta_{HP} - \delta_{HS})^2, \quad (27)$$

where the second subscript in  $\delta$  defines whether the HSP term belongs to the polymer or the solvent; e.g.  $\delta_{HP}$  is the hydrogen bond energy belonging to the polymer.  $R_a$  determines whether a polymer-solvent combination will either mix and dissolve or remain as separate phases. Hansen also introduced the Relative Energy Difference (RED). This parameter must be less than one for solubility to be possible and thus mixing to happen. Thus dissolution occurs when

$$RED = \frac{R_a}{R_O} < 1, \quad (28)$$

where  $R_O$  can be determined experimentally similarly to what shown in figure 27 and serves as the limit. What  $R_a$  does is plots various points in 3D space while  $R_O$  plots a spherical surface area in this space for a polymer. The HSPs of the polymer serve as the center of the spherical surface. Solubility is possible if  $R_a$  falls inside the surface area defined by  $R_O$ . Each polymer to solvent interaction will have its own respective  $R_a$ . Two of these are shown in figure 28 as a blue pyramid and as a red cube. The blue pyramid in the illustration falls within the spherical area and thus this

system will undergo dissolution. The red cube is outside the spherical surface area and thus this solvent polymer pair will not dissolve.

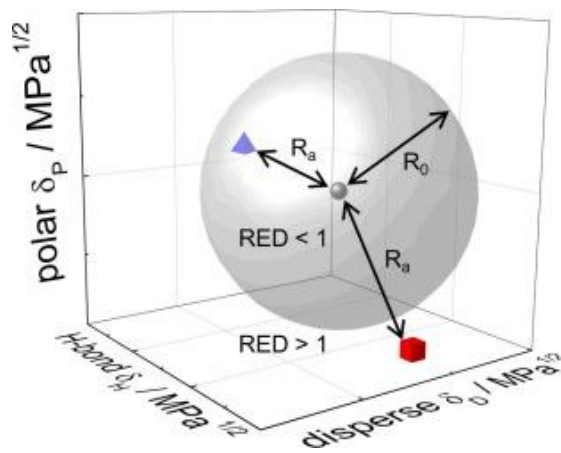


Figure 24 The Hansen Sphere. Any material that lies within the gray sphere surface will undergo dissolution. From: [74].

There are of course deviations from Hansen's model. One good example is the relative size of the solvent molecule to the solute unit molecule. A system where the solute unit molecule is relatively large to the solvent molecule is still capable of undergoing solubility, even if RED of the system is slightly greater than one. For the opposite case solubility will not happen, even if the system's RED is slightly smaller than one [72]. Never the less, the Hansen approach can deal with polar and hydrogen bonds and has widespread usage in its 50-year history in both research and industry. The HSPs for over 9,000 chemicals of various types have been computed by Hansen himself. Many industries have their own proprietary databases of HSPs [73].

## Review of Kinematic Polymer Dissolution Models

The methods developed by Flory, Hildebrand, Scatchard, and Hansen can predict whether a polymer will or will not undergo dissolution within a solvent. Such models can explain if a polymer/liquid pair will go from the initial undissolved equilibrium state to the final dissolved equilibrium state by using thermodynamics and empirical data. But these methods cannot

characterize or give an in-depth insight into the mechanism of polymer dissolution. To overcome this limitation, various models dealing with the kinematics of polymer dissolution have been developed. These are the kinetic models intended to describe the complete polymer dissolution process.

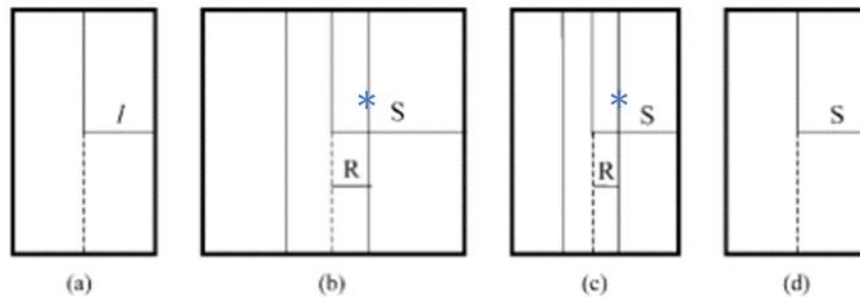


Figure 25 The main steps of polymer dissolution: (a) shows the original bulk polymer before any dissolution occurs; (b) shows the polymer swelling as solvent had penetrated in; (c) is after enough elapsed time such that single polymer chains leave the bulk. From [15].

Figure 29 shows the dissolution of bulk polymer after being immersed in a compatible solvent. The bulk polymer is an initially glassy block of length  $2L$  with solvent on both the right and left sides of the bold lines. The problem is symmetric and has mirror condition on either side of the center dotted line. In the first step, the bulk polymer undergoes swelling as the solvent diffuses into the polymer ('b' in figure 29). Here the bulk polymer increases in size due to this swelling. Moreover, there will be no initial diffusion of polymer chains from the bulk polymer into the solvent. Local regions of the bulk polymer change from a glassy to a rubbery/gel state. Subfigure 'b' of figure 29 shows this; The 'R' region is still glassy while the 'S - R' region is rubbery. This local transition happens because the solvent behaves as a plasticizer and thus lowers the  $T_g$  of local polymer regions to the operating temperature. The total quantity of polymer within the bulk polymer remains the same and does not change during this initial step. The second time step involves the diffusion of single, loose polymer chains from the bulk polymer into the solvent ('c & d' in figure 29). Polymer chains take a finite amount of time to fully

disentangle from the bulk polymer. Once untangled, polymer chains diffuse out of the bulk polymer. Chains leaving cause the total polymer quantity within the bulk polymer to decrease along with a decrease in overall size. Comparing ‘b’ with respect to ‘c’ shows that the latter is smaller in size due to polymer chain diffusion. Solvent keeps diffusing into the polymer and induces local state transition and further swelling. This process continues until the all the bulk polymer becomes loose in the solvent or a thermodynamic equilibrium is reached between the bulk polymer and the polymer chains in the solvent [16]. Figure 29d shows this equilibrium and at the same time that all the remaining polymer is rubbery. There are various models and each uses different types of governing equations to characterize the dissolution behavior.

Tu and Olano [75] designed one of the earlier mathematical polymer dissolution models. They built a one-dimensional, phenomenological model to describe the observed polymer dissolution kinematics, including three main events. The first event being the diffusion of solvent into the bulk polymer; the second event being the diffusion of polymer chains from the bulk polymer into the bulk solvent, and the final event describes the mechanics of the interface dividing the bulk polymer and the solvent. This interface is also where the bulk solvent and the bulk polymer are in contact with each other. The model divides the polymer-solvent system into three main regions. Each region has its own set of governing equations and conditions.

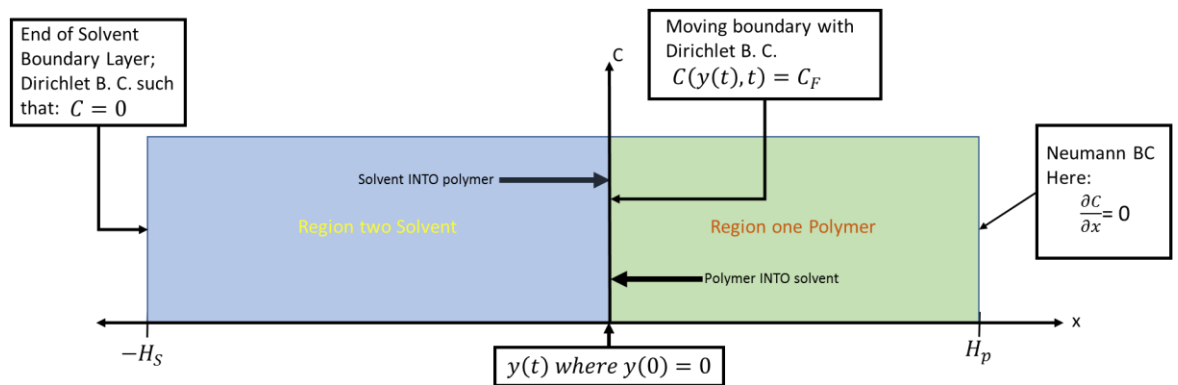


Figure 26 The three main regions for Tu & Olano's set-up at initial time

Region one in figure 28 is the bulk polymer. The solvent penetrates into the bulk polymer, causing the bulk polymer to swell. At the same time, polymer chains leave the bulk polymer and diffuse into the solvent. The bulk polymer gradually undergoes dissolution and dissolves. Tu and Olano used a nonlinear Fickian transport equation as the governing equation for this region. This governing equation is

$$\frac{\partial C_p}{\partial t} = \frac{\partial}{\partial x} \left( \frac{\partial C_p}{\partial x} C_p D_s \right), \quad (29)$$

where  $C_p$  is the volume fraction of polymer at a given location and  $D_s$  is the local diffusivity coefficient. The bulk polymer region uses mass-conservation relationships to calculate how much polymer volume fraction is present at any location within region one. Since eq. (32) is a partial differential equation, it has two boundary conditions and one initial condition. The boundary conditions are as follow:

$$\frac{\partial C_p}{\partial x} = 0 \text{ at } X = H_p \quad (30)$$

and

$$C_p = C_F(y(t), t) \text{ at } X = y(t). \quad (31)$$

$C_F$  of eq. (31) is the polymer volume fraction at the interface where the solvent and polymer meet. Region one has two boundary conditions; one for each end. The  $H_p$  boundary of the polymer region is fixed in space and no solvent or polymer flux through is possible as in eq. (30). This is similar to a Neumann Boundary Condition for the classical heat problem. The other space boundary at  $(y(t), t)$  in figure 30 is a moving boundary and thus the boundary position changes with respect to time. The moving boundary is of the Dirichlet type, having a fixed polymer volume fraction here ( $C_F$ ). This moving boundary allows the characterization of both the swelling and the eventually dissolution of the bulk polymer. Eq. (31) expresses this moving boundary. For Region one, the moving boundary allows the region to change in size, so eq. (29)

governs different spatial domains at different times. Initially, Region one is between  $x = 0$  and  $x = H_p$ . Region one is pure polymer at the very beginning. These two statements can be expressed as

$$C_p(x, t = 0) = 1 \quad \text{for } x = 0 \text{ to } x = H_p, \quad (32)$$

where a polymer volume fraction of one is equivalent to pure polymer.

Region two in figure 28 is the solvent region. The authors assumed that there will be a stable ‘boundary layer’ for polymer chains to exist within the solvent. No polymer is present beyond this boundary layer as the solvent flow will carry away any loose polymer chains. Tu and Olano derived a governing equation for the solvent boundary layer. Doing a mass conservation scheme results in the equation

$$\frac{\partial C_p}{\partial t} + \frac{dy}{dt} \frac{\partial C_p}{\partial x} = \frac{\partial}{\partial x} \left( \frac{\partial C_p}{\partial x} C_p D_p \right), \quad (33)$$

where  $D_p$  is the local diffusivity at a location in region two and  $\frac{dy}{dt}$  is the velocity of the moving boundary at the given time. Finally  $C_p$  is the polymer volume fraction at any location within region two. Solving eq. (33) will give the polymer volume fraction anywhere within Region two. Eq. (32) will also have two boundaries and one initial conditions. The boundary conditions of eq. (33) are as follows:

$$C_p = C_F(y(t), t) \text{ at } X = y(t) \quad (34)$$

and

$$C_p = 0 \text{ at } X = y(t) - H_S. \quad (35)$$

This solvent boundary layer region has two spatial ends. The far-left end of figure 28 shows the end of the boundary layer at  $-H_S$  where no polymer is present- a Dirichlet Boundary Condition having a polymer volume fraction of zero. The end of the boundary layer can move, but will remain a constant distance of  $H_S$  to the left of the other spatial boundary. Eq. (35) expresses the

other spatial boundary. The other spatial end is at  $y(t)$  and connects Region two to Region one: the bulk polymer. This boundary is the same as Region one's moving boundary of eq. (31). Like in Region one, the domain of Region two varies due to the moving boundary conditions. Moreover, Region the domain is  $x = 0$  and  $x = -H_s$  and is pure solvent at the beginning of the problem. These two statements can be expressed as

$$C(x, t = 0)_p = 0 \quad \text{for } x = -H_s \text{ to } x = 0. \quad (36)$$

Eq. (36) states that at the beginning of the problem, no polymer is present within the boundary layer. This will of course change as the polymer undergoes dissolution.

The last region is not a true region, but rather a condition to make the problem solvable. This condition deals with the moving boundary  $y(t)$  that connects Regions one and two. Since both Regions one and two have spatial boundaries at  $y(t)$ , this condition also determines the respective domain of each region. Tu and Olano expressed the condition as

$$\frac{dy}{dt} = -D_s \frac{\partial C_p}{\partial x}_{\text{polymer side}} + D_p \frac{\partial C_p}{\partial x}_{\text{solvent side}}, \quad (37)$$

where  $dy/dt$  is the velocity of the moving boundary and  $\frac{\partial C_p}{\partial x}$  is the polymer volume fraction gradient for both Regions adjacent to the moving boundary. Eq. (37) expresses the condition of the moving boundary mathematically. This governing equation accounts for two events at this polymer/solvent interface. The first term on the right hand side accounts for solvent penetrating into the bulk polymer region. The transport here is diffusion. The second term on the right hand side accounts for polymer chains leaving the bulk polymer into the solution. The transport mechanism here is also diffusion. The second term also states an interesting condition set by Tu et al. Here, polymer chains diffuse out of the bulk polymer into the solvent *immediately*. There is no time delay to allow for polymer chains disentangle from the bulk polymer first. Eq. (37) mathematically enables the bulk polymer to undergo dissolution with a compatible solvent. figure 30 shows the last region along with the polymer and solvent flows described by arrows. The

moving boundary is also present and set as  $y(t = 0) = 0$  at the start of the problem. Eq. (37) shows that polymer leaving the solvent will cause the boundary to move toward the right in figure 28 and 29 (bulk polymer shrinks), while solvent penetrating into the bulk polymer will cause the boundary to move to the left (bulk polymer swells). This results in two opposite competing mechanisms that govern how region three moves as the problem develops with respect to time.

Tu and Olano came up with an analytical solution for their system by using the method of similarities, non-dimensionalization, and reasonable assumptions to solve eqs. (29), (33), & (37) simultaneously. The valid range of the analytical solution was only for small times because of the assumptions used. Further work resulted in a numerical scheme that used finite difference methods. The numerical scheme corroborated the analytical solution and allowed to solve the system's evolution for further times.

Figure 31 shows the numerical solution of the polymer-solvent system at various time steps. This figure shows various curves having polymer volume fractions at increasing time increments labeled from 1 to 10. The 'y' axis shows the polymer volume fraction, with 1 being equal to any location being 100% polymer. Every space in the x axis is assigned a polymer concentration and the governing equations solve for it. The volume fraction of region 3 that connects the bulk polymer with the solvent boundary layer is kept as 0.25 throughout the whole problem, as per eq. (31). The location of the polymer-solvent boundary at each time increment is marked as a blue dot in figure 31. The bulk polymer region is on the right of the blue dot, while the solvent boundary layer is on the left of the blue dot for a given curve. The initial polymer-solvent boundary is at the  $x = 0$  axis for the initial time curve labeled as '1'. One can see how the solution develops by tracking the movement of the blue dot in the horizontal axis. The polymer swells initially and the blue dot moves into the negative x values. A decrease in volume fraction within the polymer shows both the solvent penetrating and polymer chains leaving the bulk polymer. Polymer chains are also present within the solvent boundary layer as there are non-

zero values to the left of the blue dot. At the polymer volume fraction curves beyond time increment three, the bulk polymer region recedes and there is a decreasing overall polymer volume fraction within the bulk polymer. This shows that at further time steps the bulk polymer undergoes dissolution.

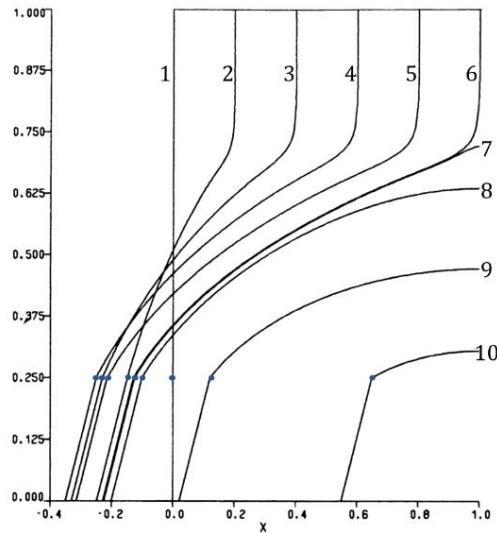


Figure 27 Tu & Olano's bulk polymer dissolution solution development with respect to time. The blue dots mark the polymer-solvent boundaries at each time increment. Each curve is also labeled with increasing time increments. The initial polymer volume fraction curve is the curve #1. From: [75].

There are other models built upon Tu and Olano's work. Devotta et al. [76] developed a polymer dissolution model for small polymer pellets having a spherical geometry. They also used two polymer-solvent systems of Polymethyl methacrylate immersed in Benzene and Polystyrene immersed in Cyclohexane to obtain experimental results for comparison. Devotta et al. additionally varied the molecular weight within each polymer-solvent system to compare with experimental results. The set-up consists of a polymer sphere submerged in a compatible solvent. Their approach can be explained with following three figures. Figure 32 shows the spherical coordinate system. Spherical coordinates are convenient for systems that are spherical or spherical-like. There are three parameters to determine a location.  $\rho$  is for the radial magnitude, while  $\varphi$  &  $\theta$  denote the angles to orient  $\rho$  with respect to the z-axis and within x-y plane respectively.

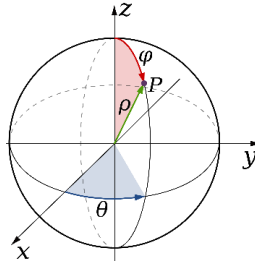


Figure 28 The spherical coordinate system. The polymer pellet will be defined by these coordinates, but the symmetry allows one to ignore the angles of theta and phi. From: [77].

Figure 33 shows the Polymer-Solvent system under spherical coordinates. The center of the pellet is at the origin of the coordinates and the pellet has a symmetric radius that can change with respect to time,  $R(t)$ . The polymer sphere has a radius of  $R(t)$ , and outside the boundary is solvent. Due to symmetry, Devotta et al. solved the problem along the radial direction with respect to time.

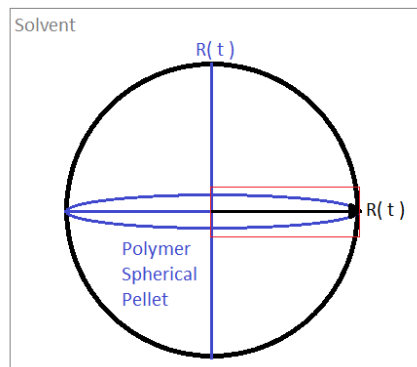


Figure 29 Showing Devotta et al problem set up. Here spherical pellet is immersed within a solvent. The red box emphasizes the 1-d simplification due to symmetry

Figure 34 shows the one-dimensional simplification of figure 31. One only solves the governing equation for the radial direction of the spherical coordinates and for the time dimension.

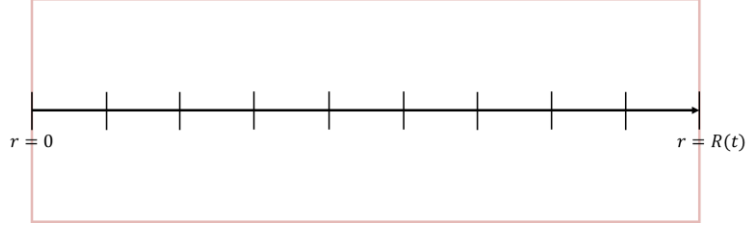


Figure 30 Boundary conditions set up based on figure above. Left end is Neumann BC and fixed while right end is Dirichlet BC and allowed to move with regards to space.

While the problem simplifies a one dimensional problem in the spherical coordinates, the governing equation should also be derived in the according coordinates. Devotta et al. Carried out the nonlinear Fickian Diffusion equation for spherical coordinates along the radial  $\rho$  axis. Doing so gave the governing equation of

$$\frac{\partial \varphi_s}{\partial t} = \frac{1}{r^2} \frac{\partial}{\partial r} \left( r^2 D_s \frac{\partial \varphi_s}{\partial r} \right) - \frac{1}{r} \frac{\partial}{\partial r} \left( r \varphi_s D_s \frac{\partial \varphi_s}{\partial r} \right), \quad (38)$$

where  $\varphi_s$  is the volume fraction of the solvent,  $D_s$  is the diffusion coefficient of the solvent, and  $r$  is any spatial location within the ‘box’ of figure 34. Since Eq. (38) is a partial differential equation, there is an initial condition and two boundary conditions. At the start of the problem, one assumes that the figure 32 ‘box’ is pure polymer and the domain at the start is from  $r = 0$  to  $r = R(t = 0)$ . These two statements can be expressed as

$$\varphi_s(r, t = 0) = 0 \text{ for } r = 0 \text{ to } r = R(t = 0), \quad (39)$$

where a solvent volume fraction equal to zero implies that there is pure polymer. Eq. (38) has the following boundary conditions:

$$\frac{\partial \varphi_s}{\partial r} = 0 \quad \text{at } r = 0 \quad \text{for all times} \quad (40)$$

and

$$\varphi_s = \varphi_{si} \quad \text{at } r = R(t) \quad \text{for all times.} \quad (41)$$

The left boundary on figure 34 is fixed in space at  $r = 0$  and no flux is allowed (eq. (40)); a Neumann boundary condition. The other boundary has a fixed solvent volume fraction quantity (eq. (41))- a Dirichlet boundary condition. This boundary can also move meaning that its location varies with respect to time as  $R(t)$ . This boundary behaves similarly to the  $y(t)$  moving boundary in Tu & Olano's preceding paper.

The moving boundary first expands and eventually recedes during the polymer dissolution simulation. The solvent volume fraction at this end is also kept constant as in eq. (41). How this boundary moves depends on two variables: the influx of solvent into the bulk polymer sphere and the dissolution of loose polymer chains into the bulk solvent. The influx of solvent causes both the polymer to swell and for  $R(t)$  to increase in size. The dissolution of loose polymer chains causes the bulk polymer to degrade and for  $R(t)$  to decrease in size. The velocity of the moving boundary is expressed as

$$\frac{dR}{dt} = \left( D_s \frac{\partial \varphi_s}{\partial r} \right)_{R_-(t)} - \left( \frac{D_p}{\varphi_{pi}} \frac{\partial \varphi_p}{\partial r} \right)_{R_+(t)}, \quad (42)$$

where  $\frac{dR}{dt}$  is the velocity of the moving boundary  $R(t)$  at any instant,  $\frac{\partial \varphi_s}{\partial r}$  is the solvent volume fraction within the polymer pellet adjacent to  $R(t)$ ,  $\frac{\partial \varphi_p}{\partial r}$  is the polymer volume fraction gradient in the solvent adjacent to  $R(t)$ , and  $\varphi_{pi}$  is the polymer volume fraction at the moving boundary  $R(t)$ . Lastly,  $\varphi_p$  is the polymer volume fraction on the solvent side of the polymer-solvent boundary denoted as  $R_+(t)$ . The polymer and solvent volume fractions at any location in the following way: the sum of both these fractions must be equal to one everywhere, since only polymer or solvent can exist within this system. This statement can be expressed as

$$\varphi_{pi} + \varphi_{si} = 1. \quad (43)$$

Eq. (43) shows this relationship for both obtaining the polymer or solvent volume fraction if one is known at any location. The second term on the right hand side of eq. (42) will be zero if the system's time is less than a characteristic time. Polymer chains need certain time to disentangle from the bulk polymer. Devotta et al. assumed this time to be equal to the reptation time of polymer,  $t_{rep}$ . This statement is expressed as

$$-D_p \frac{\partial \varphi_p}{\partial r} = 0 \text{ for } 0 < t < t_{rep} \text{ at } r = R_+(t). \quad (44)$$

Eq. (44) shows an additional feature not present in the work of Tu et al. While the governing equations for both systems are similar (see eq. (37) vs eq. (42)), Tu et al. assumed that polymer chain diffusion happened immediately. Devotta's model assumes that this phenomenon is not immediate. There are two possible cases for the second term of eq. (42) when the system's time reaches the reptation time. The first case is such that the diffusion rate will be high enough to transport the disentangled polymer chains from the bulk polymer into the bulk solvent. Thus, the rate of loose polymer chains sent to the solvent region will equal the rate of polymer chains that become disentangled. This can be stated as

$$-D_p \frac{\partial \varphi_p}{\partial r} = k_d \varphi_{pi} \text{ for } t \geq t_{rep} \text{ \& } \varphi_p < \varphi_{pi} \text{ at } r = R_+(t), \quad (45)$$

where the variable  $k_d$  here is the disentanglement rate. While  $\varphi_{pi}$  is the polymer volume fraction at the interphase  $R(t)$ . The polymer volume fraction at the solvent side of the boundary  $R_+(t)$  in eq. (42) increases as loose polymer chains travel into the solvent region. Eq. (45) is valid as long as the polymer volume fraction on the solvent side of the boundary,  $\varphi_p$  at  $R(t)_+$ , is below the polymer fraction at the interphase  $R(t)$ ,  $\varphi_{pi}$ . When these volume fractions are equal or greater, there will be no polymer concentration gradient at  $R(t)$  such that diffusion can transport the loose polymer chains into the solvent region. A new mechanism governs the process: resistance to mass transfer within the solvent, which can be mathematically described as

$$-D_p \frac{\partial \varphi_p}{\partial r} = k_l(\varphi_{pi} - \varphi_{p,b}) \text{ for } t > t_{rep} \text{ \& } \varphi_{pi} \leq \varphi_p \text{ } r = R_+(t), \quad (46)$$

where the parameter  $k_l$  is the mass transfer coefficient of the liquid. While  $\varphi_{p,b}$  is the polymer volume fraction within the bulk solvent. As a final note,  $k_l$  is dynamic and its quantity depends on the size of the polymer pellet.  $k_l$  increases in magnitude as the pellet decreases in size ( $R(t)$  becomes smaller). This change can cause  $\varphi_p$  at  $R(t)_+$  to eventually become less than  $\varphi_{pi}$  at  $R(t)_-$  and thus the condition returns to being disentanglement limited and eq. (45) governs the mechanism again. Thus, either eq. (45) or eq. (46) governs polymer diffusion at times larger than the reptation time. The one of these two with the smallest magnitude will be the one used in eq. (42).

Devotta et al solved eqs. (38) & (42) by first non-dimensionalizing them. A Finite Difference Scheme using the Crank-Nicolson method was then applied. They also put various polymer pellets within the respective compatible solvents in thermally regulated containers to experimentally measure the polymer dissolution. In experiments, a magnetic stirrer kept the pellets from aggregating and sticking to each other. Figure 35 shows both the numerical and experimental results for total dissolution time with respect to the size of the pellet for three different polymer-solvent systems. The curves show the numerical solutions while the experimental results are in data points. Both the numerical models and the experimental results showed the following:

1. The total time for complete dissolution decreased with respect to size up to a point. Pellets smaller than a cut-off size had the same dissolution time and thus flattened out.
2. The total time for complete dissolution decreases with lower molecular weights (how long the polymer chains are in average), but there is a critical molecular weight such that the dissolution time flattens out when below it.
3. When stirred, higher stirring speeds aided in lowering the dissolution time, but below a certain pellet size higher stirring speeds had no or at most minimal influence.

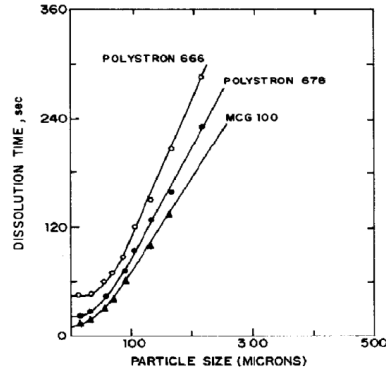


Figure 31 Results from Devotta et al showing simulation vs experimental results for polystyrene pellets submerged in cyclohexane. Both model and data show how decreasing sizes decreases dissolution time up to a point until it flattens out. From: [76].

One final model discussed here comes from the work of Wu et al [17,18]. The group introduced a more in-depth one-dimensional polymer dissolution model. It includes two main mechanisms: polymer dissolution and solvent penetration into the bulk polymer. This model is also one dimensional and the spatial set-up is shown in figure 36. This model used spatial coordinates for the un-deformed bulk polymer throughout the whole simulation. Unlike the previous other two models that had both a moving boundary condition and governing equation assigned to the moving boundary condition, here in figure 36,  $X$  is the spatial coordinate for the *un-deformed* bulk polymer without any stretching due to swelling. Wu et al. used two interesting alternatives to account for the swelling and the dissolution of the bulk polymer. The group's work is made of two parts. The first part involves building a mathematical model to characterize a polymer undergoing dissolution within a compatible solvent. A numerical finite scheme was developed to solve this mathematical model. Then they did polymer dissolution experiments to corroborate both the models and the numerical solver.

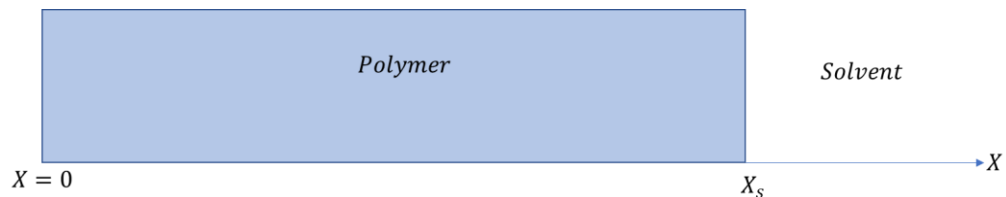


Figure 32 Polymer-solvent system of Peppas & Wu.

The bulk polymer region has a Fickian governing equation like in the previous models. There is also one additional term to deal with non-Fickian phenomena. Wu et al. derivation resulted in

$$\frac{\partial C_s}{\partial t} = \frac{\partial}{\partial x} \left( D_{12} \frac{\partial C_s}{\partial x} \right) + \frac{\partial}{\partial x} \left( \frac{D_{12} \bar{V}_1 C_s}{RT(1 - C_s)(1 - 2\chi C_s)} \frac{\partial \sigma_{xx}}{\partial t} \right), \quad (47)$$

where  $C_s$  is the solvent volume fraction,  $D_{12}$  is the mutual diffusion coefficient,  $\bar{V}_1$  is the molar volume of the solvent,  $\sigma_{xx}$  is the stress along the  $X$  coordinate system,  $R$  is the ideal gas constant, and finally  $T$  is the temperature. The parameter  $\chi$  is the same Flory parameter defined in eq. (17). Eq. (47) solves for the solvent volume fraction at any location within the bulk polymer at any time. The first term on the right hand side is the conventional Fickian term while the other is a non-Fickian term. This non-Fickian term comes from the work of Thomas and Windle. This term accounts for the observation of a large front having a large change in solvent volume fraction within the bulk polymer during the dissolution process. This front separates the swollen vs unswollen regions within the bulk polymer. The front is also the boundary between the glassy and the rubbery regions within the bulk polymer figure 29 shows this front marked as a blue asterisk during the polymer dissolution steps. At further times, this front moves deeper into the polymer to show that a larger portion of the bulk polymer has a high solvent volume fraction and different material properties [79]. Initially some solvent penetrates beyond the front, but the neighboring glassy region offers resistance against the solvent penetration and keeps the local polymer from swelling. This mechanism generates a force counter to the moving front. The stress that causes the front element to swell is the component of the hydrostatic swelling stress that is normal to the front element plane. Thomas et al. [78] related this stress to the viscoelasticity and creep properties of the polymer. The Maxwell model gives a mechanical analog to the polymer as a spring dashpot system to describe a polymer's mechanical behavior. This analog system can represent the viscoelastic dynamical mechanical behavior of the polymer. Durning [81] related the Maxwell viscoelastic model with respect to the work of Thomas and Windle to come up with an additional governing equation for the polymer region. This equation can be expressed as

$$\frac{\partial \sigma_{xx}}{\partial t} = \frac{-\sigma_{xx}}{\left(\frac{\eta}{E}\right)} + \frac{E}{(1 - C_s)^2} \frac{\partial C_s}{\partial t}, \quad 48$$

where  $\eta$  represent the polymer viscosity and  $E$  represents the polymer elasticity for the Maxwell spring-dashpot model in figure 37. Eq. (48) solves for the stress distribution that arises from solvent penetration within the bulk polymer.

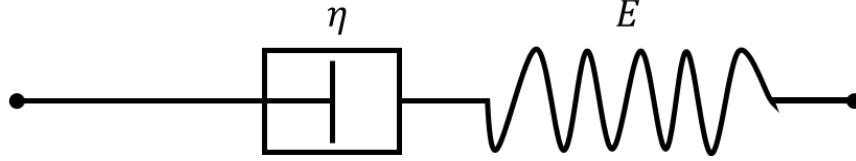


Figure 33 Maxwell model analog. The viscoelastic behavior of a polymer can be represented with this spring-dashpot arrangement.

Thus the system has two governing equations (47) & (48) now, and both have boundary and initial conditions that are defined in the following ways.

Eq. (47) describes the solvent volume fraction within the bulk polymer and has two boundary conditions. Thus, the boundary conditions for eq. (47) are as follow:

$$\frac{\partial C_s}{\partial X} = 0 \text{ when } X = 0 \text{ at any time} \quad (49)$$

and

$$C_s = C_{eq} \text{ when } X = X_S \text{ at any time.} \quad (50)$$

Where  $C_{eq}$  is the equilibrium solvent volume fraction at the polymer-solvent interface. Eq. (49)'s boundary condition is at  $X = 0$  and is of the Neumann type, meaning that no polymer or solvent flux is possible at this point. The second boundary condition is for the polymer-solvent interface. Here there is a constant polymer volume fraction and thus is a Dirichlet condition (eq. (50)).

Since  $X$  is the coordinate system for the original un-deformed bulk polymer this boundary is now fixed instead of moving like the previous two models. Eq. (47) also needs an initial condition. At

the very start of the problem, the bulk polymer is pure polymer meaning that no solvent is present at any location. This can be expressed as

$$C_s = 0 \text{ for all } X \text{ when time} = 0, \quad (51)$$

where a  $C_s$  equal to zero implies pure polymer composition.

Equation 48 solves for the stress distribution for the whole bulk polymer. Thus the spatial domain of this equation is the same as for eq. (47): the whole bulk polymer. Like the previous governing equation, this equation also has two boundary condition at the same spatial ends. Thus, the two boundary conditions are as follow:

$$\frac{\partial \sigma_{XX}}{\partial X} = 0 \text{ when } X = 0 \text{ at any time} \quad (52)$$

and

$$\sigma_{XX} = 0 \text{ when } X = X_s \text{ at any time.} \quad (53)$$

For the left end of the bulk polymer at  $X = 0$  there is a zero stress gradient and thus a Neumann boundary condition as in eq.(52). The other spatial end where the polymer meets the solvent is a free end and thus the stress here must be zero. This results in a Dirichlet boundary condition as shown in eq. (53). Wu et al. assumed that there are no residual stresses of any kind within the bulk polymer. Thus at the start of the problem, the whole polymer is stress-free. This statement mathematically translates as

$$\sigma_{XX} = 0 \text{ for all } X \text{ when time} = 0, \quad (54)$$

and thus is an initial condition for eq. (48).

All of the equations so far are for the bulk polymer system in a undeformed coordinate system. Instead of using moving boundaries, the group used the stress-strain relationship to characterize the swelling of the polymer. This method is valid since the solvent penetration causes both the polymer to swell and induces local stresses within the polymer. The local stress

field depends on the solvent volume fraction along with the polymer's viscoelastic properties. Thus it is possible to introduce a coordinate transform in the  $x$ -axis to solve for the local deformations of the bulk polymer everywhere. Doing this gives the following relationship

$$dx = (1 + \epsilon_{xx})dX, \quad (55)$$

where  $X$  is the original un-deformed bulk polymer coordinate system,  $\epsilon_{xx}$  is the local strain at a location within the polymer and  $x$  is the deformed coordinate system. One transforms the governing equations by replacing  $dX$  in eqs. (48) & (47) with  $dx$  with help of eq. (55). Solving the transformed governing equations results in the deformed bulk polymer from swelling. This methodology allows one to characterize the swelling of the polymer without having to resort to the previous methods.

Wu & Peppas' paper also gave a derivation on how to obtain the value of the solvent volume fraction at the polymer-solvent interface,  $X_S$  per eq. (50). The authors of the two preceding works did not give an argument on how to obtain this quantity. But they did state that the solvent volume fraction is constant. Wu and Peppas used the change of chemical potential and thermodynamics. This derivation depends on assuming that the physical polymer chain entanglements temporarily behave as chemical crosslinks. This assumption has merit as it takes a finite amount of time for entangled polymer chains to reptate and disentangle from the bulk polymer. Doing so allows one to apply the Flory-Rehner theory at the thin polymer sheet that is in contact with the solvent. This sheet is the thin polymer layer at  $X_S$  of figure 36 [81].

The Flory-Rehner theory states that two events change the sheet-solvent system's free energy during the mixing of a chemically cross-linked polymer network with a compatible solvent. There is a change in free energy from the mixing of the polymer with the solvent. Mixing increases the entropy and thus causes the free energy to decrease as shown in eq. (10). At the same time, the mixing causes the polymer chains within the sheet to swell and to slightly align.

The swelling and alignment of the sheet's polymer chains reduces the total number of chain configurations and thus decreases the entropy and increases the free energy [82].

Flory and Rehner divided these free energy contributions into two parts. The first contribution arises from the system's change in free energy purely from mixing [83]. This relationship can be expressed as

$$\Delta F_m = k_b T (n_s \ln(\Phi_s) + \chi_1 n_s \Phi_p), \quad (56)$$

where  $n_s$  is the number of solvent molecules,  $\Phi_s$  is the solvent volume fraction,  $\Phi_p$  is the polymer volume fraction and  $\chi_1$  is the Flory parameter. This is very similar to eq. (13) except that now the term  $n_p \ln(\Phi_p)$  is absent. There is only one very large polymer molecule due the assumed chemical crosslinks and thus the term is negligible now since  $n_p = 1$  &  $n_s \gg n_p$  [83].

The second free energy change term deals with the swelling and alignment of polymer chains within the polymer sheet in contact with the solvent as a consequence of solvent penetration. The solvent causes the polymer chains to stretch and align, thus increasing the free energy of the system. Flory and Rehner [83] used the entropy change from rubber elasticity to compute this. And gave this relationship as

$$\Delta F_{el} = \frac{k_b T v_e}{2} (\alpha_z^2 + \alpha_y^2 + \alpha_x^2 - 3 - \ln(\alpha_x \alpha_y \alpha_z)), \quad (57)$$

where each  $\alpha$  represents the expansion of the sheet in each respective direction from swelling while  $v_e$  is number of effective chains in the network. By assuming there is only swelling along the  $x$ -direction of the sheet, parts of eq. (57) simplify [17, 81]. There is no expansion along the  $y$  and  $z$ -directions meaning that

$$1 = \alpha_y = \alpha_z. \quad (58)$$

Putting the simplifications of eq. (58) into eq. (57) results in

$$\Delta F_{el} = \frac{k_b T \nu_e}{2} (\alpha_x^2 - 1 - \ln(\alpha_x)). \quad (59)$$

Panapu [81] and Wu [17] also related the expansion the x-direction to the solvent volume fraction. This relationship is given by

$$\alpha_x = \frac{V}{V_0} = \frac{1}{1 - \Phi_s} = \frac{1}{\Phi_p} = \frac{N_a V_0 + n_s \bar{v}_s}{V_0 N_a}, \quad (60)$$

where  $V$  is the swollen volume of the sheet with solvent and  $V_0$  is the original volume of the sheet without any solvent present. While  $\bar{v}_s$  is the molar volume of the solvent and  $N_a$  is Avogadro's number. One can obtain the chemical potential of the solvent at the polymer sheet by differentiating eqs. (58) & (59) with respect to solvent quantity. Thus, the chemical potential is conveyed by

$$\mu_s - \mu_s^0 = \frac{\partial(\Delta F_m)}{\partial n_s} + \frac{\partial(\Delta F_{el})}{\partial n_s}, \quad (61)$$

where  $\mu_s$  is the solvent chemical potential within the sheet and  $\mu_s^0$  is the chemical potential of the solvent at the bulk solvent. A negative result for eq. (61) means that solvent molecules will travel from the bulk solvent into the polymer sheet. A positive result means the opposite. By doing the proper partial differentiation for each free energy term and accounting all the parameters that are functions of  $n_s$  ( $\Phi_s$ ,  $\Phi_p$ , and  $\alpha_x$ ) in eqs (57) & (59), one can obtain this chemical potential difference. There will be an equilibrium when the chemical potential difference is zero [17]. This means that there will be a solvent volume fraction ( $C_{eq}$  in eq. (50)) where the total free energy change from mixing is balanced out by the total free energy change from polymer chains stretching or relaxing when a solvent molecule is added to or removed from the polymer sheet. The free energy in eq. (61) will increase when system either gains or losses a solvent molecule at this solvent volume fraction. Thus, this is a stable equilibrium minimum point as all systems seek to minimize free energy. This results in the following equation

$$0 = \mu_s - \mu_s^0 = k_b T \left( \ln(\Phi_s) + (1 - \Phi_s) + \chi(1 - \Phi_s)^2 + \frac{\bar{v}_s v_e}{V_0 N_a} \left( \frac{1}{\Phi_s} - \frac{\Phi_s}{2} \right) \right). \quad (62)$$

Thus, to find the solvent or polymer volume fraction at the gel/solvent region ( $C_{eq}$  being equivalent to  $\Phi_s$  in eq. (62)) ends up solving for  $\Phi_s$  such that eq. (62) becomes zero [17, 81].

As previously discussed, the addition of plasticizers into a polymer can lower  $T_g$  or has the equivalent effect of driving a glassy to rubbery transition with constant temperature. The polymer will turn from glass like to a rubbery gel-like state at a certain plasticizer volume fraction. Any location within the polymer that undergoes glass transition has significantly different physical properties. Further solvent penetration also eventually leads to the dissolution of the bulk polymer. Peppas and Wu came up with an interesting method to model the polymer dissolution in their model by using a method called the molecular clock. In Peppas and Wu's proposal, polymer chains begin to disentangle at any spatial location within the bulk polymer that has undergone transition from the glassy to the rubbery/gel state. The solver assigns and runs clock timer at spatial locations where the solvent volume fraction ( $C_S$ ) has become high enough to transform the polymer from glassy to rubbery state. One can state this transition solvent volume fraction as

$$C_S(X, t) = C_g, \quad (63)$$

Where  $C_g$  is the solvent volume fraction quantity that any location within the bulk polymer transitions from glassy to rubbery state. The molecular clock attached to a location begins running when the location's solvent volume fraction is at least that of eq. (63). Any location with the timer running will fully dissolve when the molecular clock's allotted time is up.

Polymer disentanglement at the locations with a running molecular clock is possible because the polymer chain segments at the rubbery regions are much more mobile and can undergo limited local diffusion. This method deals with the polymer dissolution part of the model by relating the disentanglement time to reptation time of polymer chains. Using and modifying

the scaling arguments from de Gennes theory of reptation allows one to obtain a polymer disentanglement time from reptation time to assign to the molecular clock [17].

Reptation theory by de Gennes involves reducing a many-body problem that involves many entangled polymer chains moving with respect to each other into a problem of a single polymer chain motion. All of the other polymer chains act as constrains and obstacles, limiting the mobility of the single chain. The single chain can only move efficiently in a snake-like fashion along the directional length of the red tube as shown in figure 38. The red tube represents the sole chain's path without any obstacles. If the single chain moves outside of its tube, it encounters obstacles. Thus, no part of the chain can move in a direction perpendicular to the red tube [19]. When the single polymer chain fully exits the red cylinder, it is free. The total time needed is called is the reptation time. P. de Gennes express this time proportionally as:

$$t_R \approx \frac{(L_t)^2}{D_c}, \quad (64)$$

where  $L_t$  is the length of the red tube in figure 38 and  $D_c$  is the curvilinear diffusion coefficient. In this model, the polymer chain moves within a matrix made of identical chains within a polymer melt. This is not the case when the polymer is undergoing dissolution due to a changing solvent volume fraction. But the principle remains the same; a polymer chain needs time to disentangle from the bulk polymer. Once this chain is free, it diffuses from bulk polymer into the solvent region [18].

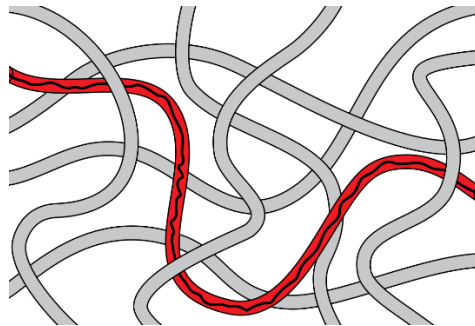


Figure 34 Pierre-Gilles de Gennes' reptation set-up. From: [19].

Wu [16] modified de Gennes reptation theory and derived the following proportional relationship for polymer chain reptation in a polymer-solvent mixture. He gave this proportional relationship as

$$t_r \sim \eta_s M^3 C_p^{6a-3}, \quad (65)$$

where  $\eta_s$  is the viscosity of the solvent,  $M$  is the molecular weight of the polymer, and  $C_p$  is volume fraction of the polymer. The parameter  $a$  describes how relatively good the solvent is with respect to the polymer in question. A good solvent will be the case where polymer to solvent molecule interactions more are favorable than polymer to polymer interactions ( $C_{ps} < C_{pp}$ ). Wu gave out the parameter of  $a = 0.75$  for a good solvent with respect to the polymer in question. In de Gennes' model, the reptation process of a single chain occurs within a pure polymer melt or within a static polymer-solvent solution. In both of these cases, the solvent volume fraction is either constant or non-existent. This is not the case during polymer dissolution. This is because the local solvent volume fraction within the bulk polymer changes with respect to time. Thus during polymer dissolution, the disentanglement of a polymer chain occurs over a range of solvent volume fractions. Wu assumed that the disentanglement process began when the local solvent volume fraction was at the critical amount to change the local polymer from glassy to rubbery state as in eq. (63)). The local polymer is fully dissolved once the molecular clock has run its allotted time. The clock's time will *not* be equal to  $t_r$ . Instead the molecular clock uses a general dissolution time based on  $t_r$ [18]. Wu derived the dissolution time as

$$t_d^0 = k_d M^\alpha C_p^\beta, \quad (66)$$

where  $k_d$  is a disentanglement time constant and  $\alpha$  &  $\beta$  factors that can be determined experimentally. Like on eq. (65), eq. (66) depends on the solvent volume fraction since  $C_s = 1 - C_p$ . Eq. (66) only works if the solvent volume fraction is constant throughout. Wu assumed the molecular clock timer at a location begins when the initial solvent volume fraction at the location

is equal to the glass transition volume fraction as  $C_s = C_g$ . Once the location's molecular clock is up, the polymer will be gone. Moreover, the new gel/solvent boundary with the solvent volume fraction found by the Flory-Rehner relationship:  $C_s = C_{eq}$  moves to this location. Each changing solvent volume fraction at this location,  $t_d^0$  contributes a little to the total disentanglement time,  $t_d$  [ 16] One can express this relationship in fraction and sum form as

$$\sum_{i=1}^n \frac{\Delta t_i}{t_d^0(C_{p,i})} = 1, \quad (67)$$

where  $\Delta t_i$  is the fractional time contribution of each respective  $t_d^0$  to the total disentanglement time for a specific solvent volume fraction. By taking  $n$  to infinity to account for infinitesimal changes in solvent volume fraction, one can turn the sum of eq. (67) into an integral[16]. Eq. (67) is transformed into

$$\int_{t_1}^{t_2} \frac{dt}{t_d^0(C)} = 1, \quad (68)$$

where  $t_2$  is the time when  $C_s = C_{eq}$  and  $t_1$  is when  $C_s = C_g$ . The dissolution time is such that:  $t_d = t_2 - t_1$ . Inserting eq. (66) into eq. (68) changes it. The new equation is

$$\frac{1}{k_d M^\alpha} \int_{t_1}^{t_2} \frac{dt}{C_p^\beta} = 1. \quad (69)$$

Figure 39 shows the molecular clock method in action. The top image shows a location in  $X$  where the polymer-solvent concentration reaches the critical value,  $C_g$ . At this location the molecular clock timer begins. The bottom figure shows the results after the molecular clock's time,  $t_d$ , at this location is up. Here the same location that previously hit the glass transition solvent volume fraction  $C_g$  is now the solvent-polymer boundary,  $X_s$ . The space between the previous solvent-polymer boundary location and  $X_\lambda$  on the top has undergone dissolution as represented by the black region of the bulk polymer. The black region represents the area of the bulk polymer that dissolves due to running the dissolution clock at this location.

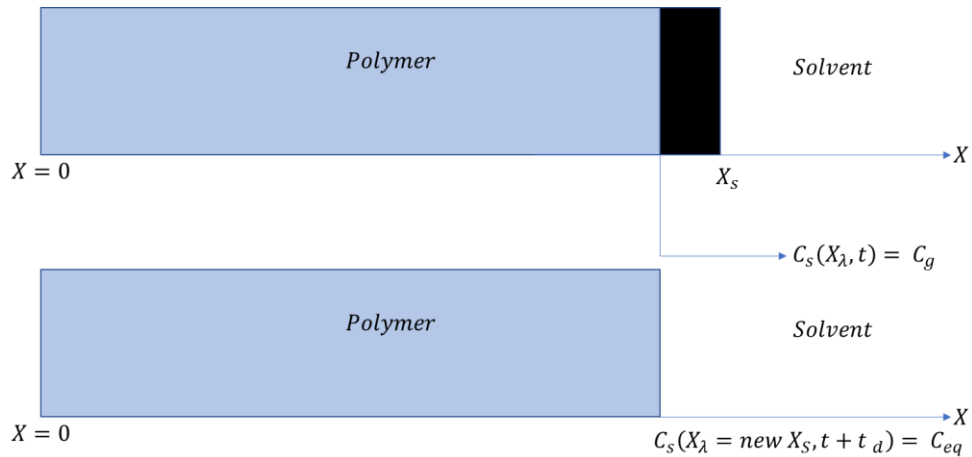


Figure 35 Schematic of the molecular clock in action.

Analytically, every space in the bulk polymer has this molecular clock timer, resulting in an infinite quantity of timers. However, since Wu et al. solved the problem numerically, there is a finite amount instead. A numerical finite difference scheme solves for the two governing eqs. (47) & (48) simultaneously. Since it is a numerical solution, the bulk polymer space contains finite discrete points. The solver solves for the solvent volume fraction and stress for all the points at each time step. Every point also has the molecular clock attached that the solver activates when the solvent volume fraction of the point in question reaches  $C_g$ .

To evaluate and compare their numerical solver, the group did polymer dissolution experiments. The group dissolved films of polystyrene in methyl ethyl ketone (MEK). Figure 40 below shows the experimental data obtained from a dissolution experiment superimposed with the solution curves of the numerical solver. The two curves track two interfaces: the solvent-gel interface ( $C_{eq}$ ) and the glassy-rubbery interface ( $C_g$ ) with respect to time. The upper line with the circle data points represents the solvent-gel interface. Here one can see the initial swelling along with the eventual receding of the polymer as both the data initially increase and then decrease. The lower curve with square data-points is the glassy-rubbery interface. The downward curve of the numerical solver shows that the solvent penetrates with greater depth and quantity into the

bulk polymer. This increasing quantity of solvent causes locations within the polymer to change from glassy to rubbery. Overall, the numerical model gives a good fit with respect to the experimental data [17,18].

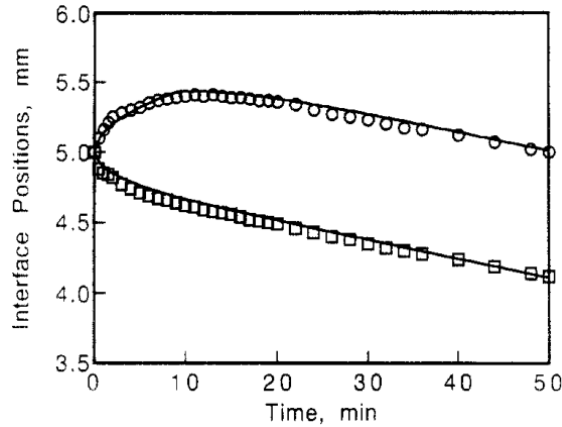


Figure 36 Experimental and numerical results of the solver for polystyrene immersed in MEK. From: [17].

As a final note, the group also dissolved Polymethyl methacrylate (PMMA) in MEK. In this polymer-solvent system, there was no polymer swelling or the formation of a rubbery region. The group did see that the PMMA surface in contact with MEK started to craze. This crazes eventually grew into cracks. The cracks joined together to ‘cut off’ pieces of the bulk polymer. Thus the dissolution mechanism here is crack propagation that causes polymer pieces to break off [18]. This dissolution mechanism is different from the other ones discussed above. Other researchers have published similar results. Interestingly, it is possible for some polymer-solvent systems to shift its dissolution mechanism from gel-formation and polymer chain reptation to the crazing and cracking mechanisms by lowering the operating temperature of the system. At a sufficiently low temperature, the rubbery-gel region disappears and the polymer disintegrates by cracking instead [16].

## Chapter IV: Own Polymer Dissolution Model

### Set-up of the Model

The previous chapter of this thesis discussed and summarized three of the many models available dealing with the polymer dissolution problem. The following is the introduction and discussion over our own model. This model builds from the models reviewed along with an additional model published by Peppas & Narasimhan [84]. Current model is one-dimensional where the overall system is divided into three main regions- each with its own governing equations. Region I is the region where the bulk polymer is present. The bulk polymer has no chemical crosslinks, but contains physical entanglements between the chains. Region II is the region where the bulk solvent and loose polymer chains are at. Region III deals with the boundary between the bulk polymer and the solvent. Figure 41 illustrates the model with the three regions.

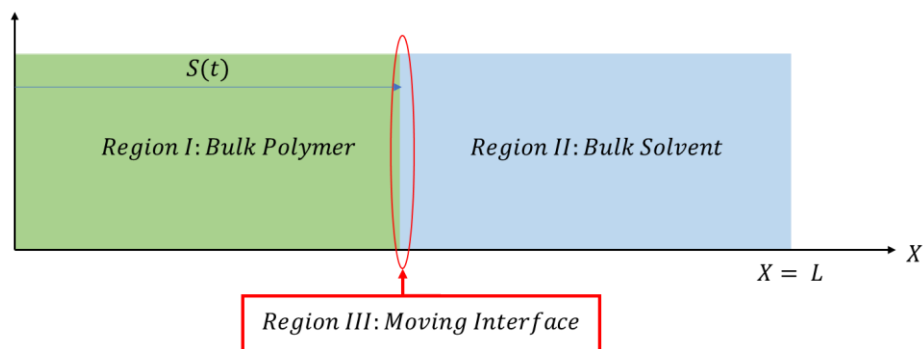


*Figure 37 Regional set-up of the problem. Region I is bulk polymer and Region II is solvent*

By including these three regions, one can model the whole process of polymer dissolution in a compatible solvent. In its entirety, polymer dissolution consists of four main steps as illustrated in figure 42. The first step involves the diffusion of solvent from Region II into Region I. Solvent penetration causes the bulk polymer (Region I) to expand and for locations within Region I to cease being a pure polymer. The total quantity of polymer within Region I is conserved and kept constant during this step. No polymer is present within the solvent (Region II)

during this step. The second step consists of the system reaching the reptation time. The reptation time is the time needed for a polymer chain to become fully disentangled from the bulk polymer. Individual polymer chains are capable of diffusing from the bulk polymer into the solvent. The total quantity of polymer within Region I will NOT conserve beyond this point. With solvent penetrating into the bulk polymer throughout the simulation process, Region I can continue to expand, even if individual polymer chains diffuse out towards Region II. The third step is when the bulk polymer starts to recede and shrink in size. This means that the solvent diffusing into Region I and inducing swelling cannot compensate for the loss of polymer chains volume-wise. The final step is complete dissolution. Complete dissolution is when all of the bulk polymer ends up as single chains within Region II. [16].

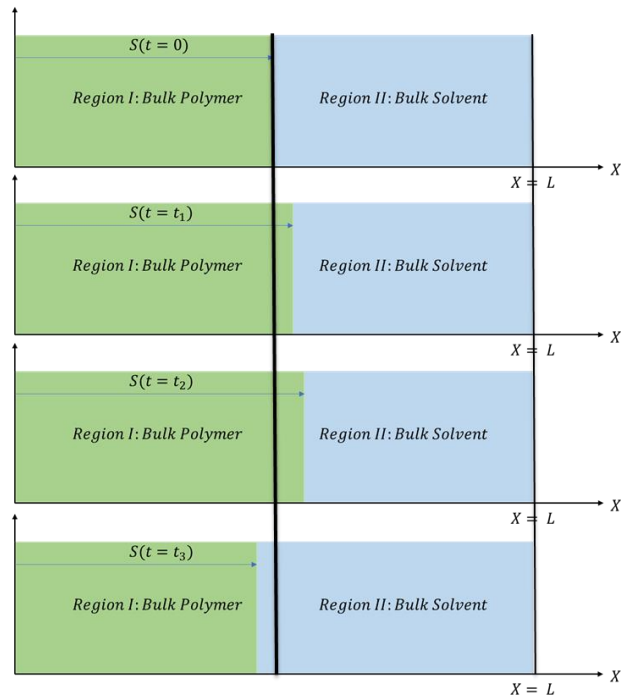


Figure 38 Change in regional sizes and domains as the polymer dissolution model progresses with respect to time

Throughout the dissolution process, volume of Region I changes with solvent penetrating in and disentangled chains diffusing out. This change indicates that the domains of both regions do not remain constant. With both Regions I and II changing in size, the parameter  $S(t)$  in Figure

41 is used to describe the boundary between them . The movement of  $S(t)$  respect to time changes both the respective domains and sizes of Regions I and II as shown in figure 42.  $S(t)$  also marks the location of Region III as shown in figure 41. This moving boundary makes the polymer dissolution problem interesting. As Regions I and II change in size, the applicable domain of their respective governing equations changes too. Figure 42 offers an example of this. At time  $t = t_1$ , the space immediately to the right of the bold center line belongs to Region I and thus the governing equation of Region I applies to this location. This is not the case at a different time such as  $t = 0$  or  $t = t_3$ . At these times, the space belongs to Region II and a different governing equation should apply. This situation makes the polymer dissolution problem belong the Stefan or Moving Boundary Problem family [85].

While the domain and size of Regions I & II are dynamic, their governing equations solve for the same thing. These equations can be used to determine the polymer volume fractions at all locations in their respective regions. Region I is a pure bulk polymer at the beginning. This gives all of Region I an initial volume fraction value of 1. The opposite happens to Region II, the region of pure solvent, at the beginning will have a volume fraction value of 0 everywhere. A special polymer volume fraction is assigned to the moving boundary from the beginning. This value is the polymer gel concentration and tells how much polymer is at the very thin layer that forms at the Stefan boundary where the bulk polymer and solvent meet. This volume fraction quantity at the moving Stefan boundary  $S(t)$  is kept as a constant and will not change as the polymer dissolution model progresses. As discussed in the previous section, Panapu, Wu, Peppas, and others gave a derivation on how to obtain this polymer volume fraction. The following summarizes the given derivation. The entanglements between the polymer chains are physical interactions. There must be no chemical crosslinks presents for a polymer to dissolve. The physical entanglements can however be *assumed* to be temporary fixed cross-links. This assumption allows the use of Flory-Rehner formula which allows one to find a polymer volume

fraction where the entropy change from mixing and the stretching of the moving boundary is at a balance such that either adding or removing solvent from this thin layer will increase the free energy. Since all systems want to minimize free energy, the polymer volume fraction will not change here. Thus, the volume fraction at the polymer-solvent interaction layer remains constant throughout.

Each one of the three regions has a governing equation along with initial and boundary conditions. For Region I, the bulk polymer, one applies the same governing equation as in [75] & [84]. The equation is a nonlinear diffusion of the Fickian type [85]. Thus, Region I's governing equation is

$$\frac{\partial C}{\partial t} = \frac{\partial}{\partial x} \left( D_1 \frac{\partial C}{\partial x} \right) \text{ for } x = 0 \text{ to } x = S(t) \text{ for all time,} \quad (70)$$

where  $C$  is the polymer volume fraction at any location and  $D_1$  is the mutual solvent-polymer diffusion coefficient. Eq. (70) also states the spatial and time domain of the governing equation. For the spatial domain,  $x$  can be anywhere between 0 and  $S(t)$ , where  $S(t)$  can change with respect to time as shown in figures 41 and 42. Eq. (70) has two boundary conditions and they are as follow:

$$\frac{\partial C}{\partial x} = 0 \text{ at } x = 0 \text{ boundary for all time} \quad (71)$$

and

$$C = C_{gel} \text{ at } x = S(t) \text{ for all time.} \quad (72)$$

$C_{gel}$  is the equilibrium polymer volume fraction obtained by using the Flory-Rehner derivation.  $S(t)$  describes the position of this boundary with respect to time, allowing to show the swelling and dissolution behavior of the bulk polymer. Eq. (71) is a Neumann boundary condition and states that no polymer or solvent can flow at  $x = 0$ . This is analog to having an insulated end

for a one dimensional heat equation problem. The work of Tu [75], Wu [18], and Devotta [76] gave this boundary condition for their respective polymer regions. Eq. (72) illustrates the second boundary condition as a Dirichlet condition and states the polymer volume fraction that the border must have. All the cited models have this boundary condition [75,76,84,18]. As discussed, the bulk polymer is pure polymer at the very start of the dissolution problem. One can express this statement as an initial condition as

$$C = 1 \text{ at } t = 0 \text{ for } x = 0 \text{ to } x = S(t = 0), \quad (73)$$

where pure polymer is equivalent to having a polymer volume fraction of 1. Eq. 70 can be linearized by making  $D_1$  a constant. One can express the linearized eq. (70) as [86]

$$\frac{\partial C}{\partial t} = \left( D_1 \frac{\partial^2 C}{\partial x^2} \right) \text{ for } x = 0 \text{ to } x = S(t) \text{ for all time,} \quad (74)$$

where now the parameter  $D_1$  will not be a function of  $x$  and is independent of the polymer volume fraction.

Region II makes the bulk solvent boundary layer and has its own set of governing equation along with boundary and initial conditions. The model uses the non-linear Smoluchowski governing equation that Tu [75] and Narasimhan [84] used for their respective models. Region II's governing equation can be expressed as [86]

$$\frac{\partial C}{\partial t} = \frac{\partial}{\partial x} \left( D_p \frac{\partial C}{\partial x} \right) - \frac{dS}{dt} \frac{\partial C}{\partial x} \text{ for } x = S(t) \text{ to } x = L \text{ for all time,} \quad (75)$$

where  $D_p$  is the diffusion constant for polymer within the solvent.  $C$  is still the polymer volume fraction concentration at any location within Region II. The term  $\frac{dS}{dt}$  is the velocity of the moving boundary,  $S(t)$ , at any time. Like Region I, Region II has two boundary conditions; one for each end in the one-dimensional space. The boundary conditions for Region II are as follow:

$$C = C_{gel} \text{ at } x = S(t) \text{ for all time} \quad (76)$$

and

$$\frac{\partial C}{\partial x} = 0 \text{ at } x = L \text{ for all time.} \quad (77)$$

The boundary condition of eq. (76) is of the Dirichlet type and is equivalent to eq. (72). This is the shared boundary of the polymer gel-solvent interface and Tu et al. [75], Devotta et al. [76] and Narasimhan et al. [84] used this condition in their respective models. Like before, the location of this boundary changes with respect to time to allow the characterization of the bulk polymer behavior of both swelling and undergoing dissolution. Eq. (77) denotes the other boundary condition at the end of the boundary layer and is a Neumann boundary condition. Like before this condition closes off the polymer dissolution system from the rest of the world. Neither the polymer chains or the solvent can pass through here.  $L$  in eq. (77) demarks the end of the bulk solvent boundary layer. Narasimhan et. al. [84] used this type of boundary condition in their model. The total length of the polymer-solvent system is equal to  $L$  and fixed. The location of  $L$  is present in figures 41 & 42. At the beginning of the problem, Region II is pure solvent with no polymer present and its domain is between  $S(0)$  and  $L$ . One can express this statement mathematically as

$$C = 0 \text{ for } x = S(0) \text{ to } x = L \text{ when } t = 0. \quad (78)$$

Since  $C$  stands for the polymer volume fraction, pure solvent means that no fraction of the volume is polymer. Like for Region I, assuming that  $D_p$  in eq. (75) is a constant allows one to linearize eq. (75). Doing so defines eq. (75) as

$$\frac{\partial C}{\partial t} = \left( D_p \frac{\partial^2 C}{\partial x^2} \right) - \frac{dS}{dt} \frac{\partial C}{\partial x} \text{ for } x = S(t) \text{ to } x = L \text{ for all time,} \quad (79)$$

where  $D_p$  is now a constant and static.

To quickly summarize, there are two regions, each with unique governing equations and both with their own initial and boundary conditions. However both regions share a moving boundary condition at  $x = S(t)$  as demonstrated by eqs. (76) & (72). This boundary is where Region I and Region II meet. The boundary can move with respect to time so it alters the size of both Region I and II. Region III accounts for this boundary and the respective governing equation solves for the velocity of this moving boundary at any time. The governing equation is

$$\frac{dS}{dt} = - \left( D_1 \frac{\partial C}{\partial x} \right)_{x=S^-} - \left( \frac{D_p}{C_{gel}} \frac{\partial C}{\partial x} \right)_{x=S^+}, \quad (80)$$

where the first term,  $\left( D_1 \frac{\partial C}{\partial x} \right)_{x=S^-}$ , is the polymer volume fraction gradient in Region I immediately to the left of the moving boundary  $S(t)$  at any time. The second term,  $\left( \frac{D_p}{C_{gel}} \frac{\partial C}{\partial x} \right)_{x=S^+}$ , is the polymer volume fraction gradient in Region II immediately to the right of the moving boundary  $S(t)$ . For the equation above, the velocity of the moving boundary depends on both the polymer gradient to the left (at Region I) and on the right (at Region II) side of the interface,  $S(t)$ . The first term states the flux of solvent into Region I, and thus how much the bulk polymer swells. The second term on the right hand side states the flux of polymer into Region II corresponding to how much of bulk polymer undergoes dissolution. Devotta et al.[76] and Narasimhan et al. [84] gave a condition similar to the stated one. One can compare eq. (42) with eq. (80). The second value on the right hand side will be zero until the simulation time is at least equal to the reptation time. After that, this value will have a non-negative value expressing the rate of disentangled polymer chains leaving the bulk polymer towards Region II. Thus, eq. (80) has conditional modifications for its second term as follows:

$$\left( D_p \frac{\partial C}{\partial x} \right)_{x=S^+} = 0 \text{ if } t < \text{reptation time } (t_{rep}) \quad (81)$$

and

$$\left(D_p \frac{\partial C}{\partial x}\right)_{x=S^+} = k_d \quad \text{if } t \geq t_{rep}. \quad (82)$$

Eq. (81) states that no loose polymer chains diffuse out from Region I until the reptation time is reached. Polymer chains can then diffuse out from Region I into Region II as per eq. (82). The parameter  $k_d$  represents the rate of loose polymer chains leaving the bulk polymer into the solvent. Eqs. (81) & (82) are based on the work published by Devotta et al. [76]. One can see this by comparing them to eqs. (44) & (45).

With the additional conditions given by eqs. (81) & (82), all requirements are met. The dissolution problem consists of simultaneously solving eqs. (74), (79), and (80). Care must be also taken to account how the domains of Regions I and II change with respect to time. As discussed, the domains belonging to each region will change with respect to time and as consequence of this so will the governing equations assigned to each spatial location. Problems with this characteristic belong a specific family. Mathematicians and physicists call this type of problem a moving boundary problem or a Stefan problem.

### The Stefan Problem and the Landau Transforms

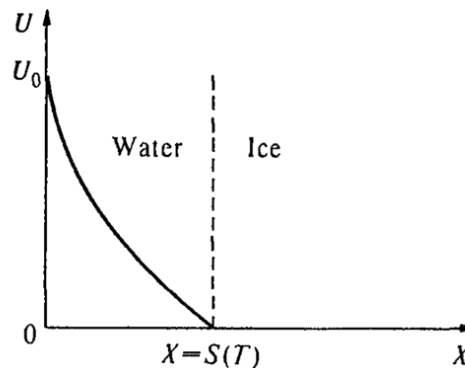


Figure 39 Classical Stefan Problem set-up. From: [82].

Stefan first postulated a problem having moving boundary condition. He considered the following: two regions- one made of water and the other one made of ice. These two regions meet

at the ice-water interface position  $x = S(t)$  in figure 43. It is known that this point must be  $273K$  or  $0\text{ }C^{\circ}$  at nominal conditions. Now the other end of the water region ( $x = 0$ ) is either kept at a constant temperature,  $U_0$ , or receives a constant heat flux, or both. Stefan's question was both how the ice-water border would move and what the temperature profile would be in the water region as the ice region melted. Any ice belonging to the ice region that melted would become a member of the water region. Thus, the size and domain of the water region grows at the cost of the ice region. By assuming an infinitely large ice region and using mass and energy conservation, Stefan derived a closed-form solution to this problem. Stefan was the first to observe and describe a specific phenomenon with this moving boundary condition. However, many other physical phenomena show this moving boundary condition such as crystallization, phase change, ablation, and of course polymer dissolution [85].

From all the models looked into, Peppas and Narasimhan [84] explicitly stated that they used a mathematical method called a Landau Transform to assist in solving their dissolution model. First introduced by Landau [87] to solve for heat conduction within a melting solid, this method became popular to solve moving boundary problems regarding various physical phenomena. The Landau transform involves transforming the spatial coordinates of a region such that the region's domain remains constant within the new coordinate system. This causes the tracking or moving front  $S(t)$  to remain static in the new coordinate system. Static  $S(t)$  not moving keeps the regions the same size throughout the whole problem time-wise and thus not one does not have to worry about which governing equation is applied to a spatial location. This is because the sizes and domains of each transformed region will be the same one as their respective initial one [85]. A Landau transform was carried out for both Regions I and II. Each region underwent different coordinate changes by their specific Landau Transforms.

For Region I, the x-coordinate now became  $\zeta_1$ . The Landau Transform for Region I is

$$\text{Let } \zeta_1 = \frac{x}{S(t)}, \quad (83)$$

where  $\zeta_1$  is the new coordinate system. In old x-coordinate system, the domain of Region I could be anywhere between zero and  $S(t)$ , with the location of  $S(t)$  changing with respect to time.

After transformation,  $\zeta_1$  can be between zero and one in quantity and remains as such throughout the whole time domain. Carrying out partial differentiation of eq. (74) with the new coordinate system given by eq. (83) gives a new governing equation. The new governing equation is

$$S^2 \frac{\partial C}{\partial t} - S \zeta_1 \frac{\partial C}{\partial \zeta_1} \frac{dS}{dt} - D_1 \frac{\partial^2 C}{\partial (\zeta_1)^2} = 0 \quad \text{for } 0 \leq \zeta_1 \leq 1 \text{ \& for all } t. \quad (84)$$

There is a new term compared to Eq. (74). When differentiating with respect to time, one has to also differentiate with respect to  $\zeta_1$  and then with respect to time. Eq. (83) shows that the new introduced coordinate  $\zeta_1$  is a function of time. Differentiating  $C$  with respect to time in the transformed coordinate system gives

$$\frac{\partial C}{\partial t} + \frac{\partial C}{\partial \zeta_1} \frac{\partial \zeta_1}{\partial t}; \text{ where } \frac{\partial \zeta_1}{\partial t} = -\zeta_1 \frac{dS}{dt} \frac{1}{S(t)}. \quad (85)$$

Region II also underwent a Landau transformation. The x coordinate system for this domain was transformed to  $\zeta_2$ . The Landau Transform for Region II is

$$\text{Let } \zeta_2 = \frac{x - S(t)}{L - S(t)}. \quad (86)$$

Under this new coordinate system, the domain of Region II is between zero and one and remains static. This again is opposite to the case of the original x-coordinate system for Region II. On the old x-coordinate system, the domain was between  $S(t)$  and  $L$ . Since  $S(t)$  changes, so does the domain of Region II in the old x-coordinate system. Like with Region I, one carries out the partial

differentiation of eq. (79) using the new  $\zeta_2$  system. The new governing equation from doing this is

$$(L - S(t))^2 \frac{\partial c}{\partial t} + \frac{\partial c}{\partial \zeta_2} \frac{dS}{dt} \zeta_2 (L - S(t)) - D_p \frac{\partial^2 c}{\partial (\zeta_2)^2} = 0 \text{ for } 0 \leq \zeta_2 \leq 1 \text{ \& for all } t. \quad (87)$$

Eq. (87) has additional terms. These terms arise due to the fact that  $\zeta_2$  is function of both time and  $x$ . So a similar but more algebraically messy process occurs like it did in eq. (85). The new spatial domains for Regions I and II are always fixed now; each one between 0 and 1. For Region I, setting  $x = 0$  for sets  $\zeta_1 = 0$  and setting  $x = S(t)$  will make  $\zeta_1 = 1$  no matter what quantity  $S(t)$  is. Something similar occurs in Region II; setting  $x = L$  will make  $\zeta_2 = 1$  while setting  $x = S(t)$  will make  $\zeta_2 = 0$  regardless of what  $S(t)$  is. The problem is now solved by solving the system of partial differential equations in the fixed domain coordinate system. A reverse Landau Transform can be executed for each respective region to obtain the original regular moving domains. Using the Landau Transform does come at a cost as one can see that the governing equations for the fixed domain are more complicated when compared to the governing equations where the domains are allowed to change. This can be seen by comparing eqs. (84) & (87) with eqs. (74) & (79).

## **Finite Difference Method and Solver Algorithms**

Stefan and Landau gave a solution to their respective problems in closed form. However, most ordinary and partial differential equations cannot be solved analytically. Thus, the set of governing equations were solved numerically using MATLAB. The transformed PDEs were solved with a Crank-Nicolson scheme along with the Finite Difference Methods. The Finite Difference methods (FDM) involves using discretization schemes to make either ordinary or partial differential equations solvable [88]. Using the right discretization along with proper set up allows one to use software to solve for the system and end up with a numerical answer to the

problem. The program also used an iterative algorithm to solve for the value of  $S(t)$  to end up with a complete answer to polymer dissolution process.

FDM is based on Taylor series expansions. For example, if one knows the functional output of a point at  $x_0$  but wants to know it at a nearby  $x$  not equal to  $x_0$ , the Taylor series expansion can give the function value at  $x$ . The Taylor series for this function is

$$f(x) = f(x_0) + \frac{d^1 f(x_0)}{dx^1} (x - x_0) + \frac{1}{2} \frac{d^2 f(x_0)}{dx^2} (x - x_0)^2 + \frac{1}{6} \frac{d^3 f(x_0)}{dx^3} (x - x_0)^3 + \dots, \quad (88)$$

where  $f(x)$  is the functional value at  $x$  one is trying to solve for and  $f(x_0)$  is the known functional value. The Taylor approximation assumes that the derivatives of  $f(x_0)$  are also known to obtain the value of  $f(x)$ . The more derivatives used, the closer to the correct answer the approximation is.

The Taylor series can also be written in a more compact form as

$$f(x) = \sum_{n=0}^{infinity} \frac{1}{n!} \frac{d^n f(x_0)}{dx^n} * (x - x_0)^n. \quad (89)$$

The Taylor series will give an exact answer if all the possible derivatives of the function are used. One can however use less terms than necessary and get an approximation. How close  $x$  is to the known value  $x_0$  also helps determine the accuracy of the approximation. This is because of the  $(x - x_0)$  present in every term and a very close distance will allow later terms with powers of  $(x - x_0)$  to become small and thus negligible. One can also use the Taylor series method to obtain the value of the derivatives by using algebraic manipulation. For example, by using Taylor expansion one can get the functional value that is both  $dx$  greater and  $dx$  less than  $f(x_0)$  taken at  $x = x_0$ . The Taylor approximation for a functional value evaluated at a position  $dx$  greater than  $x_0$  is

$$f(x_0 + dx) = f(x_0) + \frac{d^1 f(x_0)}{dx^1} * (dx) + \frac{1}{2} \frac{d^2 f(x_0)}{dx^2} * (dx)^2 + \frac{1}{6} \frac{d^3 f(x_0)}{dx^3} * (dx)^3 + \dots, \quad (90)$$

where, like before, one assumes that  $f(x_0)$  and its higher derivatives are known. The Taylor approximation for a functional value now at a point that is  $dx$  LESS than  $x_0$  is

$$f(x_0 - dx) = f(x_0) - \frac{d^1 f(x_0)}{dx^1} * (dx) + \frac{1}{2} \frac{d^2 f(x_0)}{dx^2} * (dx)^2 - \frac{1}{6} \frac{d^3 f(x_0)}{dx^3} * (dx)^3 + \dots \quad (91)$$

The fundamentals of FDM is to express the derivatives of  $f(x_0)$  as algebraic combinations of the functional values taken at  $x_0$  or adjacent to  $x_0$  such as  $f(x_0)$ ,  $f(x_0 + dx)$ , and  $f(x_0 - dx)$ . One can show how this is done in the following way. For example, one first subtracts eq. (91) from eq. (90). The subtraction gives

$$f(x_0 + dx) - f(x_0 - dx) = +2 * \frac{d^1 f(x_0)}{dx^1} * (dx) + \frac{2}{6} \frac{d^3 f(x_0)}{dx^3} * (dx)^3 + \dots \quad (92)$$

One can algebraically manipulate eq. (92) to end up with the first derivative of  $f(x_0)$  expressed by the other terms. Thus, the first derivative of  $f(x_0)$  is

$$\frac{f(x_0 + dx) - f(x_0 - dx) - \frac{2}{6} \frac{d^3 f(x_0)}{dx^3} * (dx)^3 + \dots}{2 * dx} = \frac{d^1 f(x_0)}{dx^1}. \quad (93)$$

Eq. (93) will give the exact answer for the first derivative of  $f(x_0)$ . However, one can get an approximation too. The approximation for eq. (93) is

$$\frac{f(x_0 + dx) - f(x_0 - dx)}{2 * dx} \approx \frac{d^1 f(x_0)}{dx^1}, \quad (94)$$

where the third derivative and all of the other higher derivatives represented by “...” are dropped. If  $dx$  is very small, the approximated solution is very close to the exact solution.

A similar procedure can be executed to obtain the second derivative of  $f(x_0)$  expressed in combinations of  $f(x_0)$ ,  $f(x_0 - dx)$ , &  $f(x_0 + dx)$ . The process starts by *adding* eq. (90) & (91). This addition is

$$f(x_0 + dx) + f(x_0 - dx) = 2 * f(x_0) + \frac{d^2 f(x_0)}{dx^2} * (dx)^2 + \frac{1}{12} \frac{d^4 f(x_0)}{dx^4} * (dx)^4 + \dots, \quad (95)$$

where some derivatives have canceled out due to addition while others have not. Like, with eq. (93), one can manipulate eq. (95) in a way such that the second derivative of  $f(x_0)$  equal to the combination of the other terms. Thus, the second derivative of  $f(x_0)$  is

$$\frac{f(x_0 + dx) - 2 * f(x_0) + f(x_0 - dx) - \frac{1}{12} \frac{d^4 f(x_0)}{dx^4} * (dx)^4 - \dots}{(dx)^2} = \frac{d^2 f(x_0)}{dx^2}. \quad (96)$$

Doing the same treatment as in eq. (94) approximates the second derivative of  $f(x_0)$  as

$$\frac{f(x_0 + dx) - 2 * f(x_0) + f(x_0 - dx)}{(dx)^2} \approx \frac{d^2 f(x_0)}{dx^2}. \quad (97)$$

Like before, the higher derivative terms of eq. (97) drop out since each one is multiplied by  $(dx)^4$  or a higher order term of  $(dx)$ . These simple derivations using Taylor expansions allow one to solve the previously derived family of governing eqs. (80), (84), & (87) numerically. A computer will not be able to carry out analytical mathematical operations such a differentiation or integration but can do four basic mathematical operations with ease: addition, subtraction, multiplication, and division. This is the basis of the FDM to solve problems. In FDM, the problem's spatial and time dimensions are broken up into discrete points and one solves for the values at each of these discrete points. This can be done since the Taylor series expansion showed that the derivatives of a function at a given point is approximately a combination of the values of functions evaluated at points adjacent from the point in question. One can solve for the collection of function values belonging to various points by algebraic manipulation and solving for systems of equations. This is different from solving a PDE analytically and solving for an infinite amount of points in continuous time and space. Thus, for a one-dimensional diffusion problem one ends up with a two-dimensional space: one dimension for space and the other one for time. This enables one to solve for values at specific, finite locations in space and at a given specific time.

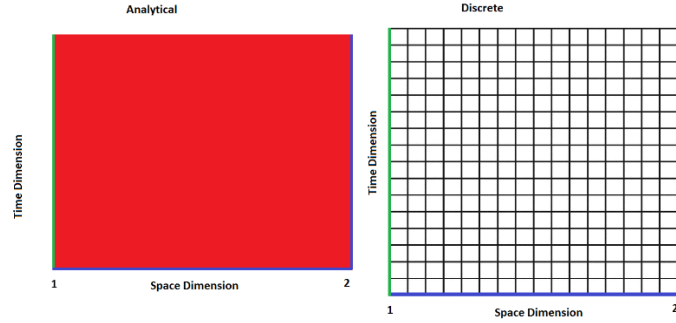


Figure 40 Continuous vs discrete space time for region one of the problem. The discrete regions are only set for the intersections of black lines. The analytical has an infinite number of locations, represented as the red field. The blue colored lines are known initial and boundary conditions that are used to compute the results.

Scientists and mathematicians have come up with various types of schemes to solve PDEs using the FDM method. It is important to know what family the governing equations belong to such that to apply the best numerical scheme. Since the governing equations of Region I and II belong to the parabolic family, the Crank-Nicolson method was chosen. The Crank-Nicolson method is a good compromise between accuracy and computing time and is unconditionally stable. This means that the solution will not blow up regardless of the size of the space or time step taken [88,89].

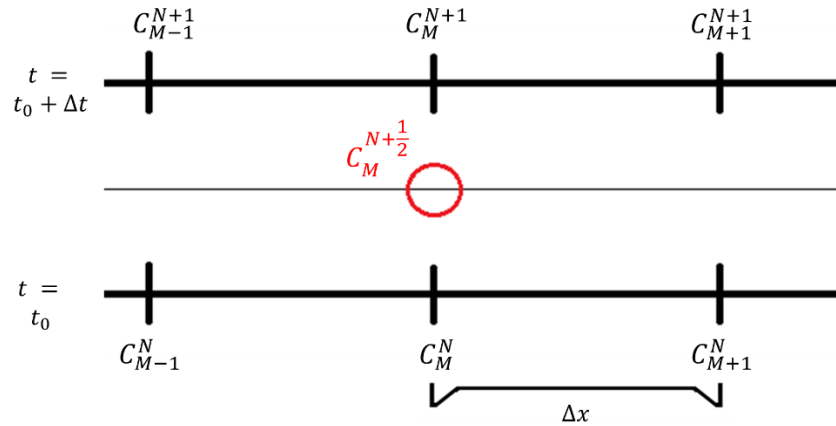


Figure 41 Showing the imaginary node halfway time-wise as a red circle. This node will be defined by the six adjacent C-labeled nodes

For starters, each discrete region will have a corresponding value in both time and space. These are marked with respect to time in superscripts and space in subscripts with respect to location for each  $C$ . First, both space and time are broken up into discrete steps. It is only at these

discrete steps that the problem will be solved for. Usually  $\delta x$  is used for the space step and  $\delta t$  is used for the time step as shown figure 45. Notice the indices put on  $C$  regarding the location with respect to time and space. With the Crank-Nicolson method however, one takes the time step at a fictional point *halfway* between the two time steps. This fictional point is the red circle in figure 45. One begins by carrying out every derivative on eq. (80) at the red circle, evaluating every term with respect to the spatial and time location of the red circle. Thus eq. (80) evaluated at the red circle is

$$-D_1 \left( \frac{\partial^2 C}{\partial \zeta_1^2} \right)_M^{N+\frac{1}{2}} - (S)^{N+\frac{1}{2}} (\zeta_1)_M \left( \frac{dS}{dt} \right)^{N+\frac{1}{2}} \left( \frac{\partial C}{\partial \zeta_1} \right)_M^{N+\frac{1}{2}} + \left( S^{N+\frac{1}{2}} \right)^2 \left( \frac{\partial C}{\partial t} \right)_M^{N+\frac{1}{2}} = 0, \quad (98)$$

where  $M$  denotes the spatial location of the red circle as a subscript and  $N + \frac{1}{2}$  does the same with respect to time as a superscript. Looking at figure 45 one can see that the subscripts and superscripts match each other for the location of the red circle., The first term in eq. (98) can be approximated by using the Crank-Nicolson method with respect to time. Here, term is approximated as an arithmetic mean involving  $\frac{\partial^2 C}{\partial \zeta_1^2}$  evaluated at time steps  $N + 1$  and  $N$ . This gives

$$-D_1 \left( \frac{\partial^2 C}{\partial \zeta_1^2} \right)_M^{N+\frac{1}{2}} \approx -\frac{D_1}{2} \left( \left( \frac{\partial^2 C}{\partial \zeta_1^2} \right)_M^{N+1} + \left( \frac{\partial^2 C}{\partial \zeta_1^2} \right)_M^N \right). \quad (99)$$

Notice that only the superscript changed from this approximation. One can then relate both double derivatives of  $C$  with respect to  $\zeta_1$  to adjacent  $C$  values at three spatial locations by using eq. (97)'s Taylor expansion. Thus, one can approximate eq. (99) as

$$-D_1 \left( \frac{\partial^2 C}{\partial \zeta_1^2} \right)_M^{N+\frac{1}{2}} \approx A * (C_{M+1}^{N+1} - 2 * C_M^{N+1} + C_{M-1}^{N+1} + C_{M+1}^N - 2 * C_M^N + C_{M-1}^N), \quad (100)$$

where  $A = \frac{-D_1}{2(\Delta\zeta_1)^2}$  and  $\Delta\zeta_1$  is the distance between nodes ( the black marked lines in figure 45) along the spatial domain. Similarly, the second term in eq. (98) undergoes the same Crank-Nicolson geometric average treatment with respect to time for  $C$  . Thus the second term is approximated as

$$(S)^{N+\frac{1}{2}}(\zeta_1)_M \left(\frac{dS}{dt}\right)^{N+\frac{1}{2}} \left(\frac{\partial C}{\partial \zeta_1}\right)_M^{N+\frac{1}{2}} \approx \frac{1}{2} \left( (S)^{N+\frac{1}{2}}(\zeta_1)_M \left(\frac{dS}{dt}\right)^{N+\frac{1}{2}} \right) \left( \left(\frac{\partial C}{\partial \zeta_1}\right)_M^{N+1} + \left(\frac{\partial C}{\partial \zeta_1}\right)_M^N \right). \quad (101)$$

Like previously only the superscript on the first derivative of  $C$  with respect to  $\zeta_1$  changes from the original  $N + \frac{1}{2}$ . One applies the Taylor approximation from eq. (94) to both partial derivatives of  $C$  with respect to  $\zeta_1$ . Doing so changes eq. (101) into

$$(S)^{N+\frac{1}{2}}(\zeta_1)_M \left(\frac{dS}{dt}\right)^{N+\frac{1}{2}} \left(\frac{\partial C}{\partial \zeta_1}\right)_M^{N+\frac{1}{2}} \approx (\zeta_1)_M B * (C_{M+1}^{N+1} - C_{M-1}^{N+1} + C_{M+1}^N - C_{M-1}^N), \quad (102)$$

where  $B = \frac{(S)^{N+\frac{1}{2}} \left(\frac{dS}{dt}\right)^{N+\frac{1}{2}}}{4\Delta\zeta_1}$ . Thus, like previously, the partial derivatives of  $C$  with respect to  $\zeta_1$  are now approximated to adjacent  $C$  values. The last term in eq. (98) undergoes the Taylor approximation in eq. (94). The partial derivative of  $C$  with respect to time in eq. (98) is approximated by two adjacent  $C$ 's. Doing so, one can approximate this partial derivative as

$$\frac{C\left(t^{n+\frac{1}{2}} + \frac{\Delta t}{2}\right) - C\left(t^{n+\frac{1}{2}} - \frac{\Delta t}{2}\right)}{2 * \frac{\Delta t}{2}} \approx \frac{\partial C\left(t^{n+\frac{1}{2}}\right)}{\partial t}, \quad (103)$$

where  $\Delta t$  is the time step denoting the distance between  $N + 1$  and  $N$  in the time domain. The approximation above is very similar to eq. (94) except that half  $\Delta t$  is used instead of  $dx$ . As a consequence of this, one can express the last term of eq. (98) as

$$\left(S^{N+\frac{1}{2}}\right)^2 \left(\frac{\partial C}{\partial t}\right)_M^{N+\frac{1}{2}} \approx C^*(C_M^{N+1} - C_M^N), \quad (104)$$

where  $C^* = \frac{\left(S^{N+\frac{1}{2}}\right)^2}{\Delta t}$ . On the equations above both  $(\zeta_1)_M$  and the diffusion coefficient  $D_1$  do not change with respect to time. The diffusion coefficient does not as it is treated as constant to linearize eq. (80). The  $\zeta_1$  does not because its location is fixed on the grid thanks to the Landau transform. One still must deal with the other terms that are functions of time. This is done in the following lines below.

The terms  $\left(S^{N+\frac{1}{2}}\right)^2$  and  $S^{N+\frac{1}{2}}$  in eq. (98) are handled by taking the geometric mean of each one like it has done to obtain the solubility parameter way back. This results in two approximations:

$$\left(S^{N+\frac{1}{2}}\right)^2 \approx S^N S^{N+1} \quad (105)$$

and

$$S^{N+\frac{1}{2}} \approx \sqrt[2]{S^N S^{N+1}}. \quad (106)$$

One must also deal with the velocity of the moving boundary at time superscript  $N + \frac{1}{2}$ . This is done similarly to the derivative of  $C$  with respect to time at eq. (103). This allows one to express the moving boundary velocity as

$$\left(\frac{dS}{dt}\right)^{N+\frac{1}{2}} \approx \frac{1}{\Delta t} (S^{N+1} - S^N). \quad (107)$$

The parameter  $S^{N+1}$  sets the location of Region III and joins Regions I and II together as in figure 41 for time step  $N + 1$ . Since  $S^{N+1}$  is the location of the moving boundary,  $S^{N+1}$  may not equal the known  $S^N$  from the previous time step. For the moment it will be set be such that  $S^{N+1} = S^{Guess}$ . This is because  $S^{N+1}$  will be found through iteration. Setting  $S^{N+1}$  to  $S^{Guess}$  for now

allows one to come up with a solvable scheme. In this method, one must first solve for both Regions I and II at a specific time step by using  $S^{Guess}$ . Following this one can use the found values to from Regions I and II to obtain  $S^{N+1}$ .

A very simple example for Region I will be done to give an understanding on how the FDM solver works. Let's consider Region I at the very start and a time step immediately afterwards as shown in figure 46. The spatial grid here is very coarse and thus only very few points are actually defined.

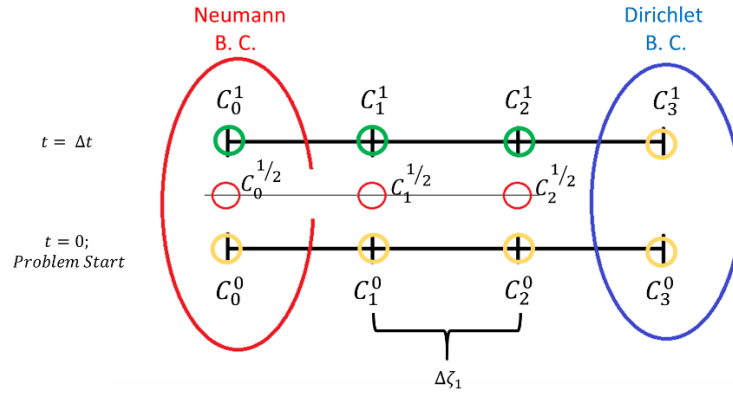


Figure 42 To solve this coarse grid, one will need three imaginary half-way nodes marked as the three red circles.

The  $C$ 's with a superscript of zero are the initial condition and thus known. The  $C$ 's within the blue circle are the Dirichlet boundary conditions at each time step and also known per eq. (72) and are also the shared moving boundary  $S(t)$ . Therefore, one only has to solve for the remaining  $C$ 's denoted with green circles in figure 46. Thus, the governing equations for Region I are taken at the spatial intervals between these two time steps shown in figure 46 above as three small red circles. One applies eq. (80) at each one of the three red circles. Eq. (80) on the red middle  $C_1^{1/2}$  circle gives

$$-D_1 \left( \frac{\partial^2 C}{\partial \zeta_1^2} \right)_1^{\frac{1}{2}} - (S)^{\frac{1}{2}} (\zeta_1)_1 \left( \frac{dS}{dt} \right)^{\frac{1}{2}} \left( \frac{\partial C}{\partial \zeta_1} \right)_1^{\frac{1}{2}} + \left( S^{\frac{1}{2}} \right)^2 \left( \frac{\partial C}{\partial t} \right)_1^{\frac{1}{2}} = 0. \quad (108)$$

One can express every partial derivative of  $C$  in eq. (108) as a combination of  $C$ 's in time and spatial nodes that will be both known ( the yellow circles in figure 46) and unknown ( green circles in figure 46). To do this, every partial derivative must undergo the Crank- Nicolson along with the respective Taylor expansion to end up with an approximation. This allow one to approximate eq. (108) as

$$0 \approx A(C_0^1 - 2 * C_1^1 + C_2^1 + C_2^0 - 2 * C_1^0 + C_0^0) + B(\zeta_1)_1(C_2^1 - C_0^1 + C_2^0 - C_0^0) + C^*(C_1^1 - C_1^0), \quad (109)$$

where  $A, B, \& C^*$  are the same parameters used in eqs. (100), (102), and (104). The same method described above can be done to the right red circle in figure 46,  $C_2^{1/2}$ . This results in the following two equations:

$$- D_1 \left( \frac{\partial^2 C}{\partial \zeta_1^2} \right)_2^{\frac{1}{2}} - (S)^{\frac{1}{2}} (\zeta_1)_2 \left( \frac{dS}{dt} \right)^{\frac{1}{2}} \left( \frac{\partial C}{\partial \zeta_1} \right)_2^{\frac{1}{2}} + \left( S^{\frac{1}{2}} \right)^2 \left( \frac{\partial C}{\partial t} \right)_2^{\frac{1}{2}} = 0 \quad (110)$$

and

$$0 \approx A(C_1^1 - 2 * C_2^1 + C_3^1 + C_1^0 - 2 * C_2^0 + C_3^0) + B(\zeta_1)_2(C_3^1 - C_1^1 + C_3^0 - C_1^0) + C^*(C_2^1 - C_2^0). \quad (111)$$

Carrying out the same procedure for the left red circle in figure 46,  $C_0^{1/2}$ , yields the following pair:

$$- D_1 \left( \frac{\partial^2 C}{\partial \zeta_1^2} \right)_0^{\frac{1}{2}} - (S)^{\frac{1}{2}} (\zeta_1)_0 \left( \frac{dS}{dt} \right)^{\frac{1}{2}} \left( \frac{\partial C}{\partial \zeta_1} \right)_0^{\frac{1}{2}} + \left( S^{\frac{1}{2}} \right)^2 \left( \frac{\partial C}{\partial t} \right)_0^{\frac{1}{2}} = 0 \quad (112)$$

and

$$\approx A(C_1^1 - 2 * C_0^1 + C_{-1}^1 + C_1^0 - 2 * C_0^0 + C_{-1}^0) + B(\zeta_1)_0(C_1^1 - C_{-1}^1 + C_1^0 - C_{-1}^0) + C^*(C_0^1 - C_0^0). \quad (113)$$

A problem arises in eq. (113). In this equation there are  $C$ 's with a subscript of negative one ( $- 1$ ). This means that the node would be located *outside* of the Neumann boundary condition

wall as shown in figure 47. This is a location outside of the polymer solvent system. However, since the Neumann boundary condition gives the derivative at every time step at  $C_0^{any}$  location as zero from eq. (71), one can use the Taylor expansion of eq.(94) to define the value of  $C_{-1}^{any}$  for any time step. One can show this relationship as

$$\frac{dC_0^{any}}{d\zeta_1} \approx \frac{C_1^{any} - C_{-1}^{any}}{2\Delta\zeta_1} = 0, \quad (114)$$

where  $C_{-1}^{any}$  is an imaginary node that exists outside of the system's domain. The literature usually cites this node as a *ghost node*. Manipulating eq. (114) will give a value for this ghost node as

$$C_{-1}^{any} = C_1^{any}. \quad (115)$$

Thus for eq. (113) all  $C$  terms with a subscript of negative one are replaced by an equivalent  $C$  with a subscript of one. One can give a very quick and intuitive argument why this is the case. The first derivative at the point  $C_0^{any}$  is equal to zero. This also means that slope in this location is equal to zero and thus a flat line. By extending this slope for the two closest neighboring spatial points,  $C_{-1}^{any}$  and  $C_1^{any}$ , both must be equal such that the slope remains as zero at the Neumann boundary [84].

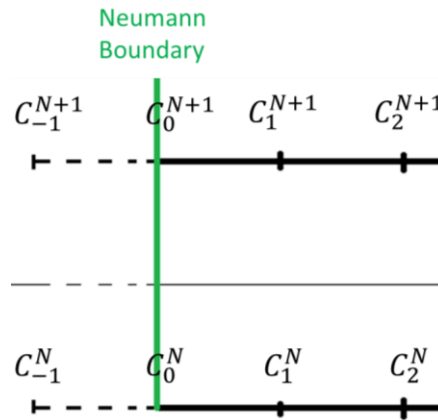


Figure 43 Showing how the 'C' nodes with subscript of -1 do not exist in physical space. These nodes are called 'ghost nodes'

The derivations above result in three equations (eqs. (109), (111), & (113)) and in three unknowns in total ( $C_0^1, C_1^1, & C_2^1$ ) that can be solved simultaneously. Figure 48 shows the re-arrangement of the equations in matrix form. The three unknowns are in vector form.

$$\begin{bmatrix} C^* - 2A & 2A & 0 \\ A - B(\zeta_1)_1 & C^* - 2A & -B(\zeta_1)_1 \\ 0 & A - B(\zeta_1)_2 & C^* - 2A \end{bmatrix} \begin{bmatrix} C_0^1 \\ C_1^1 \\ C_2^1 \end{bmatrix} = \begin{bmatrix} -2AC_1^0 + (2A + C^*)C_0^0 \\ (2A - C)C_1^0 - (A + B(\zeta_1)_1)C_2^0 + (B(\zeta_1)_1 - A)C_0^0 \\ 2AC_2^0 + (B(\zeta_1)_2 - A)C_1^0 - (A + B(\zeta_1)_2)(C_3^0 + C_3^1) \end{bmatrix}$$

Figure 44 Matrix re-arrangement of the above equations. This results in a system with 3 unknowns and 3 independent equations.

The method above describes how to obtain the three unknown values at each respective node at a specific time. The example to describe this method used a very coarse grid with a very small quantity of spatial nodes. A computer can handle many more nodes and their respective system of equations. This results in a much bigger square matrix than the one above. Regardless of matrix size, the matrix is a tridiagonal one. The best algorithm to solve this type of matrix is the Thomas Algorithm [88]. Using the Thomas Algorithm is more computationally efficient than using other more general matrix solvers such as the Gauss-Jordan.

A program in MATLAB was made to come up with a computational scheme to solve for the unknowns at a specific time step in the way discussed. A similar method as above is used to compute for the unknown spatial values in Region II at a time increment. Region II uses a different Landau transform on a different governing equation, but the methods used are the same as the ones covered for Region I. The solver begins by first solving for the values at all points of both Regions I and II for a specific time step. To do this, the solver uses the known boundary conditions, the values of the points at the last time step, and a guess value for  $S^{N+1}$  set as  $S^{guess}$ . The solver then uses the obtained spatial values for Regions I & II, at the current time step to obtain a value for  $S^{N+1}$ . This is done by first using the governing equation for Region III as given by eq. (80). This equation is

$$\frac{dS}{dt} = - \left( D_1 \frac{\partial C}{\partial x} \right)_{x=S^-} - \left( \frac{D_p}{C_{gel}} \frac{\partial C}{\partial x} \right)_{x=S^+}, \quad (116)$$

where  $D_1$  is the diffusion coefficient belonging to Region I and  $D_p$  belongs to Region II respectively. One must carry out the Crank-Nicolson approximation of eq. (116) at time step  $N + 1/2$ , since this is where the imaginary red circles in figure 46 were evaluated at. Doing this gives an approximation of the velocity of the moving boundary as

$$\left( \frac{dS}{dt} \right)^{N+1/2} \approx - \frac{D_1}{2} \left[ \left( \frac{\partial C}{\partial x} \right)_{x=S^-}^{N+1} + \left( \frac{\partial C}{\partial x} \right)_{x=S^-}^N \right] - \frac{D_p}{2C_{gel}} \left[ \left( \frac{\partial C}{\partial x} \right)_{x=S^+}^{N+1} + \left( \frac{\partial C}{\partial x} \right)_{x=S^+}^N \right]. \quad (117)$$

As discussed, the velocity of the moving boundary depends on the Polymer volume fraction gradients of Region I and Region II immediately in contact with the moving boundary. One handles the terms inside the first bracket by carrying out the Landau Transform for Region I. Then each partial derivative undergoes a Taylor approximation suggested by Langtangen [90] to approximate the partial derivatives to adjacent  $C$  values. Doing so allows one to approximate part of eq. (117) as

$$\left( \frac{dS}{dt} \right)^{N+1/2} \approx - \frac{D_1(3C_{M-1}^{N+1} - 4C_{M-2}^{N+1} + C_{M-3}^{N+1} + 3C_{M-1}^N - 4C_{M-2}^N + C_{M-3}^N)}{4 * \Delta \zeta_1 * \sqrt{S^N S^{guess}}} - \frac{k_d^{N+1} + k_d^N}{2C_{gel}}, \quad (118)$$

where the subscript ' $M$ ' denotes the spatial point where  $S$  is at in the transformed coordinate system. The ' $M - 1$ ' subscript is the nearest discrete spatial node to the left of  $S$  and in Region I. . The terms  $k_d^{N+1}$  and  $k_d^N$  are the loose polymer chain rate flows at their respective time steps  $t^N$  or  $t^{N+1}$  based on eqs. (81) & (82). One does not need to carry out the Landau transform for terms inside the second bracket in eq. (117), but instead one just needs to remember the relationships given by eqs. (81) & (82) with regards to these terms. The solver assigns both  $k_d^{N+1}$  and  $k_d^N$  a value of zero until their respective times are at least equal to the reptation time. When this is the case, either one is assigned the value of  $k_d$  from eq. (82). Langtangen's Taylor approximation is more accurate, but at the same time more complicated. It is used not only due to

higher accuracy, but because all of the  $C$ 's are on the left side and thus within Region I.

Approximating the bracketed terms with eq. (94) would require the adjacent  $C$  values on both sides of  $S$ . One cannot do this as the right-hand side  $C$  values belong to Region II and tell one nothing with regards to the polymer volume fraction gradient within Region I

Using the Taylor Approximation of eq. (94) allows to express  $\left(\frac{dS}{dt}\right)^{N+\frac{1}{2}}$  as

$$\left(\frac{dS}{dt}\right)^{N+\frac{1}{2}} \approx \frac{S^{N+1} - S^N}{\Delta t}, \quad (119)$$

where  $\Delta t$  is the size of the time step. Algebraic manipulation gives  $S^{N+1}$  approximately as

$$\Delta t \left(\frac{dS}{dt}\right)^{N+\frac{1}{2}} + S^N \approx S^{N+1}. \quad (120)$$

By using eq. (118) to replace the velocity of the moving boundary with the approximation, one finally obtains  $S^{N+1}$  for the current time step. The  $S^{N+1}$  of Eq. (120) depends on polymer volume fractions within Regions I and II as shown on the previous equations. This derived  $S^{N+1}$  is compared to the one that was taken as a guess and used to solve for the polymer volume fractions at all spatial points of Regions I and II for the given time step,  $S^{guess}$ . This will result in two cases. The first case is that  $S^{N+1}$  and  $S^{guess}$  are divergent, while the second case is that they are very alike numerically and thus convergent. If the first case occurs,  $S^{N+1}$  becomes a new  $S^{guess}$  and the Finite difference scheme is ran again for to obtain all the spatial values for Regions I & II using this new  $S^{guess}$  for the same time step. A new  $S^{N+1}$  is computed by using the new spatial values and a comparison is carried out again. After repeated attempts, one will obtain a second case for this time step where the  $S^{N+1}$  and  $S^{guess}$  values that are convergent. On the second case, a final spatial run using  $S^{N+1}$  is executed to get the final spatial values of Regions I and II for this time step. The solver then moves to the next time step,  $t^{n+2}$ , and solves for all the spatial nodes for this time by using the spatial values at the previous time step as assistance.. The new

$S^{guess}$  for this time step is taken to be  $S^{N+1}$  as an initial guess and the whole process above is repeated again for time step  $t^{N+2}$  until convergence . Figure 48 illustrates this whole process in flowchart form.

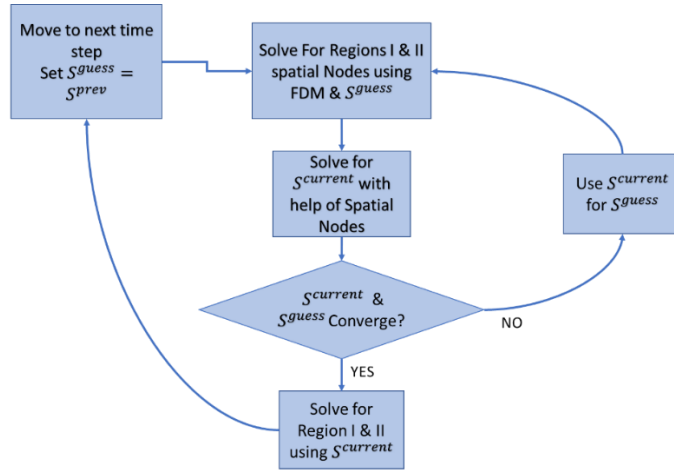


Figure 48 Flowchart showing how the MATLAB program solver tackles the problem.

## Model Results and Modifications

The MATLAB program qualitatively shows the behavior of the polymer-solvent system. Region I first swells while Region II shows no trace of polymer volume fraction at the beginning. Dissolution follows this swelling as polymer volume fractions becomes present within Region II and Region I eventually diminishes in size. Figure 49 shows the polymer volume fraction concentration profile at the very beginning of the problem. Here all of Region I is pure polymer and has a value of one in the vertical axis. Region 2 has no polymer and is thus has a value of zero. Initially Region I is from 0 to 1 in horizontal axis while Region II is the rest. A blue asterisk marks the location of Region III that connects the other two regions.

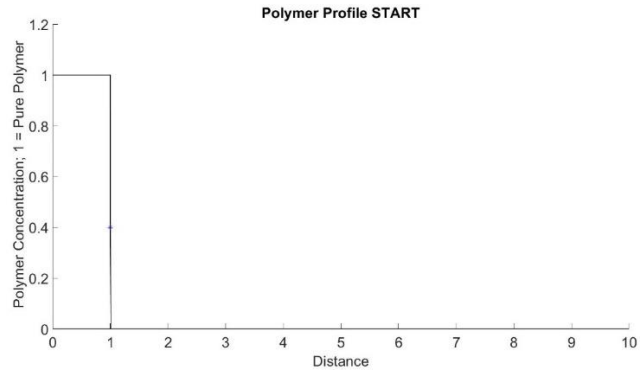


Figure 45 Polymer concentration profile at start. The blue asterisk marks the boundary between the bulk polymer and the solvent.

Figure 50 shows the evolution of the system at a later time prior to reptation. Here the polymer has become swollen with solvent, as some the locations within Region I are not fully pure anymore and thus have a volume fraction value of below one. Region II is still a pure solvent as it has zero polymer volume fraction everywhere. The expansion of the bulk polymer region one can be observed as the blue asterisk marking Region III has moved to the right with respect to figure 49.

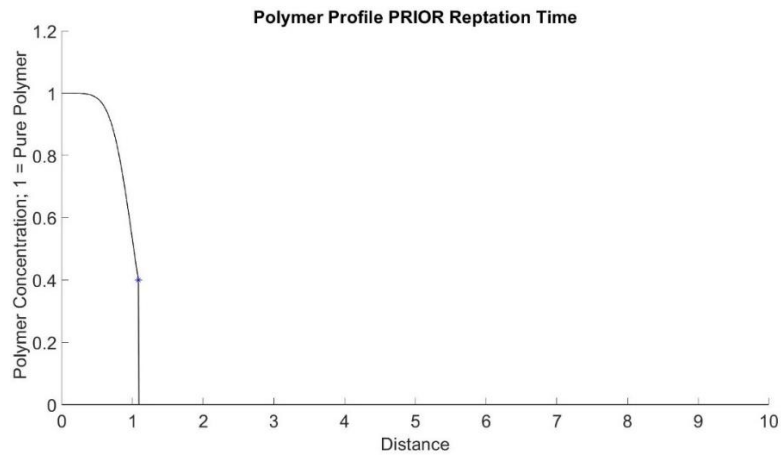


Figure 50 Polymer profile at a time prior to reptation. The asterisk shows the boundary between regions I and II. Notice that it has moved to show the expansion of the bulk polymer.

Figure 51 shows the system at a time past the reptation time. Here, Region I has decreased in size as the blue asterisk is to the left when compared to figure 50. Moreover, polymer volume fractions are now present in Region II. Since the time is greater than the reptation

time, polymer dissolution is occurring. Enough time has elapsed to allow for polymer chains to disentangle from the bulk polymer within Region I and to diffuse into Region II.

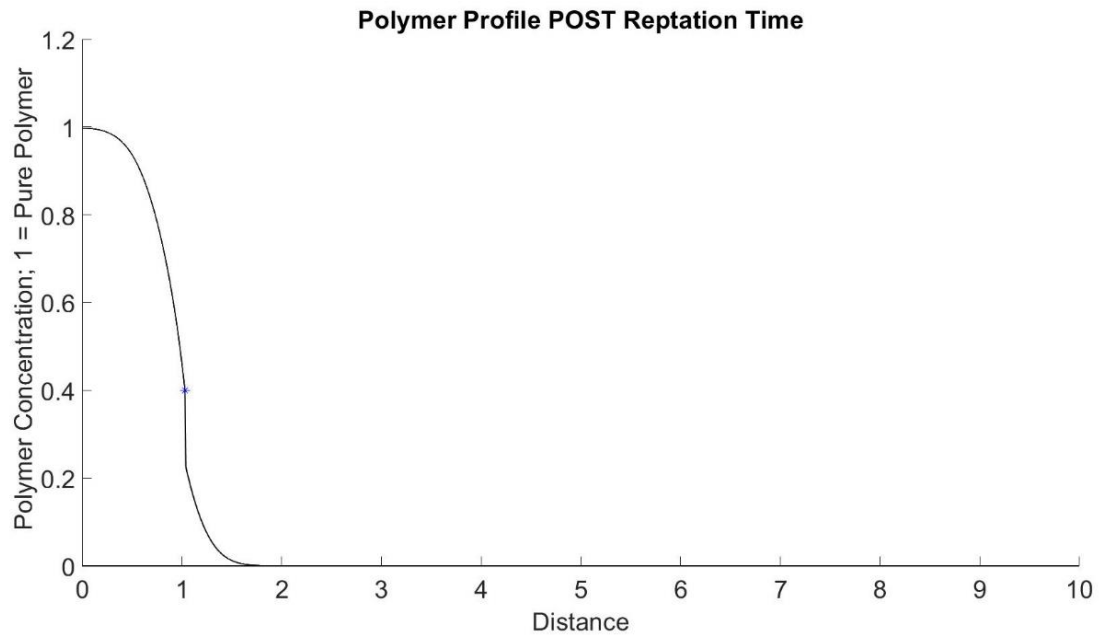


Figure 51 Polymer profile AFTER reptation. Now polymer present in the solvent region- to the right of the blue asterisk.

This polymer dissolution model showed the correct qualitative behavior, but problems arose when the model underwent closer analysis. First by adding a numerical integration scheme was added into the program. This integrator was used to show the total polymer at Region I at every time step. This integrator scheme is Simpson's 3/8<sup>th</sup> rule and computes the area under the curve to obtain the total polymer quantity. The integration scheme showed that in this model the total polymer quantity ends up NOT being conserved, even at time steps before the reptation time. Figure 52 shows proof of this. Here, the total polymer quantity as a percentage of the initial shows a steady but noticeable decrease. An initial conjecture of why this lack of conservation appeared was because the space and time steps were too large. Using large steps for FDM solvers increase the error in exchange for faster computation time. Running the program using smaller spatial and time steps did not solve for the lack of polymer conservation at Region I. And thus showed that the space and time step size was not the problem.

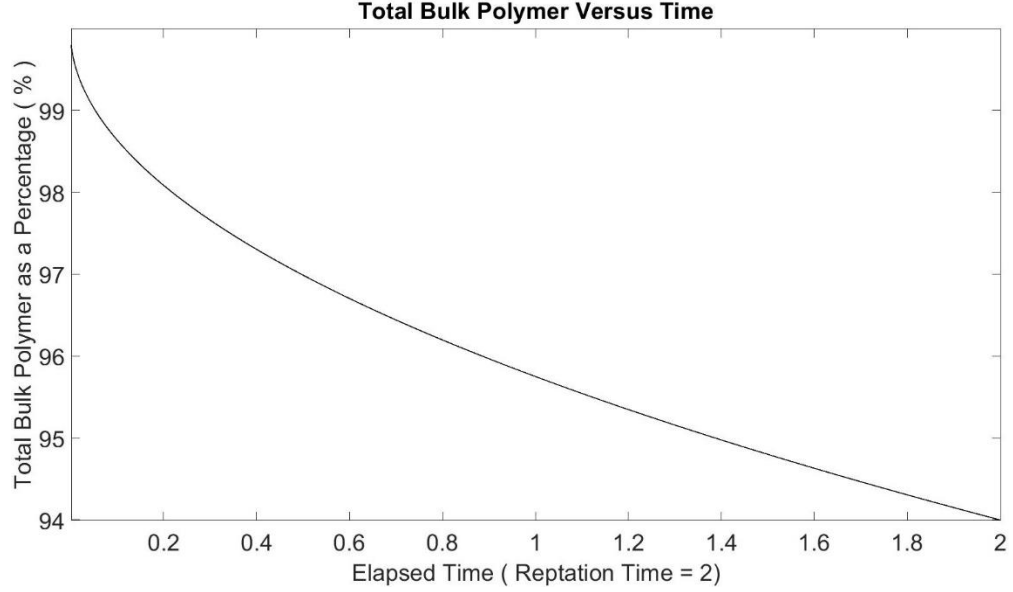


Figure 52 Total bulk polymer prior to reptation time. Mass is not conserved.

A closer inspection of the program allowed for debugging and correction of errors and typos. Moreover, an important alteration was done on the governing equation for Region III. The model used the governing equation from Peppas and Narasimhan [84]. This equation is

$$\frac{dS}{dt} = - \left( D_1 \frac{\partial C}{\partial x} \right)_{x=S^-} - \left( \frac{D_p}{C_{gel}} \frac{\partial C}{\partial x} \right)_{x=S^+} . \quad (121)$$

Both D's on the right hand side are diffusion coefficients. The first  $D_1$  is the mutual solvent-polymer diffusion coefficient within the polymer. While  $D_p$  is the mutual polymer solvent diffusion coefficient within the solvent. Both diffusion coefficient have the same units as follows:

$\frac{Length * Length}{time}$ . The first equation on the right hand side does lack the polymer volume fraction at the interface for Region III and was added accordingly. The addition modified eq. (121) to

$$\frac{dS}{dt} = - \left( \frac{D_1}{C_{gel}} \frac{\partial C}{\partial x} \right)_{x=S^-} - \left( \frac{D_p}{C_{gel}} \frac{\partial C}{\partial x} \right)_{x=S^+} . \quad (122)$$

Applying The modified equation results in a simulation that conserves the total polymer quantity in Region I. At the same time the program still shows the characteristic behavior of the polymer

both expanding, the diffusion of loose polymer chains into the solvent, and the eventual dissolution. Figure 53 shows the conservation of polymer within Region I:

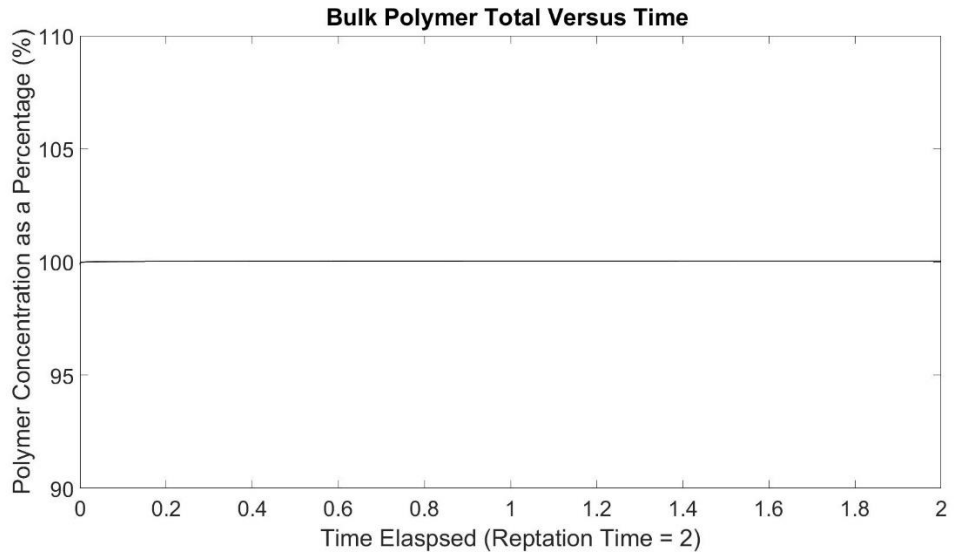


Figure 53 Bulk polymer quantity prior to reptation time. Now bulk mass is conserved.

One can see that the total polymer in Region I does not show decline prior to reaching reptation time. The polymer concentration is below 100 percent at the start. This is because the set up requires the last node to have the  $C_{gel}$  instead of a concentration of one. This artificially lowers the polymer concentration value at the start of the problem.

## **Chapter V: Conclusion & Future Work**

### **Conclusion**

This thesis introduces a numerical model and solver to reveal the swelling and dissolution of a polymer immersed in a compatible solvent. The main contribution of this work is the numerical model along with an in-depth explanation of the model's mechanism along with the results obtained from the model simulating a double moving boundary polymer dissolution problem.

With the development of new generation of dissolvable downhole tools, the oil and gas industry is looking for high performance dissolvable materials replacing conventional materials. Our group has demonstrated that packer component made from modified Polyvinyl Alcohol (PVA) can have comparable high temperature and high pressure performances as NBR components, but PVA can completely dissolve in aqueous fracking fluids. Water is not only a PVA solvent at high concentration, but it functionalizes as a plasticizer at low concentration. Thus it is of critical importance to understand the interactions between these two types of molecules.

This thesis first reviews the general concepts and characteristics of polymers. Discussions of glass transition and plasticizer effects have been included and also their effects on mechanical behavior of polymers. There was also a review on how water can behave as a plasticizer within PVA and change its mechanical behavior from plastic to rubbery-like.

PVA physiochemical properties, especially the mechanical performances changes dramatically during the swelling and dissolution process. During fracking applications, PVA elastomer components should meet the stringent and challenging performance requirements before disintegration. Thus, it is of critical importance to understand the PVA-water interaction

and be able to predict the material properties. This thesis tried to establish the numerical model to simulate and solve the polymer swelling-dissolution problem. We first looked at the thermodynamics of polymer-solution interaction to answer the important question of what determines the solubility of a solvent-polymer pair. Then we reviewed three classical kinematic models for polymer dissolution. These models provide a quantitative description of the general swelling and dissolution process: first the swelling of polymer resulted from the solvent molecule diffusion penetration, followed by polymer chains disentanglement from bulk polymer, and the receding of the polymer regions due to dissolution in solvent.

We setup the one-dimensional problem for PVA-water and derived the governing equations based on previous models. Such a double moving boundaries problem is difficult to solve analytically and various approximate approaches have been explored. In this study we first apply Landau Transform to the material system domains to handle the moving boundary problem. Then we apply the Finite Difference Method to numerically solve the problem. We also demonstrated how to use the iterative method to solve the location problem of the moving boundary at each time step. And finally we showed that the modification of governing equations is needed to maintain polymer mass conservation during the dissolution process.

In summary, the polymer dissolution problem mathematically belongs to the Stefan Problem Family. Problems of this type with moving boundaries are found in many areas of science and engineering to describe many physical phenomena such as crystallization and ablation. We believe this work can help researchers dealing with similar types of phenomena in derivation of governing equations and numerically solving the moving boundary problem.

## **Future Work Suggestions**

Einstein once famously stated that “Science is never finished.” This statement could not be more true with respect to this work. Like all science and engineering endeavors, each piece of

research and labor executed towards this work resulted in additional questions and conditions that had potential relevance for further investigation. Some ideas regarding future work, both experimental and numerical, will be discussed.

With respect to numerical future work, there are many possibilities. The governing equations published in this work had to be simplified to linear ones to be easier to deal with. The reason why is because the author at the time was a complete beginner into the Finite Difference method to numerically solve the polymer dissolution model. Linearization made the problem easier to solve, but solving the non-linear governing equations would give richer results. Another suggestion for further work is with regards to the non-Fickian Case II diffusion observed by Thomas et al. [75] and applied into polymer dissolution by Wu et al. [17]. As stated by Thomas, Case II diffusion is observed in situations where the operational temperature is low and the solvent in use is organic. Adding case II diffusion to the model published would make the model more generally applicable. Since water is not organic and the fracking well temperature is very often high, the published model should be valid in this narrow case. Including the Case II diffusion term would make the model's scope broader. One final possible suggestion for future work is to expand the model to two or even three spatial dimensions. All of the models covered and the model presented here dealt with polymer dissolution in only a one dimensional system. For more complete results, polymer dissolution must be modeled at least in two dimensions. This adds an additional layer of complexity into the dissolution problem, but doing so would set the model unique with respect to the reviewed models. Crank [82] reviewed some Stefan Problems in higher dimensions. These models demanded higher computational resources and the commonly used schemes for one dimensional problems fall short of being useful here.

Unlike numerical work, there was very little if any experimental results presented in this thesis. This is due to both time and monetary limitations as experimental work consumes both in large quantities. Devotta et al. [73] and Wu et al. [17] both published experimental work

alongside with their numerical work. The experimental work served both to corroborate their numerical models and to serve as a source for the numerical value of various parameters such as diffusion constants. Konidari [60] also published experimental results showing how the water content within PVA affected the mechanical properties of PVA. Various derivatives of PVA exists and many lack experimental data beyond what is required to be published by the manufacturer. Experimental work will be necessary for further studying the potential role of PVA as the packer component in a frac plug. For example, while undergoing dissolution, regions of the PVA will take in water and because of this there will be a gradient of material properties throughout. How this gradient influences both the mechanical behavior and the performance of the packer is an open question that will require experimental labor to give an answer to.

## References

- [1] Gold, R., 2014, *The Boom: How Fracking Ignited the American Energy Revolution and Changed the World*, Simon & Schuster, NY.
- [2] Anderson, J., 2019, “US Shale Industry Credited with Driving 10% of US GDP Growth,” *Energy In Depth*, from <https://www.energyindepth.org/us-shale-industry-credited-with-driving-10-of-us-gdp-growth>.
- [3] “What is Fracking?” *What is Fracking?*; ReFINE; from <http://www.refine.org.uk/aboutrefine/whatisfracking/>.
- [4] “Horizontal Well Stimulation: Contrast Between Plug and Perf Method and Ball and Sleeve Method for Horizontal Well Stimulation.” *Stonewall Engineering*, from: <https://info.stonewallco.com/stonewall-horizontal-well-stimulation>
- [5] Hou, Y. & Galland, P., Davies, E., Vanlue, D., and Johnson, M., 2014, “Performance tests of Boss Hog Frac Plugs under Temperature and Pressure,” Houston.
- [6] Crump, M, 2019, “Traditional Frac Plugs: How They Work.” *Rubicon Oilfield International*, from <https://www.rubicon-oilfield.com/traditional-frac-plugs-work/>.
- [7] Crump, M, 2015, “Zonal Isolation: Composite Frac Plugs Optimize Cost, Capabilities In Plug-And-Perf Completions.” *The American Oil and Gas Reporter*, from <https://www.aogr.com/magazine/cover-story/composite-frac-plugs-optimize-cost-capabilities-in-plug-and-perf-completion>.
- [8] “MVP High Temp.” *Nine Energy Service*, from <https://nineenergyservice.com/completions-technologies/dissolvables/mvp>.
- [9] Crump, M., 2019, “Composite Plug Milling: Bit Selection for 5.5’ Completions.” *LinkedIn*, from <https://www.linkedin.com/pulse/composite-plug-milling-bit-selection-55-completions-crump-p-e/>.
- [10] “Boss Hog Frac Plug,” *YouTube Video*, 2015, <https://www.youtube.com/watch?v=JJj-QG6Zyyw>

- [11] Chauffe, S. and Ray, J., 2018, "Fully Dissolvable Frac Plug Results in Efficiency Gains in Long Lateral Completions," *World Oil*, vol. 239 (6), pp. 33-37.
- [12] 2014, "Magnum Oil Tools Develops World's First Dissolvable Frac Plug." *Business Wire*, from <https://www.businesswire.com/news/home/20141118005345/en/Magnum-Oil-Tools-Develops-World%E2%80%99s-Dissolvable-Frac>.
- [13] Li J., Misselbrook, J., and Sach, M., 2010, "Sand Cleanouts with Coiled Tubing: Choice of Process, Tools and Fluids," *J. Can. Petrol. Technol.*, vol. 49(8), pp. 69–82.
- [14] Pérez-Ràfols, F. and Larsson, R., and Almqvist, A., 2016, "Modelling of Leakage on Metal-to-Metal Seals," *Tribol. Int.*, vol. 94, pp. 421–427.
- [15] C. Pirie, 2018, "Origin of the humble O-ring," *Cor Elastomers*, from <https://cormanufacturing.com/index.php/2018/08/22/origin-of-the-humble-o-ring/>.
- [16] Miller-Chou, B. A. and Koenig, J. L., 2002, "A Review of Polymer Dissolution," *Prog. Polym. Sci.*, vol. 28(8) pp. 1223–1270.
- [17] Peppas, N. A., Wu, J. C., and Meerwall, E. D. V., 1994, "Mathematical Modeling and Experimental Characterization of Polymer Dissolution." *Macromolecules*, vol. 27(20), pp. 5626–5638.
- [18] Wu, J, 1992, "Solvent Diffusion & Dissolution in Glassy Polymers," Ph.D. thesis, Department of Chemical Engineering, Purdue University.
- [19] Rubinstein, M. and Colby, R. H., 2016, *Polymer physics*, Oxford University press, Oxford, Chap. 9.
- [20] de Gennes, P. G., 1971, "Reptation of a Polymer Chain in the Presence of Fixed Obstacles," *J. Chem. Phys.*, vol. 55(2), pp. 572–579.
- [21] Saldívar-Guerra, E. and Vivaldo-Lima, E., 2013, *Handbook of polymer synthesis, characterization, and processing*, Wiley, Hoboken, NJ, Chap. 1.

- [22] Clark, J. and Reusch, W., 2020, "27.8: Polymers and Polymerization Reactions." Chemistry LibreTexts, from [https://chem.libretexts.org/Bookshelves/General\\_Chemistry/Map:\\_General\\_Chemistry\\_\(Petrucci\\_et\\_al.\)/27:\\_Reactions\\_of\\_Organic\\_Compounds/27.08:\\_Polymers\\_and\\_Polymerization\\_Reactions](https://chem.libretexts.org/Bookshelves/General_Chemistry/Map:_General_Chemistry_(Petrucci_et_al.)/27:_Reactions_of_Organic_Compounds/27.08:_Polymers_and_Polymerization_Reactions).
- [23] Rudin, A. and Choi, P., 2013, The elements of polymer science and engineering, Elsevier, San Diego, CA, Chap. 1.
- [24] Peng, H., Sun, X., Weng, W., and Fang, X., 2017, Polymer Materials for Energy and Electronic Applications, Academic Press, Amsterdam, Netherlands, Chap. 1.
- [25] Painter, P. C. and Coleman, M. M., 2009, Essentials of polymer science and engineering, DEStech Publications, Lancaster, PA.
- [26] 1999, "Hermann Staudinger and the Foundation of Polymer Science." American Chemical Society, from <https://www.acs.org/content/acs/en/education/whatischemistry/landmarks/staudingerpolymerscience.html>.
- [27] Wilson, F., 2020, "Polymer Market to Attain Valuation US\$ 158.4 Bn by 2026." PR Newswire: press release distribution, targeting, monitoring and marketing, from <https://www.prnewswire.com/news-releases/polymer-market-to-attain-valuation-us-158-4-bn-by-2026--301006585.html>.
- [28] Osswald, T. A. and Menges, G., 2012, Material Science of Polymers for Engineers, Hanser, Munich, Germany, Chap. 9.
- [29] Findley, W. N., Lai J. S. Y., and Onaran, K., 1990, Creep and Relaxation of Nonlinear Viscoelastic Materials, with an Introduction to Linear Viscoelasticity, Dover, New York, NY.

- [30] Ferrás, L.L, Ford, N., Morgado, M. L., Rebelo, M., and Mckinley, G., 2017, “How Non-Integer Order Derivatives Can be Useful to Rheology,” 3rd International Conference on Numerical and Symbolic Computation: Developments and Applications.
- [31] Reiner, M., 1964, “The Deborah number,” *Phys. Today*, vol. 17(1), pp. 62.
- [32] 2020, “Rheology of Polymers.” AZoM.com, from <https://www.azom.com/article.aspx?ArticleID=12099>.
- [33] Belfiore, L. A., 2010, *Physical Properties of Macromolecules*, Wiley, Hoboken, N. J, Chap. 1.
- [34] White, R. P. and Lipson, J. E. G., 2016, “Polymer Free Volume and Its Connection to the Glass Transition,” *Macromolecules*, vol. 49, pp. 3987–4007.
- [35] Cohen, M. D. and Turnbull, D., 1959, “Molecular Transport in Liquids and Glasses,” *J. Chem. Phys.*, vol. 31(5), pp. 1164–1169.
- [36] D. Turnbull and M. H. Cohen, 1961, “Free - Volume Model of the Amorphous Phase: Glass Transition,” *J. Chem. Phys.*, vol. 34(1), pp. 120 - 125.
- [37] Ziman, J. M., 2006, *Principles of the theory of solids*, World Books Publishing Corporation, Beijing, China.
- [38] Oliver M. and Cranford, S., 2009, “Thermal Expansion,” from <http://web.mit.edu/mbuehler/www/SIMS/Thermal%20Expansion.html>.
- [39] Dong, H. and Jacob, K. I., 2003, “Effect of Molecular Orientation on Polymer Free Volume Distribution: An Atomistic Approach,” *Macromolecules*, vol. 36(23), pp.8881-8885.
- [40] Callander, B., 2005, “Molecular Modeling of Polymer Free Volume Distribution,” Ph.D. thesis, Department of Chemical and Biological Engineering, Georgia Institute of Technology.

- [41] Wypych, J. G., Marcilla, A., and Beltran, M., 2012, Handbook of plasticizers, ChemTec Publishing, Toronto, Canada, pp. 119–131. Chap. 5.
- [42] Leaderman, H. G., 1958, “Mechanical properties of High polymers,” Annu. Rev. Phys. Chem, vol. 9, pp. 179-200.
- [43] Thomas, S., Yang, W., and Sunny, A. T., 2009, Advances in polymer processing, Woodhead Publishing, Abington, United Kingdom, Chap. 3.
- [44] 2015, “Polymer Properties Database.” Stress-Strain Behavior of Polymers, from <https://polymerdatabase.com/polymer physics/Stress-Strain Behavior.html>.
- [45] Bukhina, M. F. and Kurlyand, S. K., 2007, Low-Temperature Behaviour of Elastomers, VSP, Leiden, Netherlands, Chap. 1, pp. 11–42.
- [46] Deanin, R. D., 1990, Polymer Structure and Practical Properties: Applications in Plastics Elastomers, Coatings and Adhesives, Technomic Pub. Co., Lancaster, PA.
- [47] Harish, A., 2019, “The Challenger Disaster: Deadly Engineering Mistakes,” SimScale Blog, from <https://www.simscale.com/blog/2019/01/space-shuttle-challenger-disaster/>.
- [48] Rogers, W. L., Armstrong, N. A., Acheson, D. C., Covert, E. E., Feynman, R. P., Hotz, R. B., Kutyna, D. J., Ride, S. K., Rummel, R. W., Sutter, J. F., Walker, A. B., Wheelon, A. D., Yeager, C. E., 1986, “Report of the Presidential Commission on the Space Shuttle Challenger Accident,” Presidential Commission, Washington, D.C.
- [49] 2016, “Guide to Elastomers in Oil & Gas Industry.” Daleel Supply Chain Management Network, from <https://www.scmdaleel.com/article/guide-to-elastomers-in-oil-amp-gas-industry/249>.
- [50] Patel, H., Salehi, S., Ahmed, R., and Teodoriu, C., 2019, “Review of Elastomer Seal Assemblies in Oil & Gas Wells: Performance Evaluation, Failure mechanisms, and Gaps in Industry Standards,” J. Petrol. Sci. Eng., vol. 179, pp. 1046–1062.

- [51] Elhard, J. D, Duguid, A., and Heinrichs, M. ,2017, “Research on Safety Technology Verification for Materials and Corrosions in the U.S. Outer Continental Shelf (OCS), High Pressure High Temperature (HPHT) Material Evaluation,” Final Report, Bureau of Safety and Environmental Enforcement, Washington, D.C.
- [52] Fernandez, C. and Castaño, P., 2016, “Compatibility Behavior of Elastomers for PCP Application,” CORROSION CONFERENCE AND EXPO, vol. 1, 2016, pp.348-359.
- [53] Riou, A., 2017, “Elastomer Engineering Guide,” James Walker, Surrey, United Kingdom.
- [54] Bohnet, M., Hallensleben, M. L., Fuss, R., and Mummy, F., 2000, Ullmann's Encyclopedia of industrial chemistry, Wiley-VCH, Weinheim, Germany.
- [55] 2010, “Polyvinyl Alcohol Production.” Polyvinyl Alcohol Production 2010 – Chemical production and investment cost, from [//ihsmarkit.com/products/chemical-technology-pep-reviews-polyvinyl-alcohol-production-2010.html](https://ihsmarkit.com/products/chemical-technology-pep-reviews-polyvinyl-alcohol-production-2010.html).
- [56] 2020, “Polyvinyl alcohol.” Wikipedia, from [https://en.wikipedia.org/wiki/Polyvinyl\\_alcohol](https://en.wikipedia.org/wiki/Polyvinyl_alcohol).
- [57] Mathias, L. J., 2020, “Poly (Vinyl Acetate).” The Polymer Science Learning Center, from <https://pslc.ws/macrog/pva.htm>.
- [58] More, A., 2020, “Polyvinyl Alcohol (PVA) Market Forecast 2020-2024 By Global Industry Trends, Future Growth, Regional Overview, Size, Share Estimation, Revenue, and Outlook, Says Industry Research Biz,” MarketWatch, from <https://www.marketwatch.com/press-release/polyvinyl-alcohol-pva-market-forecast-2020-2024-by-global-industry-trends-future-growth-regional-overview-size-share-estimation-revenue-and-outlook-says-industry-research-biz-2020-05-22>.
- [59] Wilkes, C. E., Summers, J. W., Daniels, C. A., and Berard, M. T., 2020, PVC handbook. Hanser, Munich, Germany.

- [60] Konidari, M. V., Papadokostaki, K. G., and Sanopoulou, M., 2011, “Moisture-Induced Effects on the Tensile Mechanical Properties and Glass-Transition Temperature of Poly (Vinyl Alcohol) Films,” *J. Appl. Polym. Sci.*, vol. 120(6), pp. 3381–3386.
- [61] Greenspan, L., 1977, “Humidity Fixed Points of Binary Saturated Aqueous Solutions,” *J. Res. Natl. Bur. Stand. (U. S.)*, vol. 81A(1), pp. 89-96.
- [62] Hassan, C. M. and Peppas, N. A., 2000, “Cellular PVA Hydrogels Produced by Freeze/Thawing,” *J. App. Polym. Sci.*, vol. 76(14), pp. 2075–2079.
- [63] Flory, P. J., 1942, “Thermodynamics of High Polymer Solutions,” *J. Chem. Phys.*, vol. 10, pp. 51–61.
- [64] Hill, T. L., 2012, *An Introduction to Statistical Thermodynamics*, Dover Publications, Mineola, NY, Chap. 21.
- [65] 2020, “Flory–Huggins solution theory,” Wikiwand, from [https://www.wikiwand.com/en/Flory%E2%80%93Huggins\\_solution\\_theory](https://www.wikiwand.com/en/Flory%E2%80%93Huggins_solution_theory).
- [66] Wilhelm, E., 2018, “Mitigating Complexity: Cohesion Parameters and Related Topics. I: The Hildebrand Solubility Parameter,” *J. Solution Chem.*, vol. 47(10), pp. 1626–1709.
- [67] Burke, J., 1984, *Solubility Parameters: Theory and Application*, The Oakland Museum CA, Oakland, CA.
- [68] Carvalho, S. P., Lucas, E. F., González, G., and Spinelli, L. S., 2013, “Determining Hildebrand Solubility Parameter by Ultraviolet Spectroscopy and Microcalorimetry,” *J. Brazilian Chem. Soc.*, vol. 42(12), pp. 1998-2007.
- [69] C. M. Hansen, 2004, “50 Years with Solubility Parameters—Past and Future,” *Prog. Org. Coat.*, vol. 51(1), pp. 77–84.
- [70] Hansen, C.M., 1967, “The Three Dimensional Solubility Parameter and Solvent Diffusion Coefficient: Their Importance in Surface Coating Formulation,” Ph.D. thesis, The Technical University of Denmark.

- [71] Hansen, C. M., 1969, "The Universality of the Solubility Parameter," *Ind. Eng. Chem. Prod. Res. Dev.*, vol. 8(1), pp. 2–11.
- [72] Louwerse, M. J., Maldonado, A., Rousseau, S., Moreau-Masselon, C., Roux, B., and Rothenberg, G., 2017, "Revisiting Hansen Solubility Parameters by Including Thermodynamics," *ChemPhysChem*, vol. 18(21), pp. 2999–3006.
- [73] Hansen, C. M., 2020, "Hansen Solubility Parameters: Hansen Solubility Parameters." Hansen Solubility Parameters, from <https://www.hansen-solubility.com/>.
- [74] Süß, S., Sobisch, T., Peukert, W., Lerche, D., and Segets, D., 2018, "Determination of Hansen Parameters for Particles: A Standardized Routine Based on Analytical Centrifugation," *Adv. Powder Technol.*, vol. 29(7), pp. 1550–1561.
- [75] Tu, Y. O., 1977, "A Multi-Phase Stefan Problem Describing the Swelling and the Dissolution of Glassy Polymer," *Q. Appl. Math.*, vol. 35(2), pp. 269–285.
- [76] Devotta, I., Ambeskar, V., Mandhare, A., and Mashelkar, R., 1994, "The Life Time of a Dissolving Polymeric Particle," *Chem. Eng. Sci.*, vol. 49(5), pp. 645–654.
- [77] 2020, "Spherical coordinate system," Wikipedia, from [https://en.wikipedia.org/wiki/Spherical\\_coordinate\\_system](https://en.wikipedia.org/wiki/Spherical_coordinate_system).
- [78] Thomas, N. L. and Windle, A. H., 1980, "A Deformation Model for Case II Diffusion," *Polymer*, vol. 21(6), pp. 613–619.
- [79] Thomas, N. L. and Windle, A. H., 1982 "A Theory of Case II Diffusion," *Polymer*, vol. 23(4), pp. 529–542.
- [80] Durning, C. J., 1985, "Differential sorption in viscoelastic fluids," *J. Polym. Sci.: Poly. Phys.*, vol. 23(9), pp. 1831–1855.
- [81] Papanu, J. S., Hess D. H., Soane, D. S., and Bell, A. T., 1989, "Dissolution of Thin Poly(methyl methacrylate) Films in Ketones, Binary Ketone/Alcohol Mixtures, and Hydroxy Ketones," *J. Electrochem. Soc.*, vol. 136(10), pp. 3077.

- [82] Pearson, R. A. and Sperling, L. H., 2006, Introduction to physical polymer science, 4th Edition., Wiley and Sons Hoboken, NJ, Wiley and Sons, Chap. 9, pp. 427–489.
- [83] Flory, P. J., 1953, Principles of polymer chemistry, Cornell University Press, Ithaca, NY, Chap. 13, pp. 541–594.
- [84] Narasimhan, B. and Peppas, N. A., 1996, “Disentanglement and Reptation During Dissolution of Rubbery Polymers,” J. Polym. Sci. Polym. Phys., vol. 34(5), pp. 947–961.
- [85] Crank, J., 1984, Free and Moving Boundary Problems, Clarendon Press, Oxford, United Kingdom.
- [86] Crank, J., 1975, The Mathematics of Diffusion, Clarendon Press, Oxford, United Kingdom.
- [87] Landau, H. G., 1950, “Heat Conduction in a Melting Solid,” Q. Appl. Math., vol. 8(1), pp. 81–94.
- [88] Chapra, S. C. and Canale, R. P., 2004, Numerical Methods for Engineers: with Software and Programming Applications, McGraw Hill, Boston, Ma.
- [89] Leveque, R. J., 2007, Finite Difference Methods for Ordinary and Partial Differential Equations: Steady-State and Time-Dependent Problems, Society of Industrial Applied Mathematics, Philadelphia.
- [90] Langtangen, H. P. and Linge, S., 2018, Finite Difference Computing with PDEs A Modern Software Approach, Springer International Publishing, Cham, Switzerland.

## Appendices

### A. MATLAB Script

```
% *****  
% *****READ 1st*****  
% *****  
% CAUTION: RUNNING THIS WILL CLEAR ALL PAST VALUES due to 'clear all' command  
within  
% This script has as many comments as possible to give the best explanation possible  
% If a comment ends with '...', it immediately continues on the next line  
% So for example:  
% The quick brown fox jumps over the...  
% lazy dog.  
% Solution done by S. E. Y. for Dr.Sun's Functional Materials Group  
% Department of Materials and Mechanical Engineering  
% University of Houston, Texas, United States  
% 2nd Solution Attempt for 2-Phase Stefan Problem  
% Changing BC to Region II  
% Also re-writing solver for Region II to aparent mistake  
% Governing Equations will be Based on:  
%(1)"Disentanglement and Reptation During Disolution of Rubbery Polymers"  
% by: NARASIMHAN and PEPPAS  
%(2)"Mathematical Modeling and Experimental Characterization of Polymer Dissolution"  
% By: PEPPAS and WU  
%(3)"HE LIFE TIME OF A DISSOLVING POLYMERIC PARTICLE"  
% By: Devotta, Ambeskar, et al.  
%(4): "A MULTI-PHASE STEFAN PROBLEM DESCRIBING THE SWELLING AND THE....  
%DISSOLUTION OF GLASSY POLYMER"  
% By: Tu and Olano  
%Governing Equations will be kept LINEAR for now  
% Can use this model to help up for the Non-Linear Solution to Problem  
% 1-D Problem  
% Went over derivation on paper from scratch and altered program  
% accordingly  
% Seems to give out consistant data output with respect to changing dt  
% See ' 2-Phase Stefan Polymer Derivation' to see derivation &  
% arguements  
% Will use this script to as foundation to build on non-linear 2-phase stefan problem  
% May also have potential for 2-D modeling  
% *****  
% *****  
% *****  
clear all;  
clc;  
% For capturing on film; will be in same folder as where  
% will use getframe,movie and movie2avi commands  
movie = 0; % set this to '1' to make a recording of the simulation
```

```

if movie == 1
v = VideoWriter('Linear_Stefan_2Phase_Problem.avi'); % Will make a movie of the simulation if
movie set to 1;
v.Quality = 90; %Do NOT INTERRUPT PROGRAM OR ELSE WILL BE AN INCOMPLETE
MOVIE
open(v);
end
%*****Time Parameter*****
dt= .0001; % time step
t_length= 4; %total elapsed time of polymer dissolution simulation
t = 0 : dt: t_length ; % total time step is t_length/dt + 1
M= length(t);
t_rep = 2 ; % Polymer reptation time; time needed for chains to disentangle- NO dissolution prior
to this
M_rep = (t_rep/dt) + 1;
time_step= [ ' The Solutions time step is: ', num2str(dt) ] ; % to print on the plot how large the
time step is
time_rep = [ ' The Reptation time of the Polymer is : ', num2str(t_rep)]; % prints the reptation time
for the polymer
%*****

%*****Landau Transforms*****
%***** Executing Landau Transform for Region 1:*****
% eta1 = x/s(t)
% Such that will be between 0 to 1
deta1 = .001; % size of space incremenet in transformed space for region I
eta1 = 0 : deta1 : 1 ; % total number of spatial nodes will be: 1/deta1 + 1;
N1 = length(eta1); % How many Spatial nodes in total
Region_I_Step = [ 'Region I incremental step is: ', num2str( deta1) ];
%*****Executing Landau Transform for Region 2:*****
% eta2 = ( x- s(t) )/( L - s(t) )
% x = eta2*( L -s(t) ) + s(t)
deta2 = .001; %size of space incremenet in transformed space for region I
eta2 = 0 : deta2 : 1 ; % total number of spatial nodes will be: 1/deta1 + 1;
N2 = length(eta2); %How many spatial nodes in total
Region_II_Step = [ 'Region II incremental step is: ', num2str( deta2) ];
L= 10; % end of boundary layer - will use with eta2
%*****

% Allows to define length dimension of the matrix results
% use this to glue regions I and II together for a final plottable output
N = N1 + N2 - 1;

%Defining S, X, and U matrices
S = zeros( 1 , M ); % moving boundary S(t) also known as Region III; One for each time step
S( 1 ) = 1; % S location at start of problem; look at 'bar' picture....
% demarking boundary between Regions I and II
% Therefore, total length of Region I: 0 to S(t)
%         total length of Region II: L - S(t)
% Notice since S(t) changes with respect to time, the respective domains...
% also change

```



```

% dU1
% --- = 0 Therefore, will be a Neumann Boundary Condition
% dx
% *****
% @ S(t):
U_Gel = .40; % how much % vol is GEl @ S(t)
U_Solv = 1 - U_Gel; % how much % vol is SOLVENT
U1( : , N1) = U_Gel;
U2( : , 1 ) = U_Gel;% Gel/solvent layer has a characteristic concentration...
%that can be determined by use of Flory-Rehner formula
% *****
% @ S(t)+ (solvent side): BC for Region II (solvent)
% -D_p dU/dx = 0 if t < t_rep
% Also:
% -D_p dU/dx = k_d if t > t_rep
% *****
% @ B:
U2( : , N2) = 0; % Assuming once far away enough from boundary layer, will...
%be nil polymer at this level

% Diffusion Parameters With Boundary Conditions:
D_12= .02; % Poylmer Region I diffusion rate
D_p = .05;
k_d = .05 ; % Disentanglement rate
% Setting up Parameters & Conditions to Solve for Problem:
%For helping solve with the tri-diagonal matrix & Thomas Algorithm:
% These values are just placeholders to save computational time; defined
% here to prevent MATLAB from synthesizing them over and over again
% These values will make the part of the Tri-diagonal matrix that will be
% used to solve for the polymer volume fractions @ all spaces within Region I
% _____
%|f1(1) g1(1) 0    0 ...| U1(1)| |h1(1)|
%|e1(2) f1(2) g1(2) 0 ...| U1(2)| |h1(2)|
%| 0  e1(3) f1(3) g1(3) ...| U1(3)| = |h1(3)|
% 0  .  .  .  .
% Every row will only have three unknowns
e1 = zeros( 1 , N1 ); f1 = zeros( 1 , N1 ); g1 = zeros( 1 , N1 ); h1 = zeros( 1 , N1 );

% There are the same for Region II and will have same ASCII matrix
% arrangement as above:
e2 = zeros( 1 , N2 ); f2 = zeros( 1 , N2 ); g2 = zeros( 1 , N2 ); h2 = zeros( 1 , N2 );

%Place-Holders used in Tri-diagonal solver:
%will be assigned numerical values during each matrix solving step
A= 0; B = 0; C = 0; D = 0; E = 0; lambda = 0; lambda_prev = 0;
E_prev= 0;
E = ( (2 *deta2)*( L - S(1) ) )/D_p;

% For computing errors & getting condition statements to make simulation
% work:
Nicole = 0; % will keep computation in 'while' loop until condition met; will be...

```

```

%changed to 4- This allows one to iterate and solve for S(t) at a current time step
Reverse_Landau_1 = 0; % For helping transform back etas into x's s.t. can plot output...
%Kaori_1 will execute reverse Landau Transform for each value in Region I
Reverse_Landau_2 = 0; % For helping transform back etas into x's s.t. can plot output...
%Kaori_2 will execute reverse Landau Transform for each value in Region II
counter= zeros( 1, M ); % keeps track of iterations taken at each time step...
% to find a convergent S(t)- want to see how fast convergence occurs
error_counter = 250 ; % Sets limits for how many iterations are allowed within...
% a time step to find S(t)- if this was not here, program could be stuck forever
Error1 = 0 ; % This error 'turns on' if there is a failure to iterate- One...
%cannot find a convergent S(t) for a time step within an allowed iteration limit
Error2 = 0 ; % This error 'turns on' if there is a boundary mmis-match between regions 1 & 2
Error1_message =[ 'The Number of Iterations Allowed is the Following: ',
num2str(error_counter) ];
sum = zeros( 1 , M );

% for solving for first X's Location; remember landau transform
Reverse_Landau_1 = S(1); % for helping solve back to x's Landau Transform is x(k) = S(t)/eta(k)
Reverse_Landau_2 = L - S(1);
for k = 2: 1: N1
    X1(1, k) = Reverse_Landau_1*eta1(k);
end
for k = 1:1: N2 - 1
    X2(1, k) = eta2(k)*Reverse_Landau_2 + Reverse_Landau_1;
end

% *****
% *****START OF SOLVER
LOOP*****
% *****
for m = 2 : 1 : M % Counting of time steps for governing equation
    %space is nested within it and will be solve for the volume fraction
    %values for all nodes within Regions I and II within the current time
    %step
    S_guess = S( m - 1 );
    lambda_prev = lambda;
    E_prev = E;
    Nicole = 0; % Must be set to zero s.t. can enter 'while' loop iteration and solve for...
    % all volume fraction values within this time step; must set to zero at
    % every time step to go inside nested if Nicole is zero, will be able...
    %to go inside the nested 'while' loop below
    if Error1 > 0 % This tells that iteration failed at the previous time...
        %step and will exit the solver
        % Will also print out the following as an output for an error:
        disp('*****')
        disp('*****')
        disp('    Failure to iterate within allowed attempts    ')
        disp('          Exiting Program          ')
        disp(l)
        disp(Error1_message)
    end
end

```

```

disp('*****')
disp('*****')
disp('          ')
disp('          ')
break
end

while Nicole < 1 %Condition to remain at iteration until convergence is
% is achieved for all spatial at respective time step or exit if it
% fails to do so
%*****
%*****Beginning of Solver for U1*****
%*Here solving for volume fraction for all space values at Region I
%*****
% Solver for first matrix row: must solve for u1(1); Neumann BC
% Values obtained by taking Crank-Nicolson and proper
% discretization scheme at every space node
A = S_guess*S(m - 1)/dt;
B = -eta1(1)*S_guess*( ( (S_guess - S(m - 1) )/dt )*(1/(4*deta1) ) );
C = -D_12/( 2*deta1*deta1);
%
f1( 1 ) = A - 2*C; % so these two are the first row values on matrix set-up
g1( 1 ) = 2*C;

% h1(1) consists of known values; polymer volume fractions that
% are known at adjacent points will be first row value of h
h1( 1 ) = ( A + 2*C)*U1( m - 1 , 1); % ALL U( m - 1 , 1)
h1( 1 ) = h1( 1 ) + ( - 2*C)*U1( m - 1 , 2); % + ALL U1( m - 1 , 2);
% No U( m - 1 , -1) as is equal to U( m - 1 , 2)- see line above
%
%Now do Crank-Nicolson half-step approximation at every...
%imaginary half-time step node and express partial derivatives...
%At every discrete point as adjacent polymer fraction values
%'for'loop enables one to do this to all nodes except the boundary..
%condition nodes-since these two nodes have 2 row values rather...
% than three
for n = 2 : 1 : N1 - 2 % setting up matrix for middle block

% here are combinates for taking the PDE as discrete at every..
%point
A = S_guess*S(m - 1)/dt;
B = -eta1(n)*S_guess*( ( (S_guess - S(m - 1) )/dt )*(1/(4*deta1) ) );

C = -D_12/( 2*deta1*deta1);
% so every the volume fraction at every spatial node will be...
% a combination of three nodes
e1( n ) = -B + C;
f1( n ) = A - 2*C;
g1( n ) = B + C;
% Here are past and known values that help solve for U1( n)...
% for the current time step

```

```

% ALL U0-same space in the past:
h1( n ) = (A + 2*C)*U1( m - 1, n);
% ALL U+1: adding right adjacent spaces in the past:
h1( n ) = h1( n ) + (-B - C)*U1( m - 1 , n + 1 );
% All U-1: adding left adjacent spaces in the past:
h1( n ) = h1( n ) + ( B - C)*U1( m - 1 , n - 1 );
end
% Solving for last Node in matrix (Dirichlet Condition)
A = S_guess*S(m - 1)/dt;
%      B = -eta1(N1-1)*S_guess*( ( S_guess - S(m - 1) ) /dt )*(1/(4*deta1) ) );

C = -D_12/( 2*deta1*deta1);
e1( N1 - 1 ) = -B + C;
f1( N1 - 1 ) = A - 2*C;
g1( N1 - 1 ) = 0;

h1( N1 - 1 ) = ( A + 2*C)*U1( m - 1, N1 - 1); % ALL UN1-1 variables
h1( N1 - 1 ) = h1( N1 - 1 ) + ( B - C)*U1( m - 1 , N1 - 2); % ALL U N1 - 2 Variables
h1( N1 - 1 ) = h1( N1 - 1 ) -2*( B + C)*U_Gel; % All U_Gel Variables
% Beginning of Thomas Algorithm Solver
% Since matrix is tridiagonal, can solve very efficiently:
% alter matrix starting with second row such that:
% row2 = row2 - row1*(e2/f1) = f2' g2' and reduce to 2 non zero row values
% do the same for all other rows using: row_n = row_n - row_(n-1)*(e(n-1)/f(n)
% such that all row are reduced to having only 2 non zeros values...
% except the last one, which will have only ONE non zero value f_last
% get U_last from h_last/f_last = U_last;
% use U_last to help solve for U_(last-1) from row above, as has two...
% non-zero values keep doing this all polymer volume fractions found...
% Computer can do this with brutal efficiency...
for k = 2 : 1 : (N1 - 1)
    alpha1= e1(k)/f1(k - 1);
    e1( k ) = e1( k ) - f1( k - 1)*alpha1;
    f1( k ) = f1( k ) - g1( k - 1)*alpha1;
    h1( k ) = h1( k ) - h1( k - 1)*alpha1;
end
U1(m , N1 - 1) = h1( N1 - 1)/f1( N1 - 1 );
for k = (N1 - 2 ) : -1 : 1
    U1( m , k) = (h1(k) - g1(k)*U1( m , k + 1 ) )/f1(k);
end
% End of Thomas Algorithm Solver

% *****
% *****END OF U1 SOLVER PART; HAVE U1 VALUES*****
% *****

% *****
% *****Beginning of Solver for U2*****
% *****
% For the first row in the matrix
%-----

```

```

%      |+
%      S(t)
% Solving for node IMMEDIATELY to the right of S(t); eta2(2)
% First node is shared with Region I, but CANNOT be used as using it..
% will give a gradient in Region II and polymer will diffuse out...
% immediately. Will have to then modify it such that is a Neumann BC.
% According to paper, will have Neumann B.C. & depends on t_reptation
% This Neumann condition states that polymer flux occurs at times greater...
% than reptation and polymer becomes present in the solvent at this...
% time.
%re-writing A, B, C, & D from Stefan_Two_Phase_Polymer

A = ( L*L -2*L*S_guess +S(m - 1)*S_guess ) / dt;

B = ( L*S(m) - L*S( m - 1 ) - S_guess*S( m ) + S( m - 1 )*S( m ) )*(eta2( 2 ))/(
4*deta2*dt);

%      B = (1/ (4 * deta2 * dt) )*( eta2( n ) )*( L*( S_guess -S( m - 1 ) ) ) ;
C = -(D_p*.5)/( deta2*deta2 );

E = (2*deta2*( L - S( m ) ) )/D_p;% special value for Neumann B.C.
if t(m) < t_rep %This 'if' statement will check if enough time has elapsed
    lambda = 0;
else
    %s.t. lambda = ( (2*deta2*( L - S( m ) ) )/D_p ) *k_d
    lambda = k_d *E;
end

f2( 2 ) = A - 2*C;
g2( 2 ) = 2*C ;

h2( 2 ) = (A + 2*C)*U2( m - 1 , 2 ); % All U2( m - 1 , 2 ) Variables
h2( 2 ) = h2( 2 ) + ( -2*C ) *U2( m - 1 , 3 ); % All U2( m - 1 , 3 ) Variables
h2( 2 ) = h2( 2 ) + ( B - C )*( lambda_prev + lambda); % All respective lambdas

%Here, can solve for the rest of the values equally since all...
%have similar set-up.
for n = 3 : 1 : N2 - 2 % setting up matrix for the rest of the values
%re-writing A, B, C, & D from Stefan_Two_Phase_Polymer
A = ( L*L -2*L*S_guess +S(m - 1)*S_guess ) / dt;
B = ( L*S(m) - L*S( m - 1 ) - S_guess*S( m ) + S( m - 1 ) *S( m ) )*(eta2( n ))/(
4*deta2*dt);

%      B = (1/ (4 * deta2 * dt) )*( eta2( n ) )*( L*( S_guess -S( m - 1 ) ) ) ;
C = -(D_p*.5)/( deta2*deta2 );

e2( n ) = -B + C;
f2( n ) = A - 2*C;
g2( n ) = B + C ;

h2( n ) = (A + 2*C)*U2( m - 1 , n ); % All U2( m - 1 , n ) Variables

```

```

h2(n) = h2(n) + (-B - C)*U2(m - 1, n + 1); % All U2(m - 1, n + 1) Variables
h2(n) = h2(n) + (B - C)*U2(m - 1, n - 1); % All U2(m - 1, n - 1) Variables
end
%For solving the last row:
A = (L*L - 2*L*S_guess + S(m - 1)*S_guess) / dt;

B = (L*S(m) - L*S(m - 1) - S_guess*S(m) + S(m - 1)*S(m))*(eta2(N2 - 1))/(
4*deta2*dt);
% B = (1/(4 * deta2 * dt))*(eta2(n))*(L*(S_guess - S(m - 1)));
C = -(D_p*.5)/(deta2*deta2);

e2(N2 - 1) = -B + C;
f2(N2 - 1) = A - 2*C;
g2(N2 - 1) = B + C;

h2(N2 - 1) = (A + 2*C)*U2(m - 1, N2 - 1); % All U2(m - 1, N2 - 1) Variables;
h2(N2 - 1) = h2(n) + (-B - C)*U2(m - 1, N2); % All U2(m - 1, N2) Variables;
h2(N2 - 1) = h2(n) + (B - C)*U2(m - 1, N2 - 2); % All U2(m - 1, N2 - 2) Variables;
h2(N2 - 1) = h2(n) - g2(N2 - 1)*U2(m, N2); % Subtracting known U2(m, N2) from
system part
% Do not have to solve for the last row, as the last spatial node..
% At region II will have zero polymer volume fraction, since it...
% is the end of the boundary layer and polymer gets swept away.

% Beginning of Thomas Algorithm Solver
% Same method as described above for Region I
for k = 3 : 1 : (N2 - 1)
alpha1 = e2(k)/f2(k - 1);
e2(k) = e2(k) - f2(k - 1)*alpha1;
f2(k) = f2(k) - g2(k - 1)*alpha1;
h2(k) = h2(k) - h2(k - 1)*alpha1;
end
U2(m, N2 - 1) = h2(N2 - 1)/f2(N2 - 1);
for k = (N2 - 2) : -1 : 2
U2(m, k) = (h2(k) - g2(k)*U2(m, k + 1))/f2(k);
end
% End of Thomas Algorithm Solver

% *****
% *****End of Solver for U2*****
% *****

% *****
% *****Solving for S at specific time*****
% *****

% Here discretizing Region III condition for the moving boundary:
% ds/dt = D*du/dx - D*du/dx
% S(m) = (ds/dt)*dt + S(m - 1)
S(m) = -(D_12/(4*S_guess*deta1*U_Gel))*(3*U1(m, N1 - 1) - 4*U1(m, N1 - 2)...
+ U1(m, N1 - 3) + 3*U1(m - 1, N1 - 1) - 4*U1(m - 1, N1 - 2) + U1(m, N1 - 3))/1;
% S(m) = S(m) + (D_p/(2*deta2*U_Gel))*(3*U2(m, 1) - 4*U2(m, 2) + U2(m, 3));

```

```

% Here script checks if sufficient time elapsed such that polymer chain...
% diffusion to solvent occurs occurs:
if t(m) >= t_rep % Will check to see if enough time has passed for disentanglement
    S( m ) = S( m ) - (.5/ U_Gel)*(k_d + lambda_prev/E_prev) ;
end
    S( m ) = S( m )*dt + S( m - 1 );
% Computing Error with current guess vs guess at previous iteration
% Here is where one compares the S(t) obtained from the polymer volume..
% Fraction values from Region I & II versus the S_guess that was USED...
% To obtain the polymer fraction Values for regions I & II
S_Error(m) = abs( ( S(m) - S_guess )/S_guess ); %Error is compared RELATIVELY
if S_Error(m) < .0000001
    %Here means that for this iteration loop, convergence was achieved...
    % within the time step, so can go to the next time step
    Nicole = 4; % Nicole condition set such that can exit 'while' loop
    % *****
    % *****Must run Thomas Algorithm one more time to get*****
    % *****Final U values with Converged S value*****
    % *****
    % *****Beginning of Solver for U1*****
    % *****
    % Running solver for all locations within the time step again, but...
    %notice that now using S(m); NOT S_guess to solve
    % Solver for first matrix row: must solve for u1(1); Neumann BCfgfw

    A = S( m )*S( m )/dt;
    B = -eta1(1)*S( m )*( ( S( m ) - S(m - 1) )/dt )*(1 / (4*deta1) ) );
    C = -D_12/( 2*deta1*deta1);

%
    f1( 1 ) = A - 2*C;
    g1( 1 ) = 2*C;

    h1( 1 ) = ( A + 2*C)*U1( m - 1, 1); % ALL U( m - 1, 1)
    h1( 1 ) = h1( 1 ) + ( - 2*C)*U1( m - 1, 2); % + ALL U1( m - 1, 2);
    % No U( m - 1, -1) as is equal to U( m - 1, 2)- see line above

%

for n = 2 : 1 : N1 - 2 % setting up matrix for middle block

    A = S( m )*S( m )/dt;
    B = -eta1(n)*S( m )*( ( S( m ) - S(m - 1) )/dt )*(1 / (4*deta1) ) );
    C = -D_12/( 2*deta1*deta1);

    e1( n ) = -B + C;
    f1( n ) = A - 2*C;
    g1( n ) = B + C;

    h1( n ) = (A + 2*C)*U1( m - 1, n); % ALL U0
    h1( n ) = h1( n ) + (-B - C)*U1( m - 1, n + 1 ); % ALL U+1

```

```

    h1(n) = h1(n) + (B - C)*U1(m - 1, n - 1); % All U-1
end
% Solving for last Node in matrix (Dirichlet Condition)
A = S(m)*S(m)/dt;
B = -eta1(N1-1)*S(m)*((S(m) - S(m - 1))/dt)*(1/(4*deta1));
C = -D_12/(2*deta1*deta1);
e1(N1 - 1) = -B + C;
f1(N1 - 1) = A - 2*C;
g1(N1 - 1) = 0;

h1(N1 - 1) = (A + 2*C)*U1(m - 1, N1 - 1); % ALL UN1-1 variables
h1(N1 - 1) = h1(N1 - 1) + (B - C)*U1(m - 1, N1 - 2); % ALL U N1 - 2 Variables
h1(N1 - 1) = h1(N1 - 1) - 2*(B + C)*U_Gel; % All U_Gel Variables
% Beginning of Thomas Algorithm Solver
for k = 2 : 1 : (N1 - 1)
    alpha1 = e1(k)/f1(k - 1);
    e1(k) = e1(k) - f1(k - 1)*alpha1;
    f1(k) = f1(k) - g1(k - 1)*alpha1;
    h1(k) = h1(k) - h1(k - 1)*alpha1;
end
U1(m, N1 - 1) = h1(N1 - 1)/f1(N1 - 1);
for k = (N1 - 2) : -1 : 1
    U1(m, k) = (h1(k) - g1(k)*U1(m, k + 1))/f1(k);
end
% End of Thomas Algorithm Solver

% *****
% *****END OF U1 SOLVER PART; HAVE U1 VALUES*****
% *****

% *****
% *****Beginning of Solver for U2*****
% *****
% For the first row in the matrix
%-----
%      |+
%      S(t)
% Solving for node IMMEDIATELY to the right of S(t); eta2(2)
% According to paper, will have Neumann B.C. & depends on t_reptation

%re-writing A, B, C, & D from Stefan_Two_Phase_Polymer

A = (L*L - 2*L*S(m) + S(m)*S(m))/dt;
B = (L*S(m) - L*S(m - 1) - S(m)*S(m) + S(m - 1)*S(m))*(eta2(2))/(
4*deta2*dt);
%      B = (1/(4 * deta2 * dt))*(eta2(n))*(L*(S_guess - S(m - 1)));
C = -(D_p*.5)/(deta2*deta2);

E = (2*deta2*(L - S(m)))/D_p;% special value for Neumann B.C.

```

```

if t(m) < t_rep %This 'if' statement will check if enough time has elapsed
    lambda = 0;
else
    %s.t. lambda = ( (2*deta2*( L - S( m ) )/D_p ) *k_d
    lambda = k_d *E;
end

f2( 2 ) = A - 2*C;
g2( 2 ) = 2*C ;

h2( 2 ) = (A + 2*C)*U2( m - 1 , 2 ); % All U2( m - 1 , 2 ) Variables
h2( 2 ) = h2( 2 ) + ( -2*C ) *U2( m - 1 , 3 ); % All U2( m - 1 , 3 ) Variables
h2( 2 ) = h2( 2 ) + ( B - C ) * ( lambda_prev + lambda ); % All respective lambdas

for n = 3 : 1 : N2 - 2 % setting up matrix for the rest of the values
    %re-writing A, B, C, & D from Stefan_Two_Phase_Polymer

    A = ( L*L - 2*L*S( m ) + S( m ) * S( m ) ) / dt;
    B = ( L*S(m) - L*S( m - 1 ) - S( m ) * S( m ) + S( m - 1 ) * S( m ) ) * ( eta2( n ) ) / (
4*deta2*dt);
%    B = ( 1 / ( 4 * deta2 * dt ) ) * ( eta2( n ) ) * ( L * ( S_guess - S( m - 1 ) ) );
    C = -(D_p*.5)/( deta2*deta2 );

    e2( n ) = -B + C;
    f2( n ) = A - 2*C;
    g2( n ) = B + C ;

    h2( n ) = (A + 2*C)*U2( m - 1 , n ); % All U2( m - 1 , n ) Variables
    h2( n ) = h2( n ) + ( -B - C ) *U2( m - 1 , n + 1 ); % All U2( m - 1 , n + 1 ) Variables
    h2( n ) = h2( n ) + ( B - C ) *U2( m - 1 , n - 1 ); % All U2( m - 1 , n - 1 ) Variables
end
%For solving the last row:

%    A = ( L*L - 2*L*S( m ) + S( m - 1 ) * S_guess ) / dt;
%    B = ( L*S(m) - L*S( m - 1 ) - S( m ) * S( m ) + S( m - 1 ) * S( m ) ) * ( eta2( N2 - 1 ) ) / (
4*deta2*dt);
%    B = ( 1 / ( 4 * deta2 * dt ) ) * ( eta2( n ) ) * ( L * ( S_guess - S( m - 1 ) ) );
    C = -(D_p*.5)/( deta2*deta2 );

    e2( N2 - 1 ) = -B + C;
    f2( N2 - 1 ) = A - 2*C;
    g2( N2 - 1 ) = B + C;

    h2( N2 - 1 ) = (A + 2*C)*U2( m - 1 , N2 - 1 ); % All U2( m - 1 , N2 - 1 ) Variables;
    h2( N2 - 1 ) = h2( n ) + ( -B - C ) *U2( m - 1 , N2 ); % All U2( m - 1 , N2 ) Variables;
    h2( N2 - 1 ) = h2( n ) + ( B - C ) *U2( m - 1 , N2 - 2 ); % All U2( m - 1 , N2 - 2 ) Variables;
    h2( N2 - 1 ) = h2( n ) - g2( N2 - 1 ) *U2( m , N2 ); % Subtracting known U2( m , N2 ) from
system part

% Beginning of Thomas Algorithm Solver

```

```

for k = 3 : 1 : (N2 - 1)
    alpha1= e2(k)/f2(k - 1);
    e2( k ) = e2( k ) - f2( k - 1)*alpha1;
    f2( k ) = f2( k ) - g2( k - 1)*alpha1;
    h2( k ) = h2( k ) - h2( k - 1)*alpha1;
end
U2(m , N2 - 1 ) = h2( N2 - 1 )/f2( N2 - 1 );
for k = (N2 - 2 ) : -1 : 2
    U2( m , k ) = (h2(k) - g2(k)*U2( m , k + 1 ) )/f2(k);
end
% End of Thomas Algorithm Solver

% *****
% *****End of Solver for U2*****
% *****
%ELSE statement below in case there is DIVERGENCE between the S_guess...
%& and the S(m)
% Now will iterate and solve solve for the volume fraction values @...
% Regions I and II for spatial node, but now the new S_guess is the...
% S( m ) value that was obtained from the previous iteration
else
    S_guess = S( m ); % new S_guess value to help compute volume fractions
    counter(m) = counter(m) + 1; % counter increased
end
if counter(m) >= error_counter % here will check if executed too many iterative solve attempts
    Error1= 1; % error gets turned on- will allow to exit program all together
    l=[ ' Iteration Failure: Error Occurred @ time step: ', num2str(m) ];

    break % Allows one to exit while loop due to failure to iterate

end
% *****
% *****Transforming Etas back to X's such that can be plotted*****
% *****
% Now transforming back values to their locations for a time step.
% Here each spatial node in Regions I & II undergoes a reverse Landau..
%transform into the original coordinate system.Thus, can show outputs..
% where the polymer swells and undergoes dissolution.
Reverse_Landau_1 = S( m ); % for helping solve back to x's
Reverse_Landau_2 = L - S( m );
for k = 2: 1: N1
    X1(m, k) = Reverse_Landau_1*eta1(k);
end
for k = 1:1: N2 - 1
    X2(m, k ) = eta2(k)*Reverse_Landau_2 + Reverse_Landau_1;
end
end % End of 'while' loop with 'Nicole' Condition

```

```

end % End of time step (i.e: m to M) to solve at each time
%*****
%*****END OF SOLVER
LOOP*****
%*****

% Defining X3 & U3 which will unite both regions together
X3 = zeros( M , N1 + N2 - 1 );
U3 = zeros( M , N1 + N2 - 1 );

%Assuring that there is no mis-match between boundaries
for m = 1: 1 : M
    if X1( m , N1) ~= X2( m , 1)
        Error2 = 1;
        Message1 = [ ' Error: X Boundary Mis-Match between Phase 1 & Phase 2. Happened at time
step: ' , num2str(m) ] ;
        disp('*****')
        disp('*****')
        disp(Message1)
        disp('*****')
        disp('*****')
        break
    else
        % Sticking both Phase regions together s.t. one can plot them
        X3( m , : ) = [ X1( m , : ) X2( m , 2:N2) ];
        U3( m , : ) = [ U1( m , : ) U2( m , 2:N2) ];
    end
end
% Sticking both phases together s.t. will be able to be plotted
X3( 1 , : ) = [ X1( 1 , : ) X2( 1 , 2:N2) ];
U3( 1 , : ) = [ U1( 1 , : ) U2( 1 , 2:N2) ];

%*****
%*****Computing Total Polymer at a Given Time*****
%*****
% Beginning of Simpson's for EVEN number of Nodes; Make sure N1 is EVEN
% Here, uses original moving coordinates, so cannot do Simpson's straight..
% off.Must deal with each case carefully as in original coordinates spacing...
% will not be equal between nodes due to swelling and dissolution of...
% polymer region.

for m = 1 : 1 : length(t) %Executues Simpson's for the current time step
    for k = 1: 2 : N1 - 5
        % Simpson's 1/3 Segment:
        y0 = U1( m , k )/(( X1( m , k ) - X1( m , k + 1) )*( X1( m , k )...
            - X1( m , k + 2) ));
        y1 = U1( m , k + 1 )/(( X1( m , k + 1 ) - X1( m , k ) )*( X1( m , k + 1 )...
            - X1( m , k + 2) ));
        y2 = U1( m , k + 2 )/(( X1( m , k + 2 ) - X1( m , k + 1) )*( X1( m , k + 2 )...

```

- X1(m, k));

sum(m) = sum(m) + y0\*((X1(m, k+2).^3)/3 - (.5\*(X1(m, k+2).^2))\*(X1(m, k+1)...  
+ X1(m, k+2)) + X1(m, k+1)\*X1(m, k+2)\*X1(m, k+2));

sum(m) = sum(m) + y1\*((X1(m, k+2).^3)/3 - (.5\*(X1(m, k+2).^2))\*(X1(m, k)...  
+ X1(m, k+2)) + X1(m, k)\*X1(m, k+2)\*X1(m, k+2));

sum(m) = sum(m) + y2\*((X1(m, k+2).^3)/3 - (.5\*(X1(m, k+2).^2))\*(X1(m, k+1)...  
+ X1(m, k)) + X1(m, k+1)\*X1(m, k)\*X1(m, k+2));

sum(m) = sum(m) - y0\*((X1(m, k).^3)/3 - (.5\*(X1(m, k).^2))\*(X1(m, k+1)...  
+ X1(m, k+2)) + X1(m, k+1)\*X1(m, k+2)\*X1(m, k));

sum(m) = sum(m) - y1\*((X1(m, k).^3)/3 - (.5\*(X1(m, k).^2))\*(X1(m, k)...  
+ X1(m, k+2)) + X1(m, k)\*X1(m, k+2)\*X1(m, k));

sum(m) = sum(m) - y2\*((X1(m, k).^3)/3 - (.5\*(X1(m, k).^2))\*(X1(m, k+1)...  
+ X1(m, k)) + X1(m, k+1)\*X1(m, k)\*X1(m, k));

end

% Simpsons's 3/8 final segment

k = N1;

y1 = U1(m, k-3)/(X1(m, k-3) - X1(m, k-2))\*(X1(m, k-3)...  
- X1(m, k-1))\*(X1(m, k-3) - X1(m, k));

y2 = U1(m, k-2)/(X1(m, k-2) - X1(m, k-3))\*(X1(m, k-2)...  
- X1(m, k-1))\*(X1(m, k-2) - X1(m, k));

y3 = U1(m, k-1)/(X1(m, k-1) - X1(m, k-3))\*(X1(m, k-1)...  
- X1(m, k-2))\*(X1(m, k-1) - X1(m, k));

y4 = U1(m, k)/(X1(m, k) - X1(m, k-3))\*(X1(m, k)...  
- X1(m, k-2))\*(X1(m, k) - X1(m, k-1));

sum(m) = sum(m) + y1\*( (.25\*(X1(m, k).^4) - ((X1(m, k).^3)/3)\*(...  
X1(m, k-2) + X1(m, k-1) + X1(m, k)) + .5\*(X1(m, k).^2)\*(...  
X1(m, k-2)\*X1(m, k-1) + X1(m, k-2)\*X1(m, k) + ...  
X1(m, k-1)\*X1(m, k)) - X1(m, k)\*(X1(m, k-2)\*X1(m, k-1)\*X1(m, k)) );

sum(m) = sum(m) - y1\*( (.25\*(X1(m, k-3).^4) - ...  
((X1(m, k-3).^3)/3)\*(X1(m, k-2) + X1(m, k-1) + X1(m, k))...  
+ .5\*(X1(m, k-3).^2)\*(X1(m, k-2)\*X1(m, k-1) + ...  
X1(m, k-2)\*X1(m, k) + X1(m, k-1)\*X1(m, k))...  
- X1(m, k-3)\*(X1(m, k-2)\*X1(m, k-1)\*X1(m, k)) );

sum(m) = sum(m) + y2\*( (.25\*(X1(m, k).^4) - ...  
((X1(m, k).^3)/3)\*(X1(m, k-3) + X1(m, k-1) + X1(m, k))...  
+ .5\*(X1(m, k).^2)\*(X1(m, k-3)\*X1(m, k-1) + ...  
X1(m, k-1)\*X1(m, k) + X1(m, k-3)\*X1(m, k)) - ...  
X1(m, k)\*(X1(m, k-3)\*X1(m, k-1)\*X1(m, k)) );

sum(m) = sum(m) - y2\*( (.25\*(X1(m, k-3).^4) - ...  
((X1(m, k-3).^3)/3)\*(X1(m, k-3) + X1(m, k-1) + X1(m, k))...  
+ .5\*(X1(m, k-3).^2)\*(X1(m, k-3)\*X1(m, k-1) + X1(m, k-1)\*X1(m, k)...  
+ X1(m, k-3)\*X1(m, k)) - X1(m, k-3)\*(X1(m, k-3)\*X1(m, k-1)\*X1(m, k)) );

```

sum( m ) = sum( m ) + y3*( (.25*(X1( m , k ).^4)) - ...
((X1( m , k ).^3)/3)*( X1( m , k - 3) + X1( m , k - 2)...
+ X1( m , k ) ) + .5*( X1( m , k ).^2 )*( X1( m , k - 3)*X1( m , k - 2)...
+ X1( m , k - 3)*X1( m , k ) + X1( m , k - 2)*X1( m , k ) ) - ...
X1( m , k )*( X1( m , k - 3)*X1( m , k - 2)*X1( m , k ) ) );
sum( m ) = sum( m ) - y3*( (.25*(X1( m , k - 3 ).^4)) -...
((X1( m , k - 3 ).^3)/3)*( X1( m , k - 3) + X1( m , k - 2 ) + X1( m , k ) ) +...
.5*( X1( m , k - 3 ).^2 )*( X1( m , k - 3)*X1( m , k - 2) + X1( m , k - 3)*X1( m , k )...
+ X1( m , k - 2)*X1( m , k ) ) - X1( m , k - 3)*( X1( m , k - 3)*X1( m , k - 2)*X1( m , k ) )
);

sum( m ) = sum( m ) + y4*( (.25*(X1( m , k ).^4)) - ...
((X1( m , k ).^3)/3)*( X1( m , k - 3) + X1( m , k - 2) + X1( m , k - 1 ) )...
+ .5*( X1( m , k ).^2 )*( X1( m , k - 3)*X1( m , k - 2) + X1( m , k - 2)*X1( m , k - 1 )...
+ X1( m , k - 1)*X1( m , k - 3 ) ) - X1( m , k )*( X1( m , k - 2)*X1( m , k - 1)*X1( m , k - 3)
) );
sum( m ) = sum( m ) - y4*( (.25*(X1( m , k - 3 ).^4)) -....
((X1( m , k - 3 ).^3)/3)*( X1( m , k - 3) + X1( m , k - 2 ) + X1( m , k - 1 ) )...
+ .5*( X1( m , k - 3 ).^2 )*( X1( m , k - 3)*X1( m , k - 2) + X1( m , k - 2)*X1( m , k - 1 )+...
X1( m , k - 1)*X1( m , k - 3 ) ) - X1( m , k - 3)*( X1( m , k - 2)*X1( m , k - 1)*X1( m , k - 3)
);
end
% *****
% *****End of Total Poylmer Computation*****
% *****

% *****
% *****All Computations Done; Can Plot Results*****
% *****

% Following is just script to give graphic outputs to polymer dissolution..
% problem. Will make a movie if movie set to 1 at beginning or give a....
% combination of plots in the case where movie set to 0 ( zero)
if (Error1 < 1) && (Error2 < 1) && movie ==1
    timer1 = ' Current time is: ';
    integration1 = ' Total UNDISSOLVED Polymer : ';
    timer3 = [ ' Total time is: ' num2str( t( M ) ) ];
for m = 1: 1 : M % This loop is for making movie. Makes a graph for each frame
    hold off
    axis([ 0 L 0 1.2])
    plot( X3( 1 , : ) , U3( 1 , :), 'r' ); % Plot concentration at beginning
    hold on
    axis([ 0 L 0 1.2])

    plot( X1( m , N1) , U_Gel , 'g*') % Will 'track' solvent/gel layer
    plot( X3( m , : ) , U3( m , :), 'k' ); % Plotting Concentration at each time
% plot( X3( M , : ) , U3( M , :), 'c' ); % Plotting final Concentration
% plot( X3( M_rep , : ) , U3( M_rep , :), 'b' );
    axis([ 0 L 0 1.2])
    title( ' Solution of LINEAR STEFAN PROBLEM WITH TWO PHASES ' );

```

```

xlabel( x_label);
ylabel( ' Polymer Concentration - Pure polymer is 1 (100%)' );
legend({' Start ', Solvent/Gel Layer ', ' Current '},'Location','northeast');
legend('boxoff');

% Setting plot written information
timer2 = num2str(t(m)) ;
integration2 = num2str(sum( m ) );
text( 7 , .5 , timer1);
text( 7.5 , .425 , timer2);
text( 7 , .35 , timer3);
text( 4 , .6 , time_rep);
% text( 5 , .3 , integration1);
% text( 7 , .225 , integration2);
frame = getframe(gcf);
writeVideo( v , frame );

end
%Now plot without a movie. Will give a polymer volume fraction profile for...
%beginning, when reptation time is reached, and for final time.
elseif (Error1 < 1) && (Error2 < 1) && movie ==0
axis([ 0 L 0 1.2])
plot( X3( 1 , : ) , U3( 1 , :), 'r' ); % Plot concentration at beginning
hold on
axis([ 0 L 0 1.2])
plot( X3( M , : ) , U3( M , :), 'c' ); % Plotting final Concentration
plot( X3( M_rep , : ) , U3( M_rep , :), 'b' ); %Plotting Concentration..
% at the reptation time.
axis([ 0 L 0 1.2])
title( ' Solution of LINEAR STEFAN PROBLEM WITH TWO PHASES ' );

xlabel( x_label );
ylabel( ' Polymer Concentration - Pure polymer is 1 (100%)' );
legend({' Start ', ' Final ', ' Apogee '},'Location','northeast');
legend('boxoff');
text( 5 , .5 , time_step );
text( 7 , .35 , timer3);
text( 4 , .55 , Region_I_Step);
text( 4 , .70 , Region_II_Step);
else
disp( ' Since an error(s) occurred, will not print plot.' )
disp( ' Try looking at workspace values to get an idea.' )
disp( ' Check for errors that are set to "1" at the Workspace table.' )
disp( ' Consult with Script commentary to see what went wrong.' )

end

```

